

phase separation micro molding

**laura vogelaar**

© Laura Vogelaar, 2005

Phase Separation Micro Molding

Laura Vogelaar

Ph.D. Thesis, University of Twente, The Netherlands

ISBN 90-365-2221-8

Printed by PrintPartners Ipskamp B.V., Enschede, The Netherlands

Cover: Optical diffraction of sunlight through transparent microstructures having a periodic hole pattern. The microstructures are floating in non-solvent (water), and the reflection is projected on silicon molds. Photography Bernke Papenburg, advice Carole Messerli.



# **PHASE SEPARATION MICRO MOLDING**

## **PROEFSCHRIFT**

ter verkrijging van  
de graad van doctor aan de Universiteit Twente,  
op gezag van de rector magnificus,  
prof.dr. W. H. M. Zijm,  
volgens besluit van het College voor Promoties  
in het openbaar te verdedigen  
op vrijdag 8 juli 2005 om 15:00 uur

door

**Laura Vogelaar**

geboren op 5 september 1975  
te Rotterdam

Dit proefschrift is goedgekeurd door de promotor:

Prof.dr.-ing. M. Wessling

en de assistant promotor:

Dr.ir. R. G. H. Lammertink.

## voorwoord

Op de kaft van dit boekje staat maar één naam en dat klopt niet. Eigenlijk zou de kaft vol moeten staan met namen van iedereen, zonder wie dit proefschrift er nooit in de huidige vorm was geweest. Ik hoop dat jullie ook tevreden zijn met een plaatsje in dit voorwoord.

Het werk de afgelopen jaren was vooral erg leuk door mijn mede-MTO-ers. De leuke sfeer in de groep, koffiepauzes, borrels en Geus avonden zal ik erg gaan missen. Als jullie ooit horen van iemand die met weemoed in de etalage van de multivlaai staat te staren, of een pitcher bier bestelt, terwijl ze dat niet eens drinkt, dan weet je wie het is... Een aantal van jullie wil ik met name noemen.

Matthias wil ik natuurlijk vooral bedanken voor zijn ‘op de fiets’ idee om fasescheiding te combineren met een mal. Dat fietstochtje heeft mij de afgelopen jaren goed bezig gehouden. Bedankt dat je dit werk aan mij hebt toevertrouwd, en voor je enthousiasme de afgelopen jaren. Ik hoop dat dit boekje weergeeft wat je toen al fietsend in gedachten had.

Rob, als ik nog tijd had gehad al je originele ideeën uit te voeren was dit boekje minstens twee keer zo dik geweest. Daarnaast ben ik je ook nog dank schuldig voor al het praktische werk dat je hebt gedaan en je treffende op- en aanmerkingen op mijn schrijfwerk de afgelopen maanden. Zonder jouw inbreng was het lang niet zo leuk geweest aan dit boekje te werken. Je inzet en enthousiasme als begeleider werken erg motiverend.

Jonathan stond voor de onmogelijke taak om iemand, die alle polymeren plastic noemt en al het glaswerk flesje, op weg te helpen op een chemisch lab. Bedankt voor de goede samenwerking! CT is toch best aardig... Bernke, enorm bedankt voor al je werk aan tissue engineering tijdens je afstuderen en aan de lotusstructuren tijdens je assistentschap. Daarnaast natuurlijk ook voor je fotofiekunsten, die de omslag sieren. Ik vind het een geruststellend idee dat je verder gaat als aio en het PS $\mu$ M-werk dus in goede handen is. Hartelijk dank aan Dirk Grijpma en André Poot van de PBM groep, Dimitris en het lab van

het Medisch Spektrum Twente, die aan het tissue engineering werk hebben bijgedragen. Thanks to Hanquan, who performed her graduation assignment within my project, parts of which are described in this thesis. Thank you for your efforts.

Lydia wil ik bedanken voor haar assistentie in de eerste jaren van mijn project, het was leuk om met je samen te werken. Verder hebben Peter, Thomas, Jorg, en Micky als studentassistent of voor een studieopdracht meegeholpen aan delen van dit boekje, waarvoor natuurlijk hartelijk dank. Miriam en Jörg bedankt voor de samenwerking op de warmtebehandelingen, Marcel voor alle hulp bij computerellende, Antoine voor de zorgen op financieel gebied en omdat je een fijne wijkgenoot bent, Greet voor alle antwoorden op administratieve vragen, Maik voor de hulp bij metingen aan contacthoeken en oppervlaktetspanning, Clemens voor het filmpje op de optische microscoop, Wilbert voor het tekenen van het 3D plaatje, en Herman voor de foto van de knikkervormige waterdruppel en de hulp bij SEM-problemen.

Verder wil ik mijn (oud-)kamerogenoten Sybrand, Jonathan, George, Jens, Alisia, Bernke en voor korte tijd ook Pedro en Alexei bedanken. Ik heb het erg gezellig gevonden op onze kamer, 1330 is echt prettig!

Natuurlijk kan ik dit dankwoord niet schrijven zonder Aquamarijn / Nanomi te bedanken: Wietze, Cees, Ben en Gert, bedankt voor jullie bijdrage en belangstelling.

Mijn vrienden en vriendinnen heel erg bedankt voor alle leuke momenten, het is goed te weten dat ik altijd op jullie kan rekenen. Daarnaast zijn er een aantal vriendinnen die een wat concretere bijdrage aan mijn promotie hebben geleverd. Antoinette, ik vind het fijn dat er altijd iemand was die de ups en downs van promoveren zo goed begrijpt, en ik wens je veel succes bij jouw laatste loodjes. Carole, bedankt voor het advies over de foto voor de omslag (daardoor is het toch nog gelukt). En natuurlijk mijn paranimfen: Suuzz, dank voor je verrassende, creatieve ideeën voor de lay-out van dit boekje. Je staat altijd voor me klaar en verdient zeker een plaats op het podium (ook al heb je er om gezeurd...). En Sas, ik vind het heel bijzonder dat we al zo lang vriendinnen zijn. Toen we twee kaarsjes uitbliezen op de verjaardagstaart stond je me al terzijde, en ik vind het fijn dat dat nu nog steeds zo is.

Tot slot mijn ouders en broer, die altijd achter me staan. Wat dat voor me betekent, valt niet in een simpel dankwoord te vatten.

Lauka

## contents

introduction	1
<b>chapter 1</b> why micro molding? introduction on the role of micro molding in microfabrication	5
<b>chapter 2</b> phase separation micro molding: a new, generic approach towards microstructuring a wide range of materials	19
<b>chapter 3</b> freestanding microstructures fabricated by phase separation micro molding	43
<b>chapter 4</b> perforated microstructures prepared by phase separation micro molding: application as polymeric microsieves and free standing polymeric etch and deposition masks	61
<b>chapter 5</b> scaffolds for tissue engineering prepared by phase separation micro molding	75
<b>chapter 6</b> self cleaning surfaces: phase separation micro molding as a route to superhydrophobicity	91
<b>chapter 7</b> polyaniline microactuator fabricated by phase separation micro molding	105
summary	113
samenvatting	115
curriculum vitae	117



## scope of this thesis

The central topic of this thesis is the development of a novel microfabrication method, Phase Separation Micro Molding (PS $\mu$ M). PS $\mu$ M is a replication method based on phase separation of a polymer solution. A very broad range of materials has been structured, including both polymers and inorganic materials. From the preparation of several different microstructures out of various materials, insight has been gained on the strengths and weaknesses of PS $\mu$ M as a microfabrication method. PS $\mu$ M has a few characteristics, which are unprecedented in microfabrication. In this thesis, these characteristics are exploited in different applications. Freestanding microstructures have been fabricated as a result of corner flow assisted PS $\mu$ M. Their evolution is described according to experimental results and a model. The fabrication of perforated microstructures is demonstrated and such microstructures are applied as polymeric microsieves and etch and deposition masks. Furthermore a tissue engineering scaffold, a self-cleaning surface, and a pH-sensitive microactuator were developed based on the benefits, which PS $\mu$ M offers as a microfabrication technique.

## brief introduction

Traditionally microfabrication is the driving force behind the developments within microelectronics.<sup>1</sup> However as a consequence of the many possibilities of integration and miniaturization in many other technologies microfabrication has also established a permanent position. For example integrated optics, microfluidics and certain biomedical applications rely completely on the use of microfabrication. For the applications outside

microelectronics different requirements are valid based on e.g. costs and material properties.<sup>2</sup> The traditionally prevailing microfabrication technology, photolithography, cannot always meet these requirements. Photolithography is relatively expensive, especially when the necessary feature sizes approach the far sub-micrometer regime.<sup>3</sup> The range of materials that can be processed is limited. Furthermore there is a fundamental boundary to progress to smaller feature sizes, caused by the use of optical projection.

Conventional micro molding methods avoid the limitations of photolithography.<sup>4</sup> They are cost-effective since they are based on simple replication. The range of materials that is available for microfabrication is expanded by the introduction of a certain amount of melt processable and cross linkable polymers. Since there is no optics involved, there is no fundamental limitation for fabrication of structures in the nanometer regime (feature sizes as small as 2 nm have recently been demonstrated).<sup>5</sup> Therefore micro molding methods play an important role especially for low-cost fabrication of micro- and nanostructures or for the processing of materials that are necessary for applications outside microelectronics. The micro molding method that is the topic of this thesis, phase separation micro molding, complements the spectrum of microfabrication technologies. First of all PS $\mu$ M holds the above mentioned advantages of micro molding methods, second because new functionalities emerge from the possibility to prepare porous microstructures, and finally it also further expands the range of applicable materials.<sup>6</sup>

## structure of this thesis

The thesis consists of an introduction to the role of micro molding methods in microfabrication, a description of the Phase Separation Micro Molding process, and some applications to illustrate its strengths. The PS $\mu$ M process is relatively easy and very reliable. Furthermore PS $\mu$ M covers a very broad range of materials, some of which could not be used in microfabrication before. Perforated microstructures can be prepared in a single fabrication step, as well as certain three-dimensionally freestanding configurations. PS $\mu$ M is also unique in its possibility to fabricate porous microstructures having a wide range of well-controllable morphologies. The applications that are described in this thesis merely focus on exploitation of the above-mentioned characteristics.



In **Chapter 1** a literature-based introduction on micro molding is given. A brief description of the present field of microfabrication, in which traditionally photolithography dominates, illustrates the role micro molding methods fulfill herein. Micro molding techniques against an elastomeric master, collectively known as ‘soft lithography’, and against rigid masters, e.g. hot embossing and nano-imprint, will be described in more detail.

The process of phase separation micro molding is described in **Chapter 2**. The chapter reveals how the intrinsic porosity can be tuned by controlling various parameters of the phase separation process. The effect of shrinkage is discussed, and, as it turns out, this shrinkage of the polymer during the phase separation is crucial for some important characteristics of PS $\mu$ M. There are both positive and negative sides to this shrinkage, which is responsible for very easy release conditions and the preparation of perforated microstructures on one hand, but also involves a risk for deformations on the other hand. Furthermore the chapter lists the very broad range of materials that have been used in PS $\mu$ M, including amorphous and crystalline polymers, block copolymers and some polymers with a specific functionality. Finally, the chapter will also comment on the preparation of microstructures from inorganic materials by combination of PS $\mu$ M with additional processing.

**Chapter 3** describes the preparation of freestanding microstructures by PS $\mu$ M. Such microstructures would be at least very difficult (not to say impossible) to fabricate by any other fabrication method. In PS $\mu$ M the freestanding configuration of the microstructures is the result of air entrapment when a polymer solution is applied on molds with polygonal holes. The corners of the holes allow the polymer solution to flow into the polygonal trench while displacing the air. PS $\mu$ M fixates the configuration of the flowing polymer solution in a freestanding microstructure. Comparison of experimental results with a model describing corner flow provides insight in the mechanism of the polymer solution flowing in the polygonal trenches.

The preparation of perforated, completely open microstructures is set out in detail in **Chapter 4**. Process conditions that promote perforation are revealed. Two applications are described in the chapter, namely the use of perforated microstructures as polymeric microsieves and as etch or deposition masks. Uniform size reduction of the microstructures is demonstrated, by the introduction of a heat treatment that causes the intrinsic porosity to collapse.

**Chapter 5** focuses on the preparation of a scaffold for tissue engineering purposes. The scaffold consists of porous microstructured sheets from a biodegradable material. The porosity of the microstructure serves the purpose of nutrient transport, while the relief profile can be utilized for directional cell growth. Cell culturing experiments reveal that cells proliferate well on such scaffolds and even have a slight tendency to grow directionally. Glucose diffusion through such scaffolds indicates that nutrients can be transported, although the porosity of the scaffold requires further improvement.

In **Chapter 6** a self-cleaning surface is prepared using PS $\mu$ M from a commercially available hydrophobic polymer. The self-cleaning effect of the surfaces relies on a hierarchical roughness. This hierarchical roughness consists of the microstructure and a roughness on a smaller length scale, which results from the interplay between porosity and crystallinity during the phase separation. The roughness structure mimics the structure on the leaves of the lotus plant that exhibit a natural self-cleaning effect. For the optimal combination of microstructure and surface roughness a contact angle of 167° is measured, while hardly any hysteresis could be detected, confirming good self-cleaning properties.

A pH-sensitive microactuator is developed in **Chapter 7**. The actuation of the device relies on the asymmetric pore morphology throughout the microstructure. This asymmetry is very typical for liquid induced phase separation. Initial results are presented on actuation of the microstructure as a response to a change in pH.

## references

<sup>1</sup> M. J. Madou, *Fundamentals of Microfabrication*, CRC Press, Boca Raton, U.S. **2002**.

<sup>2</sup> Y. Xia and G. M. Whitesides, *Angew. Chem. Int. Ed.* **1998**, *37*, 550.

<sup>3</sup> S. R. Quake and A. Scherer, *Science* **2000**, *290*, 1536.

<sup>4</sup> Reviews on micro molding: Y. Xia and G. M. Whitesides, *Angew. Chem. Int. Ed.* **1998**, *37*, 550; S. R. Quake and A. Scherer, *Science* **2000**, *290*, 1536; M. Geisler and Y. Xia, *Adv. Mater.* **2004**, *16*, 1249; Y. Xia, J. A. Rogers, K. E. Paul, G. M. Whitesides, *Chem Rev.* **1999**, *99*, 1823; D. Qin, Y. Xia, J. A. Rogers, R. J. Jackman, X. M. Zhao, G. M. Whitesides, *Topics in Current Chemistry* **1998**, *194*, 1; H. Becker, C. Gartner, *Electrophoresis* **2000**, *21*, 12; Y. Xia, G. M. Whitesides, *Annu. Rev. Mater. Sci.* **1998**, *28*, 153; B. D. Gates, Q. Xu, C. Love, D. B. Wolfe, G. M. Whitesides, *Annu. Rev. Mater. Res.* **2004**, *34*, 339; M. Hecke and W. K. Schomburg, *J. Micromech. Microeng.* **2004**, *14*, R1.

<sup>5</sup> B. D. Gates and G. M. Whitesides, *J. Am. Chem. Soc.* **2003**, *125*, 14986.

<sup>6</sup> L. Vogelaar, R. G. H. Lammertink, J. N. Barsema, W. Nijdam, L. A. M. Bolhuis-Versteeg, C. J. M. van Rijn, M. Wessling, *Small* **2005**, *1*, 645 ; L. Vogelaar, J. N. Barsema, W. Nijdam, C. J. M. van Rijn, M. Wessling, *Adv. Mater.* **2003**, *15*, 1385.



## chapter 1

## why micro molding?

### introduction on the role of micro molding in microfabrication

In only a few decades, microfabrication has developed into a vast and ever expanding field. It is impossible to imagine the state of technology today without microfabrication. Traditionally, photolithography has been the method of choice, but lately micromolding methods find increasing application. This chapter reviews the different microfabrication methods, and will focus on the benefits that micro molding methods can offer with respect to photolithography.



*Above: Memory of my first molding experiments. Thanks to Milo for providing the mold.*

# 1

## 1.1 introduction

Microfabrication has been the workhorse behind the explosive growth in microelectronics during the past decades. The demands to continuously increase the density of components on a chip can only be fulfilled by advancements in the technology to define architectures on a micrometer to nanometer scale. Microfabrication has not only supported the developments in microelectronics, but has emerged in several other technologies as well.<sup>1</sup> Well-known examples are micromechanics, micro-electromechanical systems (MEMS), integrated optics, photonics, microfluidics (lab on a chip, micro Total Analysis Systems), information storage devices, biochips, displays, micro reactors, and several types of sensors. In the areas where microfabrication is applied, miniaturization and integration have led to new functions, a reduction in time, costs, reagents, sample size, or power consumption, and furthermore portability and improved detection limits.<sup>2</sup>

## 1.2 direct writing methods

Methods to realize structures on such small length scales can be divided in direct writing methods and replication methods.<sup>3,4</sup> Initial generation of a pattern on a micrometer scale is in almost all cases accomplished by a direct writing method. For example, writing with a focused laser beam is often employed to produce photomasks that contain the structure necessary for photolithography. Other examples of direct writing methods are writing by atomic force microscopy (AFM), near field scanning optical microscopy (NSOM), electron beam (e-beam) lithography, focused ion beam (FIB) lithography, laser-induced chemical vapor deposition, inkjet printing and dip-pen lithography. In some cases high resolutions can be achieved, e.g. the minimum dimension that can be written by e-beam lithography is as small as 10 nm.<sup>4,5</sup> However, the main limitation of writing methods is their serial character that makes them too slow and expensive for application on a large scale in the fabrication of commercial devices. Writing methods however will remain the basis for generation of masks or molds for replication methods.

## 1.3 photolithography

Geissler and co-workers define the purpose of replication as 'to reproduce (or duplicate) the structural information on the surface of a mask or master using a different material in a single step, rapidly, and with high fidelity'.<sup>3</sup> Replication is in general more cost-effective since a master structure can be replicated many times, at relatively short time scales compared to writing methods. The replication method that is used mostly in microfabrication is photolithography or optical lithography.

A schematic representation of photolithography is depicted in Figure 1. Photolithography relies on the chemical change in a photoresist upon exposure to light, affecting for example the solubility of the resist.<sup>1</sup> A thin layer of resist is exposed to a pattern from a mask mostly by UV light. When the resist is subsequently developed, the pattern on the mask is transferred in the resist. The photoresist can be used as a mask for etching, herewith transferring the pattern in the underlying substrate.

Projection of the mask structure on the photoresist can be achieved by bringing the mask in close contact with the resist layer during the illumination. However this includes the risk of damaging the mask or resist and yields a 1:1 projection of the mask. Therefore in commercial applications a so-called wafer stepper is used, in which a lens system projects a reduced image of the mask at a larger distance.<sup>3</sup> These systems are very costly and increase in complexity (and therefore costs) as the required feature size of the projected patterns decreases. Distortion of the projection by dust particles should be avoided and therefore lithography is performed in a cleanroom environment, which is an additional boost of the costs of photolithography.

A fundamental barrier for the minimum feature size that can be projected is Rayleigh's resolution limit, which strongly depends on the wavelength of the light.<sup>2,6</sup> For use of UV light, the lower boundary in feature size is estimated at 150 nm.<sup>4</sup> The limit is lowered when a shorter wavelength is employed (like extreme UV or X-rays), although also for these wavelengths the boundary in resolution will eventually be met. The use of optical projection will therefore inherently complicate the achievement of smaller feature sizes. Additionally, the requirements on the chemistry of the photoresist are getting more stringent in the progression towards higher resolutions.<sup>4</sup> Meanwhile Moore's law states, the number of transistors that can be integrated on a single silicon chip doubles every 18 months.<sup>6,7</sup> The

## chapter 1

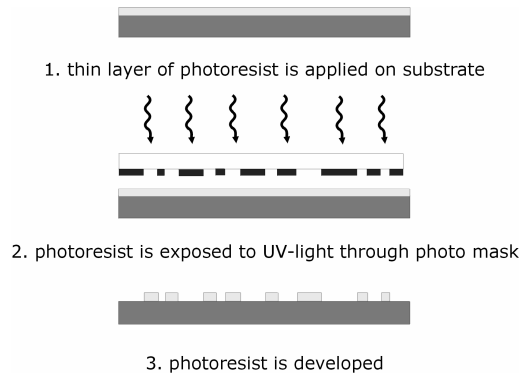


figure1 *Schematic representation of photolithography.*

resolution required in microelectronics will soon approach the fundamental limitation of photolithography, and it will be increasingly difficult to adapt to Moore's law.

The patterns generated by lithography are transferred in the underlying material by etching, or transferred in other layers by deposition. The materials that can be used in the traditional combination of photolithography and subsequent etching or deposition steps are mainly silicon (crystalline or amorphous), glass, quartz, metals, and some polymers, and are sometimes referred to as 'rigid materials'.<sup>8</sup> These materials are excellent choices for the traditional application in microelectronics, but are very limited when it comes to other applications. Silicon is brittle, expensive, opaque in the UV and visible region, and has a surface chemistry that is complicated to manipulate.<sup>2</sup> Especially in integrated optics, microfluidics and biomedical applications the material properties of silicon are too restricted. Therefore alternative methods that expand the range of applicable materials find use especially in these areas.

The limited transparency of the involved materials and the high costs are a drawback for the use of photolithography in integrated optics. Microfluidic devices by nature require a certain minimum area over which they extend, and therefore need a relatively high volume of material. The high cost of the material and the fabrication method and the limitations in geometrical design and surface chemistry can be disadvantageous for application of photolithography in microfluidics.<sup>9</sup> Also biomedical applications require a delicate surface chemistry.<sup>10,11,12</sup>

The limitations of optics considering feature size and the limited choice in materials were the two main reasons to start the development of alternatives for photolithography, namely micro molding methods. Other reasons are the high costs and the inability to pattern non-planar surfaces.<sup>2</sup> Micro molding relies on replication of a master or mold, having a microstructured relief profile on its surface. The rest of this chapter will clarify micromolding methods, mainly categorized in two classes. The first part will discuss soft lithography, where the mold or master structure is formed by an elastomeric (soft) material.<sup>2,13,14</sup> The second part will go into detail on micro molding methods using a rigid mold, e.g. hot embossing, nano imprint and micro injection molding.<sup>15</sup> The focus is restricted to techniques that can transfer arbitrarily chosen patterns, and therefore self assembly as a means of pattern generation will not be considered.<sup>3</sup>

## 1.4 soft lithography

Soft lithography is the collective name for a set of techniques, which all use an elastomeric stamp or mold to transfer a pattern to a substrate.<sup>2,13,14,16</sup> The ‘soft’ master structure is prepared mostly from poly(dimethyl siloxane) (PDMS), by curing on a microstructured mold. Presently, the collective of soft lithography consists of microcontact printing ( $\mu$ CP), nanotransfer printing (nTP), replica molding (REM), microtransfer molding ( $\mu$ TM), micromolding in capillaries (MIMIC), capillary force lithography (CFL) and solvent assisted micro molding (SAMIM). Figure 2 illustrates the collective of soft lithographic techniques schematically. Soft lithography was mainly developed within the group of G.M. Whitesides.<sup>17</sup>

Microcontact printing is the means of soft lithography that has found until now the most practical application. In  $\mu$ CP the elastomeric microstructure is used as a stamp.<sup>18</sup> An ink is applied on the mold, dried and then the mold is brought into contact with a substrate. The ink is transferred to the substrate and can be used in subsequent process steps. To scale-up the process the patterned elastomer can also be applied on a cylindrical role to create a rolling stamp.<sup>19</sup> Self Assembling Monolayers (SAMs) are often chosen as the ink. Examples of such SAMs are alkanethiolates, which can be applied on gold or silver,<sup>18,20,21,22</sup> silanes, which can be applied on siliconoxide,<sup>23</sup> or siloxanes, which can be applied on OH-terminated

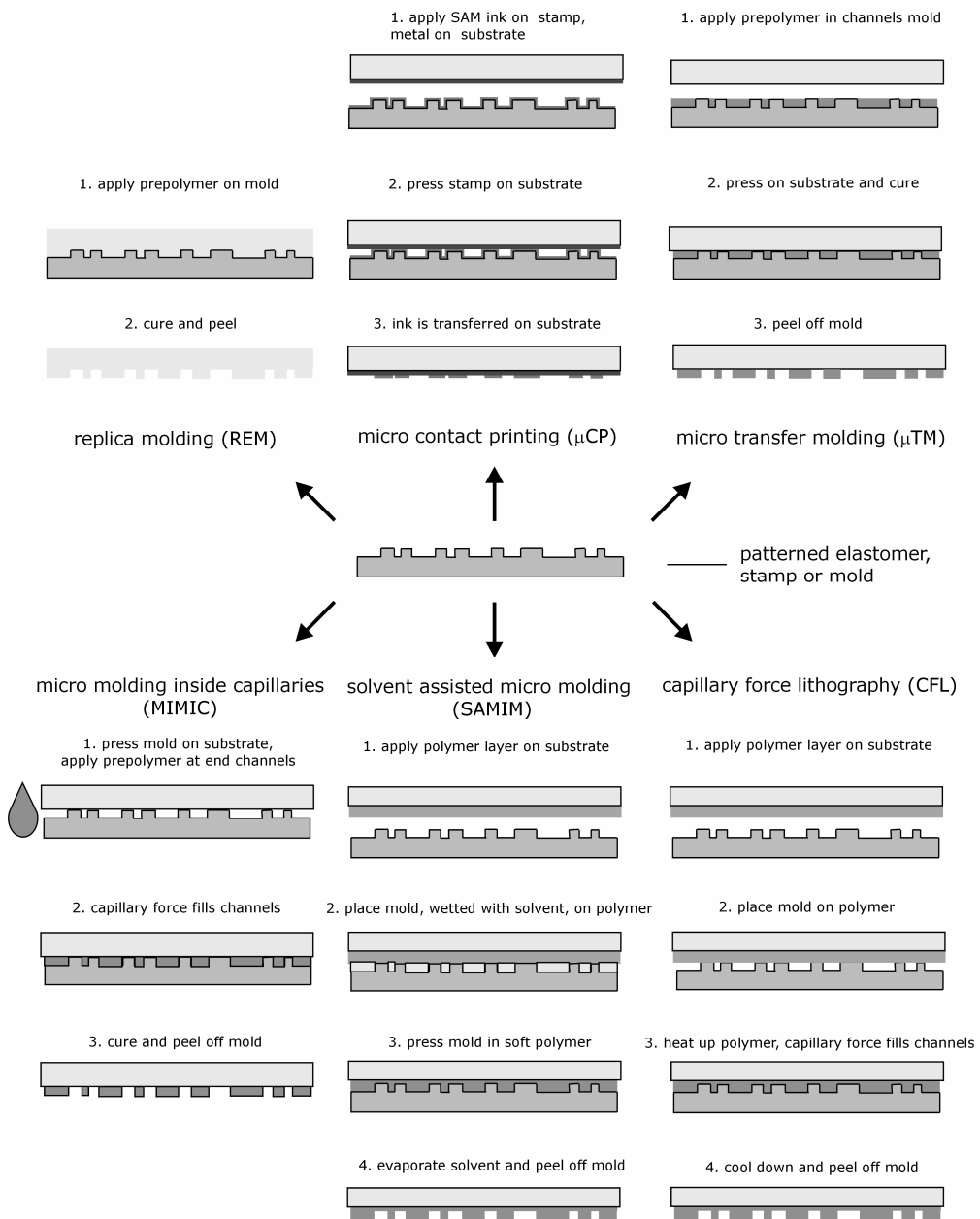


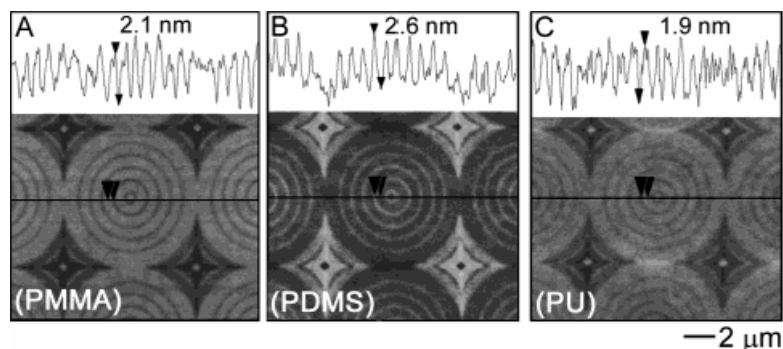
figure 2 Schematic representation of the collective of soft lithographic techniques. Soft lithography presently consists of Replica Molding, Micro Contact Printing, Micro Transfer Molding, Micro Molding Inside Capillaries, Solvent Assisted Micro Molding and Capillary Force Lithography. All these techniques use a patterned elastomer to transfer a pattern.



surfaces.<sup>24</sup> They form highly ordered layers of molecules only 1-3 nm thick. Because the layers are so thin, there is little loss in edge definition.<sup>2</sup>

The patterned SAMs can be used in wet etching or as templates for the deposition of other materials or controlled wetting and dewetting. However SAMs can not withstand conventional reactive ion etching.<sup>2</sup>  $\mu$ CP can replicate accurately on length scales down to  $\sim 35$  nm.<sup>4,25,26,27</sup> The success of  $\mu$ CP relies on conformal contact between the stamp and the substrate to be patterned, for which the use of an elastomeric stamp has suitable mechanical properties.<sup>3</sup> On large areas, contact between mold and substrate has to be guaranteed. Also the defect rate in the self-assembly of the monolayer affects the reliability of the process. Although the defect density is relatively low, it is still too high for the requirements for fabrication of high-resolution microelectronic devices.<sup>2</sup>

Formation of microstructures on non-planar surfaces has also been demonstrated by  $\mu$ CP. The flexibility of the stamp allows the patterning of curved surfaces, which is impossible with photolithography.<sup>2,28,29</sup> In a number of areas of optics and optoelectronics patterning of curved areas is especially useful, as well as for the fabrication of certain micromechanical components.<sup>2</sup> A patterned curved surface can also be used as the initial step to fabricate complex, three-dimensional microstructures.<sup>30,31</sup>



**figure 3** Example of soft lithography on the nanometer scale: replica molding of a pattern having a minimum feature size of 2 nm. The AFM image shows a pattern of concentric circles and pyramids of a) poly(methyl methacrylate) (PMMA), b) a PDMS stamp replicated against the PMMA, and c) a poly(urethane) structure prepared by replica molding on the PDMS stamp. Reproduced from reference 37 (permission American Chemical Society).

A technique, which is conceptually similar to  $\mu$ CP to pattern gold layers in well-defined three dimensional constructs is nanotransfer printing (nTP).<sup>32,33,34</sup> The difference is that in the case of nTP a solid layer (e.g. gold) is deposited on the elastomeric stamp, and transferred on a substrate that is coated with a SAM (e.g. a thiol).

In replica molding (REM) a prepolymer is spread on an elastomeric mold and cured. The mold is peeled off and a polymeric replica is the final product.<sup>35,36</sup> The advantage of the use of an elastomeric opposed to a rigid mold is the low surface tension and elasticity of the mold, which facilitate the release.<sup>2</sup> Furthermore the original master, used to prepare the PDMS mold, is preserved for a longer time.<sup>4</sup> Replica molding was demonstrated mostly with the use of poly(urethane) on a PDMS mold. The challenge for REM in the future remains to structure a wider range of functional materials, e.g. electrical or optical materials.<sup>4</sup> A minimum feature size of 2 nm has recently been demonstrated (see Figure 3).<sup>37</sup>

In microtransfer molding ( $\mu$ TM) the PDMS mold is coated with a prepolymer, where the excess of prepolymer is removed from the surface. The mold is then pressed against a substrate and cured.  $\mu$ TM can be used to fabricate multiple layer constructs, since it is able to pattern nonplanar surfaces.<sup>38</sup> A disadvantage of  $\mu$ TM is that a very thin residual layer can be formed on the substrate in between the molded features, complicating etching of the underlying substrate.<sup>2</sup>

Micromolding in capillaries (MIMIC) does not have this disadvantage. In MIMIC the PDMS mold is first pressed on the substrate, where capillary force is then exploited to fill the thus created channel structure with a prepolymer.<sup>39</sup> The prepolymer is subsequently cured and the mold removed. The channels on the mold have to be interconnected, which limits the choice of geometries using MIMIC. Another disadvantage of MIMIC is that the rate of filling depends on the geometry of the channel structure and becomes increasingly slow for longer and wider structure. The interfacial properties of the prepolymer liquid can slow down the filling process as well.<sup>2</sup> Another method that makes use of capillary force is capillary force lithography (CFL), where a PDMS mold is placed on a thin polymer layer that is subsequently heated. Once capillary force has allowed the polymer to fill up the mold, cooling down fixes the structure.<sup>40,41,42</sup>

Solvent assisted micromolding (SAMIM) creates a microstructure in polymeric substrates by pressing a PDMS mold, wetted with a good solvent, onto the substrate. The solvent swells or dissolves a thin layer of polymer that conforms to the mold. The mold remains in contact with the substrate while the solvent evaporates. Removal of the mold leaves a complementary relief structure on the polymer.<sup>43</sup> The choice of solvent is not trivial

for the effectiveness of SAMIM since it should wet the mold and have a high evaporation rate, but at the same time should not swell the mold or affect the conformal contact between mold and substrate. The minimum feature size achieved with SAMIM is 60 nm.<sup>43</sup>

In all soft lithographic techniques, the use of an elastomer as a mold has the advantage that the mold can be deformed mechanically, herewith adjusting the shape of the microstructures and expanding the possibilities considering the replicated patterns.<sup>4,44</sup> Moreover the dependence on the absence of dust particles is less restricted, since contaminations will be swallowed up in the PDMS precursor and therefore not influence the soft lithography process. Hence it is not necessary to perform the replica molding of PDMS in a clean room.<sup>2</sup> The ‘soft’ mechanical properties of elastomers on the other hand have the disadvantage of deformation during the replication process. Possible errors include pairing of features (collapse due to e.g. capillary force), sagging of the mold (contact between substrate and lower part of the mold as a result of the exerted pressure) and shrinking in between different cycles.<sup>2,45</sup> Improvement of the mechanical properties of the mold can be achieved by using an other mold material or composite stamps.<sup>46,47,48</sup>

## 1.5 micro molding against a rigid mold

Products fabricated by micro molding against a rigid master have already found widespread application, and can be found in every household as compact discs, digital video discs, and holographic images on bank passes.<sup>1,4</sup> The fabrication of CDs succeeds via a combination of injection molding and embossing.<sup>15</sup> Both of these techniques are based on thermoplastic deformation of a polymer. Micro molding methods, which make use of a rigid mold, are illustrated in Figure 4.

The first example of micro molding against a rigid mold is the basis of soft lithography, namely curing of an elastomer while in contact with a mold. Frequently PDMS is the elastomer of choice. Apart from the use as a stamp or mold, patterned elastomers also find use for example as microfluidic or optical devices. Microstructured elastomers have mechanical properties that are favorable for direct use e.g. as mechanical microfluidic parts.<sup>10</sup>

In hot embossing a microstructured mold is pressed with high force into a polymer film, which is heated above its glass transition temperature. The mold fills with polymer, which is then cooled down below the  $T_g$  and released from the mold.<sup>3,9,15</sup> Hot embossing is

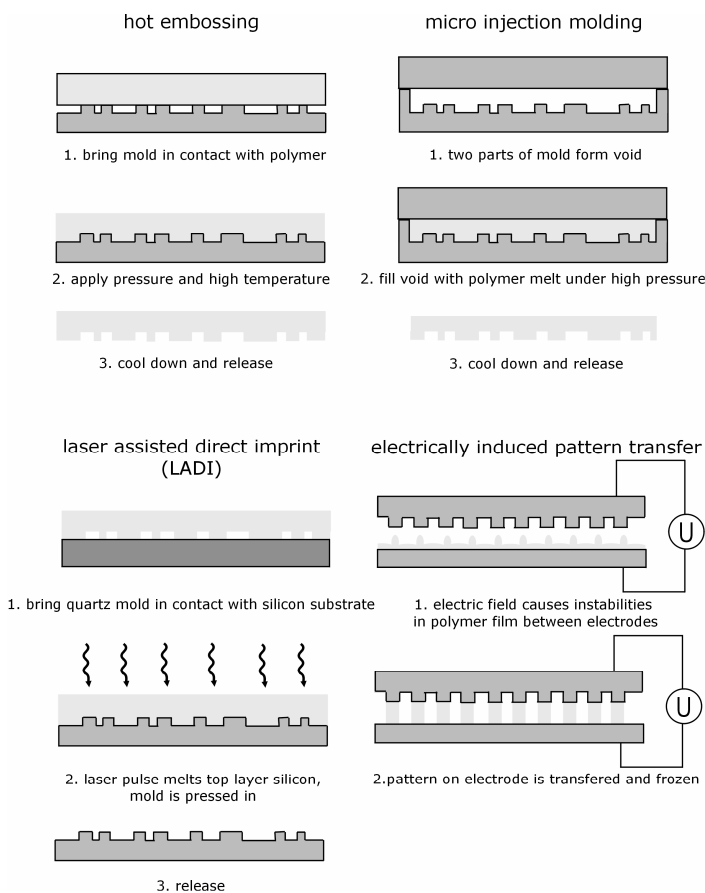
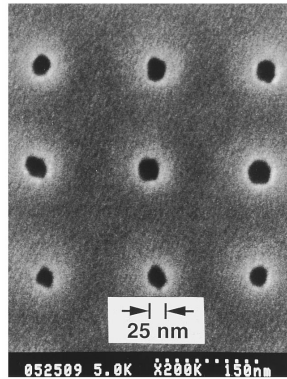


figure 4 Schematic representation of micro molding methods that make use of a rigid master or mold, namely hot embossing (or nano-imprint lithography), micro injection molding, laser assisted direct imprint (LADI) and electrically induced pattern transfer.

applicable on a rather large range of polymers, however a prerequisite is thermoplastic behavior. Popular materials are especially poly(methyl methacrylate) and poly(carbonate).<sup>9</sup>

Typical molding temperatures are in the order of 50-150°C, depending on the thermal transitions of the involved polymer, while the pressures that are used are on the order of 0.5-2 kN/cm<sup>2</sup>. The temperature and pressure may be modified by addition of plasticizers in the polymer to give access to modification of a broader range of polymers by hot embossing.<sup>49</sup> However, this way the properties of the polymer product are also affected. The



**figure 5** *Example of nano-imprint of a pattern having a minimum feature size of 25 nm. The SEM image displays a pattern of dots imprinted in poly(methyl methacrylate). Reproduced from reference 54 (permission American Institute of Physics).*

temperature difference in an embossing cycle should be 25 to 40 °C, in order to minimize thermally induced stress in the material.<sup>50</sup> The time that a cycle requires is typically 3-10 minutes, but may even go up to 30 minutes.<sup>9</sup> Hot embossing is performed under vacuum, since entrapment of air in the mold would hinder the replication.

The high pressure that is exerted on the mold during the hot embossing process makes a very high mechanical strength of the mold absolutely necessary. Silicon molds, that are relatively easy to access, are less suitable for long-term hot embossing processes due to their brittle nature.<sup>15</sup> Metals or metal alloys are therefore more suitable materials for the fabrication of molds.<sup>15</sup>

Most problems in hot embossing however are not present during the molding, but during the release of the structure from the mold. These problems can cause rupture or deformation of the microstructures.<sup>9</sup> Especially microstructures with a high aspect ratio suffer from release problems. Therefore generally aspect ratios are limited, depending on parameters like material, dimensions and position on the mold.<sup>15</sup> Contraction of the polymer during the cooling step seems to complicate the demolding process. Release problems can be reduced when the mold has slightly inclined sidewalls.<sup>15,51</sup> Silicon has the common problem of potential stiction with many polymers.<sup>9</sup> The use of anti-adhesive coatings on the mold improves the release of the replica from the mold.<sup>51</sup> Nevertheless there is a risk of interaction

between the coating and the polymer, thus influencing the surface chemistry of the molded product.<sup>52</sup> Choice of a completely different mold material, which intrinsically possesses an anti-adhesive behavior, solves this problem.<sup>53</sup> Distortions in the embossed product can also originate from the thermal cycling.<sup>4,50</sup>

In nanoimprint the embossing process is executed on a nanometer scale.<sup>4,54,55,56,57</sup> The nanoimprint process was proven successful even for lateral dimensions as small as 25 nm (see Figure 5).<sup>54,55,57</sup>

Micro injection molding is a replication method that is also based on thermal deformation. Here a polymer melt is injected at high pressures into the cavity formed by a microstructured mold. Temperatures of the melt are generally between 150 and 400 °C. Volume changes and thermal shrinkage therefore have to be taken into account in the design of the mold. A cycle requires 1-3 minutes.<sup>9</sup> The fast cycle times make that in almost all cases industrial series production is based on injection molding.<sup>15</sup>

Replication of a structure smaller than 100 nm in dimensions was also demonstrated by electrically induced pattern transfer, in which a patterned electrode in proximity of a polymer film causes structure formation. The replication process works well, which is interesting from a phenomenological point of view, although replication is currently demonstrated on a small area, and the technique is not yet suitable as a replication method for commercial purposes.<sup>58</sup>

A micro molding method on silicon was demonstrated using laser-assisted direct imprint (LADI). A patterned quartz mold is pressed on the silicon. A single excimer laser pulse through the mask melts the top layer of the silicon, while the mold is pressed into the melt. Once the silicon is solidified and the mold removed, a silicon microstructure has been fabricated. The embossing time is less than 250 ns. Minimum feature sizes are presently 140 nm, but expected to decrease into the nanometer range.<sup>6,59</sup>

## 1.6 conclusions

Although photolithography is still the driving force behind the fabrication of microelectronics, the versatile spectrum of micro molding methods can provide a useful alternative. Micro molding methods offer a very broad range of materials and are inexpensive, which make them advantageous in particular for use in integrated optics, microfluidics and biomedics. Moreover, the use of optics in photolithography is believed to

be an unbridgeable limitation for fabrication of features with nanometer dimensions. Micro molding methods do not have a fundamental boundary for patterning in the nanometer range. Using soft lithography a minimum feature size as small as 2 nm is reported, while nanoimprint lithography has yielded a pattern with a minimal dimension of 25 nm. An additional merit of soft lithography is the use of a flexible mold, which facilitates the patterning of non-planar surfaces.

Micro molding methods can therefore be considered complementary to the presently dominating microfabrication method, photolithography. The expansion of the range of materials, necessary to further broaden the scope of microfabrication towards new applications, the low costs, and the absence of a fundamental limitation of the resolution promise an ongoing development and growth of micro molding methods.

## references

- <sup>1</sup> M. J. Madou, *Fundamentals of Microfabrication*, CRC Press, Boca Raton, U.S. **2002**.
- <sup>2</sup> Y. Xia and G. M. Whitesides, *Angew. Chem. Int. Ed.* **1998**, *37*, 550.
- <sup>3</sup> M. Geisler and Y. Xia, *Adv. Mater.* **2004**, *16*, 1249.
- <sup>4</sup> Y. Xia, J. A. Rogers, K. E. Paul, G. M. Whitesides, *Chem Rev.* **1999**, *99*, 1823.
- <sup>5</sup> A. N. Broers, W. W. Molzen, J. J. Cuomo, N. D. Wittels, *Appl. Phys. Lett.* **1976**, *9*, 596.
- <sup>6</sup> R. F. Pease, *Nature* **2002**, *417*, 802.
- <sup>7</sup> G. E. Moore, *Electronics* **1965**, *38*.
- <sup>8</sup> D. Qin, Y. Xia, J. A. Rogers, R. J. Jackman, X. M. Zhao, G. M. Whitesides, *Top. Cur. Chem.* **1998**, *194*, 1.
- <sup>9</sup> H. Becker, C. Gartner, *Electrophoresis* **2000**, *21*, 12.
- <sup>10</sup> S. R. Quake and A. Scherer, *Science* **2000**, *290*, 1536.
- <sup>11</sup> G. M. Whitesides, E. Ostoni, S. Takayama, X. Y. Jiang, D. E. Ingber, *Ann. Rev. Biom. Eng.* **2001**, *3*, 335.
- <sup>12</sup> T. H. Park, M. L. Shuler, *Biotechnol. Prog.* **2003**, *19*, 243.
- <sup>13</sup> Y. Xia, G. M. Whitesides, *Annu. Rev. Mater. Sci.* **1998**, *28*, 153.
- <sup>14</sup> B. D. Gates, Q. Xu, C. Love, D. B. Wolfe, G. M. Whitesides, *Annu. Rev. Mater. Res.* **2004**, *34*, 339.
- <sup>15</sup> M. Hecke and W. K. Schomburg, *J. Micromech. Microeng.* **2004**, *14*, R1.
- <sup>16</sup> J. A. Rogers, R. G. Nuzzo, *Materials Today* **2005**, *8*, 50.
- <sup>17</sup> Y. Xia, *Adv. Mater.* **2004**, *16*, 1245.
- <sup>18</sup> A. Kumar, G. M. Whitesides, *Appl. Phys. Lett.* **1993**, *63*, 2002.
- <sup>19</sup> Y. Xia, D. Qin, G. M. Whitesides, *Adv. Mater.* **1996**, *8*, 1015.
- <sup>20</sup> A. Kumar, H. A. Biebuyck, G. M. Whitesides, *Langmuir* **1994**, *10*, 1498.
- <sup>21</sup> X. M. Yang, D. A. Tryk, K. Hasimoto, A. Fujishima, *Appl. Phys. Lett.* **1996**, *69*, 4020.
- <sup>22</sup> Y. Xia, E. Kim, G. M. Whitesides, *J. Electrochem. Soc.* **1996**, *143*, 1070.
- <sup>23</sup> N.L. Jeon, K. Finnie, K. Branshaw, R. G. Nuzzo, *Langmuir* **1997**, *13*, 3382.
- <sup>24</sup> Y. Xia, M. Mrksich, E. Kim, G. M. Whitesides, *J. Am. Chem. Soc.* **1995**, *117*, 9576.
- <sup>25</sup> B. Michel, A. Bernard, A. Bietsch, E. Delamarche, M. Geissler, D. Juncker, H. Kind, J. P. Renault, H. Rothuizen, H. Schmid, P. Schmidt-Winkel, R. Stutz, H. Wolf, *IBM J. Res. Dev.* **2001**, *45*, 697.
- <sup>26</sup> H. A. Biebeck, N. B. Larsen, E. Delamarche, B. Michel, *IBM J. Res. Dev.* **1997**, *41*, 159.
- <sup>27</sup> H. W. Li, B. V. O. Muir, G. Fichet, W. T. S. Huck, *Langmuir* **2003**, *19*, 1963.
- <sup>28</sup> W. R. Childs, R. G. Nuzzo, *Adv. Mater.* **2004**, *16*, 1323.
- <sup>29</sup> K. E. Paul, M. Prentiss, G. M. Whitesides, *Adv. Func. Mater.* **2003**, *13*, 259.
- <sup>30</sup> R. J. Jackman, S. T. Brittain, A. A. Adams, M. G. Prentiss, G. M. Whitesides, *Science* **1998**, *280*, 2089.
- <sup>31</sup> S. T. Brittain, O. J. A. Schueller, H. Wu, S. Whitesides, G. M. Whitesides, *J. Phys. Chem. B* **2001**, *105*, 347.
- <sup>32</sup> S. Jeon, E. Menard, J. U. Park, J. Maria, M. Meitl, J. Zaumseil, J. A. Rogers, *Adv. Mater.* **2004**, *16*, 1369.
- <sup>33</sup> E. Menard, L. Bilhaut, J. Zaumseil, J. A. Rogers, *Langmuir* **2004**, *20*, 6871.

## chapter 1

- <sup>34</sup> J. Zaumseil, M. A. Meitl, J. W. P. Hsu, B. R. Acharya, K. W. Baldwin, Y. L. Loo, J. A. Rogers, *Nano Lett.* **2003**, *3*, 1223.
- <sup>35</sup> Y. Xia, J. J. McClelland, R. Gupta, D. Qin, X. M. Zhao, L. L. Sohn, R. J. Celotta, G. M. Whitesides, *Adv. Mater.* **1997**, *9*, 147.
- <sup>36</sup> Y. Xia, E. Kim, X. M. Zhao, J. A. Rogers, M. Prentiss, G. M. Whitesides, *Science* **1996**, *273*, 347.
- <sup>37</sup> B. D. Gates and G. M. Whitesides, *J. Am. Chem. Soc.* **2003**, *125*, 14986.
- <sup>38</sup> X. M. Zhao, Y. Xia, G. M. Whitesides, *Adv. Mater.* **1996**, *8*, 837..
- <sup>39</sup> E. Kim, Y. Xia, G. M. Whitesides, *Nature* **1995**, *376*, 581.
- <sup>40</sup> K. Y. Suh, Y. S. Kim, H. H. Lee, *Adv. Mater.* **2001**, *13*, 1386
- <sup>41</sup> K. Y. Suh, H. H. Lee, *Adv. Funct. Mater.* **2002**, *12*, 405.
- <sup>42</sup> C. M. Bruinink, M. Peter, M. de Boer, L. Kuipers, J. Huskens, D. N. Reinhoudt, *Adv. Mater.* **2004**, *16*, 1086.
- <sup>43</sup> E. Kim, Y. Xia, X. M. Zhao, G. M. Whitesides, *Adv. Mater.* **1997**, *9*, 651.
- <sup>44</sup> Y. Xia, G. M. Whitesides, *Langmuir* **1997**, *13*, 2059.
- <sup>45</sup> E. Delamarque, H. Schmid, B. Michel, H. Biebuyck, *Adv. Mater.* **1997**, *9*, 741.
- <sup>46</sup> J. P. Rolland, E. C. Hagberg, G. M. Denison, K. R. Carter, J. M. de Simone, *Angew. Chem. Int. Ed.* **2004**, *43*, 5796.
- <sup>47</sup> P. J. Yoo, S. J. Choi, J. H. Kim, D. Suh, S. J. Baek, T. W. Kim, H. H. Lee, *Chem. Mater.* **2004**, *16*, 5000.
- <sup>48</sup> T. W. Odom, J. C. Love, D. B. Wolfe, K. E. Paul, G. M. Whitesides, *Langmuir* **2002**, *18*, 5314.
- <sup>49</sup> L. Tan, Y. P. Kong, S. W. Pang, A. F. Yee, *J. Vac. Sci. Technol. B* **2004**, *22*, 2486.
- <sup>50</sup> Y. J. Juang, L. J. Lee, K. W. Koelling, *Polym. Eng. Sci.* **2002**, *42*, 539
- <sup>51</sup> H. Becker, U. Heim, *Sensor. and Actuat. A-Phys.* **2000**, *83*, 130.
- <sup>52</sup> R. W. Jaszewski, H. Schiff, B. Schnyder, A. Schneuwly, P. Gröning, *Appl. Surf. Sci.* **1999**, *143*, 301.
- <sup>53</sup> M. M. Alkaisi, R. J. Blaikie, S. J. McNab, *Microelectr. Eng.* **2001**, *57-58*, 367.
- <sup>54</sup> S. Y. Chou, P. R. Krauss, P. J. Renstrom, *Appl. Phys. Lett.* **1995**, *67*, 3114.
- <sup>55</sup> S. Y. Chou, P. R. Kraus, P. J. Renstrom, *J. Vac. Sci. Technol. B* **1996**, *14*, 4129.
- <sup>56</sup> H. Schiff, R. W. Jaszewski, C. David, J. Gobrecht, *Microelectronic Eng.* **1999**, *46*, 121.
- <sup>57</sup> H. Schiff, C. David, M. Gabriel, J. Gobrecht, L. J. Heyderman, W. Kaiser, S. Köppel, L. Scandella, *Microelectronic Eng.* **2000**, *53*, 171.
- <sup>58</sup> E. Schaeffer, T. Thurn-Albrecht, T. P. Russell, U. Steiner, *Nature* **2000**, *403*, 874.
- <sup>59</sup> S. Y. Chou, C. Keimel, J. Gu, *Nature* **2002**, *417*, 835.





## chapter 2 phase separation micro molding:

### a new, generic approach towards microstructuring a wide range of materials

*L. Vogelaar*

*R. G. H. Lammertink*

*J. N. Barsema*

*W. Nijdam*

*L. A. M. Bolhuis-Versteeg*

*C. J. M. van Rijn*

*M. Wessling*

Phase Separation Micro Molding (PS $\mu$ M) is a versatile microfabrication technique, capable to structure a very broad range of polymers, including block copolymers, biodegradable and conductive polymers without the need for cleanroom facilities. By incorporating a subsequent process step, carbon, ceramic, and metallic microstructures can also be fabricated from a polymeric or hybrid precursor. The replication process is straightforward and cost effective. It relies on phase separation of a polymer solution while in contact with a structured mold. Intrinsic shrinkage during the phase separation facilitates the release of the replica from the mold, which increases the reliability of the process even at small feature sizes, thin polymer films, or high aspect ratio structures. Under suitable circumstances perforation of the polymer film can be obtained, resulting in completely open ‘through’ microstructures. Furthermore, porosity can be introduced in a microstructure, which may result in unknown functionalities.

*Parts of this chapter have been published previously in Small and Advanced Materials.<sup>1,2</sup>*

*Above: Microstructure prepared by Phase Separation Micro Molding*

## 2.1 introduction

Microfabrication is best known as the driving force behind the increased performance in microelectronics. The ongoing quest in semiconductor industry to evermore increase the amount of electrical components on a chip has created a fascinating field of techniques to microfabrication and nanofabrication is still expanding.<sup>3</sup> In the last decades the opportunities of integration and miniaturization have been noticed in a large range of other disciplines as well. Numerous applications varying from lab on a chip<sup>4</sup>, biomedical scaffolds<sup>5</sup>, integrated optics and photonics<sup>6</sup>, and novel sensors<sup>7</sup> all find their origin in microfabrication. New applications set new demands on the material and surface properties of the microstructure. A biomedical application may require biocompatibility or biodegradability.<sup>8</sup> Microfluidic applications may need certain solvent resistance or surface characteristics.<sup>9</sup> However, not every material is accessible for microfabrication due to the limitations set by the corresponding microfabrication processes. The classical combination of photolithography and subsequent etching still dominates microfabrication. Although this combination succeeds well in realizing highly complicated architectures on the micrometer scale, it offers a limited freedom of choice in materials, in which silicon or silicon based glasses make up the larger part. Silicon is an excellent choice in microelectronics, but it is not obvious why it should be used in most of the other present or prospective applications. Ideally the choice of a material is based only on the material properties necessary for the application, without limitations evoked by the fabrication method.<sup>10</sup>

Replication methods, like hot embossing or soft lithography, have significantly expanded the range of materials, by addressing polymers.<sup>11,12,13,14</sup> Replication of a mold or stamp to define a microstructure can offer great benefits compared to conventional lithography. The replicas are in general more cost effective<sup>12</sup> and there is no fundamental limitation considering the minimum feature size.<sup>11,15</sup>

Unfortunately, even with the large extension of the range of materials, offered by micromolding, the material to be used in microfabrication cannot be chosen completely arbitrarily. Only polymers that can be processed well from the melt are applicable for hot embossing, while soft lithography uses primarily elastomers, like PDMS. Therefore not all polymers can be processed easily by these replication methods. Besides, there is also not yet an easy solution for the microfabrication of certain ceramics.<sup>16,17</sup> Phase separation micro molding (PS $\mu$ M) is a replication technology based on phase separation of a polymer solution, a process used mostly in the fabrication of synthetic membranes, for instance hemodialysis

and blood oxygenation membranes, ultrafiltration membranes, molecular gas separation and desalination membranes.<sup>18,19</sup> This process covers a very broad spectrum of polymers, most of which were not applicable in microfabrication before. In Phase Separation Micro Molding (PS $\mu$ M), phase separation is combined with replication of structures on a micro- to submicrometer scale. In this way a novel microfabrication technique is created, which significantly expands the range of available materials.<sup>1,2</sup>

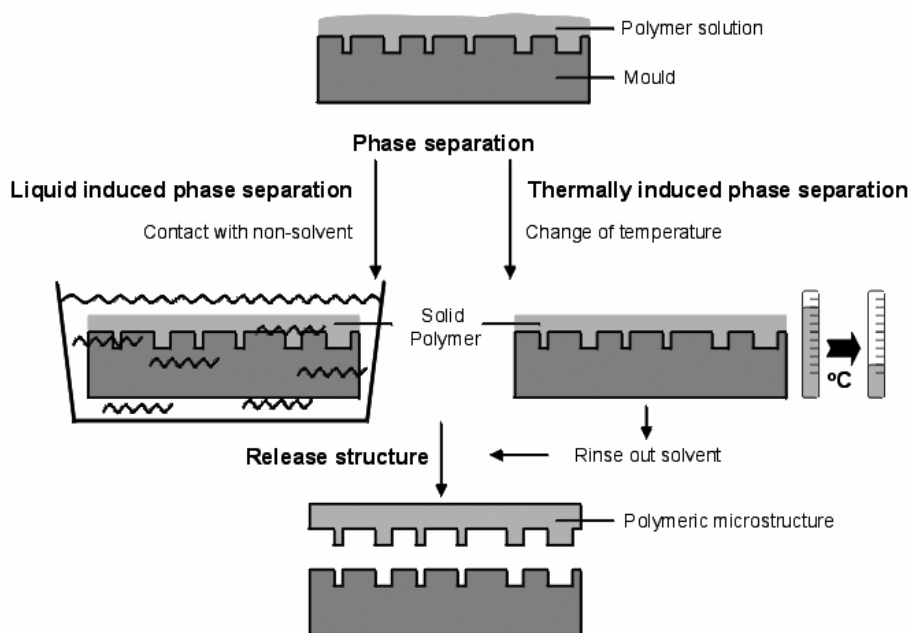
Even though phase separation has never been brought into the arena of microfabrication, we find it has some key features that complement the existing spectrum of microfabrication techniques well. Phase separation micromolding (PS $\mu$ M) not only extends the range of materials, but also offers the possibility to introduce porosity, which can lead to new functionalities, and provides a very reliable means of replication. PS $\mu$ M therefore opens avenues to large-scale microfabrication from an extremely broad range of materials, under easy and cost-effective process conditions.

In this chapter, first a background is provided in phase separation of polymer solutions and how this can be incorporated in phase separation micro molding. Some interesting characteristics of the PS $\mu$ M process will be discussed. Subsequently the fabrication process of microstructures using a large range of polymers is illustrated, including amorphous as well as crystalline polymers, block copolymers, polymers for biomedical applications and a conductive polymer. Also the fabrication of a carbon, ceramic and metallic microstructure is demonstrated.

## 2.2 phase separation micro molding process

A schematic representation of the PS $\mu$ M process is given in Figure 1. In PS $\mu$ M a polymer solution is applied on a mold, having a micrometer-sized relief structure on the surface. The application of the solution on the mold is performed normally by casting. When the thickness of the layer of polymer solution is a critical parameter, a set-up was used in which the height of the casting knife can be adjusted by micrometer positioners, ensuring accuracy of the film thickness. The polymer solution is solidified by phase separation and during the solidification assimilates the profile on the mold.

Phase separation is utilized for decades for the fabrication of synthetic membranes.<sup>18,19</sup> There are different means to induce the phase separation of a polymer



**figure 1** Schematic representation of the Phase Separation Micro Molding process. On a mold, having a micrometer sized relief profile on the surface, a layer of polymer solution is applied. The polymer solution is solidified by either thermally induced (change of temperature of the solution) or liquid induced phase separation (immersion in a non-solvent). During the solidification the polymer assimilates the profile on the mold. The polymer microstructure is easily released from the mold.

solution into a solid polymer and a solvent. Phase separation micro molding has been performed by way of thermally induced phase separation, and more frequently by liquid induced phase separation. In phase separation the thermodynamic equilibrium of a polymer solution is disturbed. When passing the thermodynamic phase boundary (in temperature or composition), the polymer will no longer be soluble in the film of solution, causing the solution to phase separate in a polymer-rich and a polymer-lean part. The polymer-rich part solidifies and assimilates the relief profile on the mold. Subsequently the microstructured polymer film is released from the mold.

Depending on the composition of the solution and the non-solvent, the resulting polymer film may exhibit an intrinsic porosity after the phase separation. Phase separation on a mold can therefore result in porosity within a microstructured polymer product. Figure 2b depicts such a porous microstructure. Although at first sight porosity may seem useless and may even seem unwanted, these previously unavailable morphologies will lead to new functionalities of the polymer microstructure. For instance the inner surface created by the porosity can serve adsorptive or catalytic purposes, which are yet unknown functionalities in microfabrication. For a typical biomedical application such as tissue engineering scaffolds, porosity in a microstructure might offer a solution for problems related to the required transport of nutrients or growth of cells through the scaffold. Microstructuring a porous scaffold of a biodegradable material can positively influence the growth direction of the cells, optimizing the properties of the tissue.<sup>20</sup> The microstructure maintains the preferential growth of the cells while the porosity facilitates transport through the scaffold. For a non-porous scaffold material the transport of oxygen and nutrients is hindered and the cells within the deeper inner part of the scaffold are smothered.<sup>21</sup> The preparation of a porous scaffold for tissue engineering purposes is the topic of chapter 5.

In thermally induced phase separation the distortion of the equilibrium of the solution is caused by a change in temperature. The temperature of the solution is changed from a temperature at which the solvent is a good solvent for the polymer, to a temperature at which the solvent is poor. The composition of the polymer solution, the temperature, and the cooling rate determine the porosity of the resulting material.<sup>22</sup> Most of the structures discussed in this paper have however been made by liquid induced phase separation. In liquid induced phase separation a polymer solution demixes in the presence of a non-solvent (for which preferably water is chosen). The non-solvent is miscible with the solvent of the polymer solution, causing a diffusion driven exchange of solvent and non-solvent in the polymer film. The scheme in Figure 2a represents a phase diagram illustrating the liquid

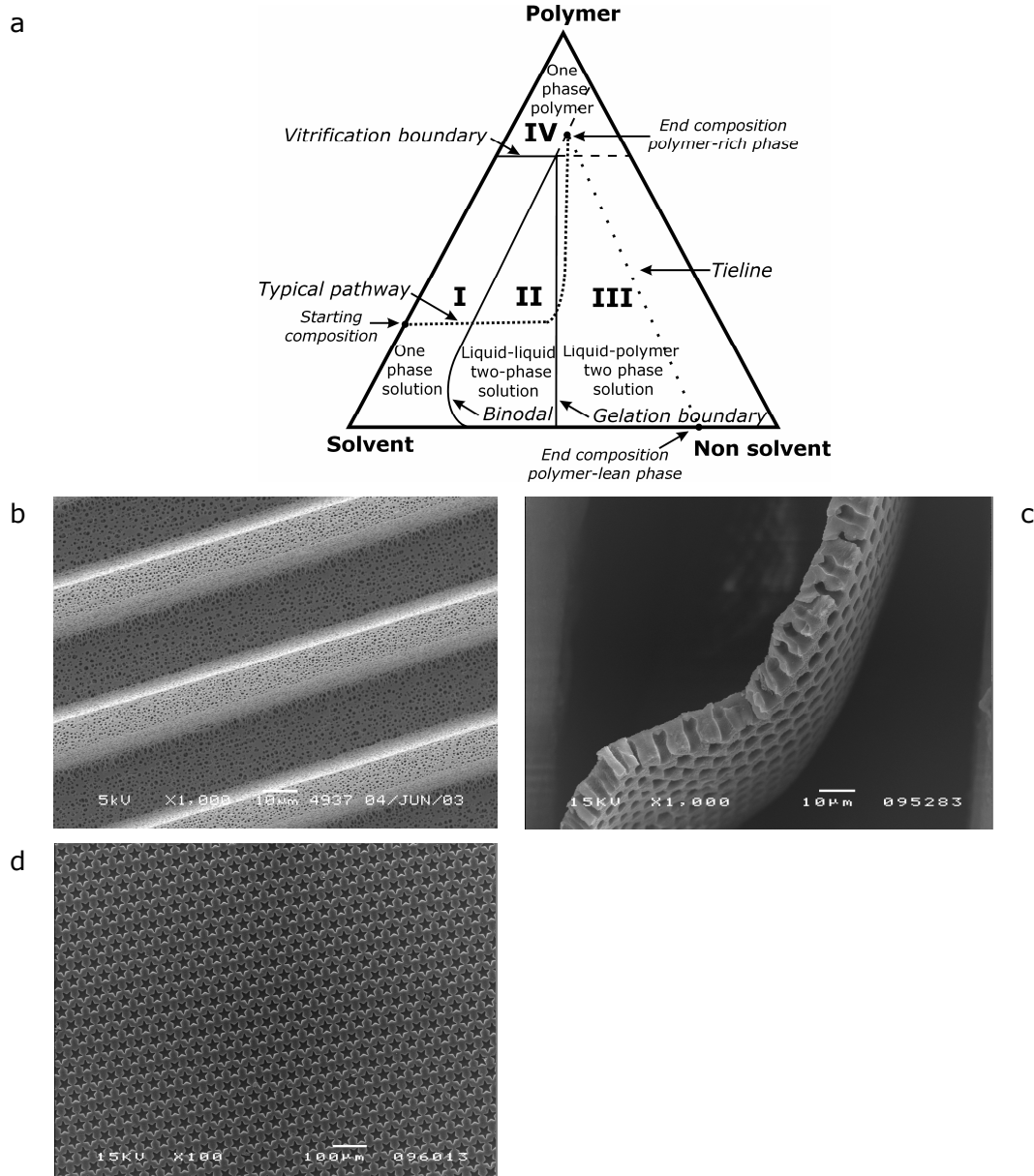


figure 2a Schematic ternary phase diagram and a typical pathway of a solution of an amorphous polymer subjected to liquid induced phase separation [13,8]. The three axes represent the concentrations of polymer, solvent and non-solvent in the system. Solutions in region I are homogeneous liquids. After crossing the binodal boundary, in region II two liquid phases coexist in the solution, one being rich in polymer, the other one consisting of merely solvent and non-solvent. In region III the solution separates in a liquid polymer lean phase and a glassy polymer rich phase. In the vitrification area IV the polymer solidifies. The dotted line starting on the solvent-polymer axis represents a typical pathway of a solution in liquid induced phase separation. In the endpoint, on the binodal boundary, the solution reaches its final configuration. The solution is split in a liquid polymer lean phase and a glassy, solid polymer rich phase, represented by the end points of the tieline.

**b** *Porous microstructure. The microstructure was prepared from a polyetherimide/ polyvinyl- pyrrolidone solution. The presence of the PVP in the solution causes a homogeneous, interconnected pore network throughout the microstructure.*

**c** *Cross section of dense microstructure, comprising circular imprints, made of polyvinylidene fluoride (PVDF). The phase separation was realized in two subsequent steps: first an exposure to water vapour, then an immersion in water. Both the inner part and the surface of the microstructure are completely dense.*

**d** *Microstructure of stars, pattern made from polyethersulfone (PES). The film was exposed to a flow of nitrogen, almost saturated with water vapour. Subsequently the film was immersed in water. The inner structure is porous although the surface is completely dense. The high uniformity of the pattern extends over areas of centimetres squared, without any defects, while the corners of the stars show sharp edge definition.*

induced phase separation process in a ternary system consisting of polymer, solvent and non-solvent.<sup>18,23</sup> As soon as the composition has passed the binodal boundary, the polymer solution becomes unstable and phase separates in polymer-rich and polymer-lean regions. In a polymer film prepared by liquid induced phase separation, the pores stem from the polymer-lean phase, whereas the solid polymer is formed from the polymer-rich phase. When an appropriate composition of the polymer solution is used, the solid polymer regions will be continuous and the phase separation yields a solid polymer film. It is well known from the field of membrane technology under which conditions phase separation will be successful. PS $\mu$ M can therefore benefit from all the preparative details, tips and tricks from the kitchen of membrane preparation.<sup>18,19</sup>

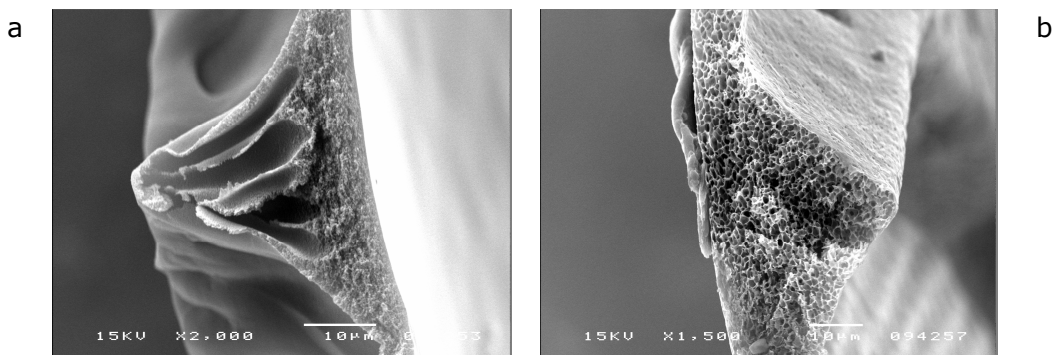
The pore morphology can vary in between a very open, sponge-like configuration with an interconnected pore network (like the microstructure depicted in Figure 2b), a few isolated pores surrounded by polymer and even a completely dense configuration, yielding optically transparent polymer films (like the microstructure depicted in Figure 2c). Whilst the inner structure of the polymer product can be porous, the surface may still be dense. As can be seen, the microstructure, which is depicted in Figure 2d, does not exhibit any pores at the surface. However the inner part of this microstructure is porous. The porosity of both the surface and the inner structure is completely determined by the conditions under which the phase separation takes place, e.g. the composition of the polymer solution and the non-solvent. The porosity can therefore be tailored by choosing the right composition of the solution and non-solvent. As a rule of thumb a higher polymer concentration and a higher molecular weight of the polymer result in a denser polymer film. The pore morphology strongly depends on the kinetics of the exchange between solvent and non-solvent as well. A

slower demixing process in general results in a denser polymer. The demixing is delayed for instance by choice of a non-solvent having low miscibility with the solvent. Also the use of either polymeric or low molecular weight additives can slow down the demixing process. Another option to influence the exchange of solvent and non-solvent is by either adding a small amount of non-solvent to the solution, or by adding solvent to the non-solvent.

During a relatively fast demixing process macrovoids can form: large fingerlike cavities below the surface of the film.<sup>18,19</sup> Although macrovoids in general do not appear at the surface, they locally disturb the mechanical properties and can therefore lead to defects in the microstructure on the surface of the polymer film. Macrovoids in a microstructured polymer are depicted in Figure 3a. Formation of macrovoids can be prevented by adaptation of the recipes, for example by including certain additives in the solution. Another method that may prevent the formation of macrovoids is to precede the liquid induced phase separation by a vapor induced phase separation.<sup>24,25,26,27</sup> The polymer solution on the mold is first exposed to an environment of nitrogen, saturated with non-solvent vapor. The non-solvent vapor dissolves into the polymer solution, causing the phase separation to set in as can be seen from the turbidity of the film. The non-volatile solvent, however, remains in the solution. Subsequently the mold and the polymer film are immersed in a non-solvent bath, which extracts the remaining solvent from the film and finalizes the phase separation. When the liquid induced phase separation is combined with such a vapor step, we observe a homogeneous pore distribution, reduced skin formation, and absence of macrovoids. A typical example of preventing macrovoid formation by an additional vapor step is given in Figure 3b.

Inclusion of additives provides additional control over the intrinsic porosity of the microstructure. An example of an additive, which is used to yield a product with a uniform, interconnected pore network, is the water-soluble polymer polyvinylpyrrolidone.<sup>28</sup> Above a certain minimum concentration and molecular weight the presence of the polyvinylpyrrolidone will increase the amount of coagulation nuclei and thus suppress the macrovoid formation.





**figure 3a** *Cross-section of a polymeric microstructure exhibiting macrovoid formation. The microstructure in this figure was prepared from a solution of polyimide in NMP; the phase separation was performed in water.*

**b** *Similar structure, on the same mold and from the same recipe, when a non-solvent vapor step is included prior to the immersion in the non-solvent. The film of polymer solution is exposed to a saturated vapor until the film is completely turbid. The film exhibits a homogeneous pore distribution and macrovoids have not been formed.*

## 2.3 effect of shrinkage

A particular advantage of PS $\mu$ M over the existing micromolding techniques is the remarkable ease by which a structure can be released from the mold. In many cases the polymer microstructure comes off the mold without or with hardly any external force applied, and detaches spontaneously in the non-solvent bath. The time span between immersion and spontaneous release requires generally only a few minutes, and in some cases even less than a minute. In other replication methods, e.g. hot embossing and soft lithography, the release from the mold is not straightforward, especially in the fabrication of high aspect ratio structures or thin films. A conformal contact between the mold and the structured material causes release problems related to sticking, breaking or other stress related deformations of the polymer structure or the mold.<sup>13,29</sup>

During the solidification the polymer layer shrinks.<sup>30</sup> We ascribe the easy release in PS $\mu$ M to the shrinkage in parallel orientation with the film, taking place during the solidification. The shrunken polymer leaves a small gap between the mold and the replica, and therefore the polymer film is already loose from the mold. For the phase separation processes described here in most of the cases we observed shrinkage up to approximately 5%

## chapter 2

in between the mold features in horizontal orientation, parallel with the mold and the film. The perpendicular shrinkage depends strongly on the process parameters, such as the composition of the polymer solution.

The easy release from each mold seems to be rather independent of the surface composition of the mold. The surfaces of the different used molds consist of silicon (with a native oxide layer), siliconoxide, siliconnitride or gold. The absence of release problems leads to a very low defect rate. Therefore, the uniformity of the microstructures prepared by PS $\mu$ M extends over areas up to several centimeters squared. The high uniformity of the microstructures is illustrated in Figure 4, showing excellent replication of a high aspect ratio structure. Also the molds do not show any damage after the replication, and thus the PS $\mu$ M process can be considered very reliable. The line pattern in Figure 5 gives an indication for the achievable minimum feature. The current minimum feature size is around 150 nm. However, this minimum feature size was restricted by the fabrication process of the mold rather than by the replication process. Therefore the boundaries of the PS $\mu$ M concerning the minimum feature size have not yet been explored fully, and the actual minimum feature size is still unknown. Looking at the nature of the phase separation process and the many possible combinations of polymer - solvent systems we anticipate the actual minimum feature size to be even smaller. The present aspect ratio, height/width, was around 5, however also the maximum aspect ratio was merely limited by the mold.

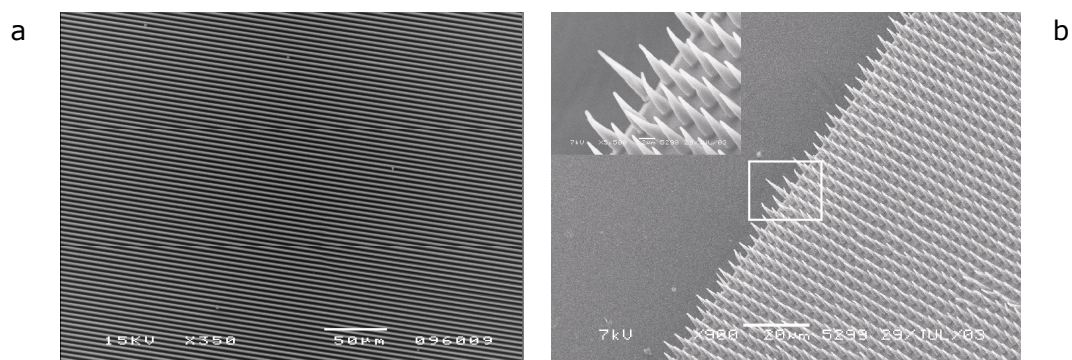
Because of the easy release conditions, the process conditions of PS $\mu$ M are very favourable to implement a continuous process. Large-scale flat sheet membrane production takes place in a continuous role-to-role apparatus. In liquid induced PS $\mu$ M there is no need for high pressures or high temperatures. Together with the easy release of the structure these favourable process conditions ensure there is no obvious bottleneck in the up scaling of the lab scale process to a continuous process. The costs of the microstructures fabricated by PS $\mu$ M are already very low in a discontinuous process, and will be even lower when continuous mass fabrication is realised.

Although the shrinkage is one of the major advantages of PS $\mu$ M concerning the absence of release problems, it has the tendency to reduce the curvature of a microstructure in phase separation processes at larger amounts of shrinkage. In these cases very sharp corners tend to round. A typical example of the reduction of curvature by excessive shrinkage is illustrated by the microstructure depicted in Figure 6a. Ultimately, this phenomenon can lead to complete absence of replication in the case of recipes with a lot of

shrinkage on relatively shallow molds. Experiments were performed on molds with shallow relief profiles, ranging from a depth of 100 nm to 800 nm (see Table 1). A recipe known to yield a relatively large amount of shrinkage, exhibited no apparent replication of the pattern on the shallowest molds. Nevertheless, by reducing the amount of shrinkage, the replication of shallow mold profiles and sharp corners is improved. A reduction of shrinkage can be achieved for example by choosing a higher polymer concentration, addition of solvent in the non-solvent or addition of a small amount of non-solvent in the solution.

Shrinkage on a micro mold also gives rise to deformations. Due to the relief structure of the mold, the film thickness varies locally. Since the relative shrinkage is uniform the absolute amount of shrinkage also varies locally. During the phase separation the film will contract towards areas with larger absolute shrinkage (the initially thicker parts). When there is a distinct transition in film thickness, the microstructures will be stretched out towards the local contraction. Also a transition in the amount of micro structured area per unit area is a risk of these deformations. As an example a microstructure, demonstrating this phenomenon is given in Figure 6b. The width of the replicas in Figure 6b is dependent on the distance between the mold features. This dependence is illustrated by the graph in Figure 6c. However the shrinkage is uniform and predictable, therefore the deformation of the structure can be taken into account during the mold design so that the resulting polymer replica has the desired shape.

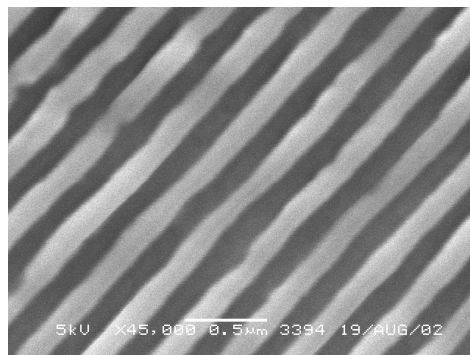
Besides to the absence of release problems, the shrinkage of the polymer upon solidification opens routes to simple fabrication of completely open microstructures. An example of an open microstructure is depicted in Figure 7. If a film of polymer solution is applied just a little higher than the mold features, the shrinkage of the film towards the mold during solidification can cause the mold features to punch through the film. The mold perforates the polymer, resulting in a completely open microstructure. The fabrication of perforated microstructures by PS $\mu$ M is discussed in more detail in chapter 4.



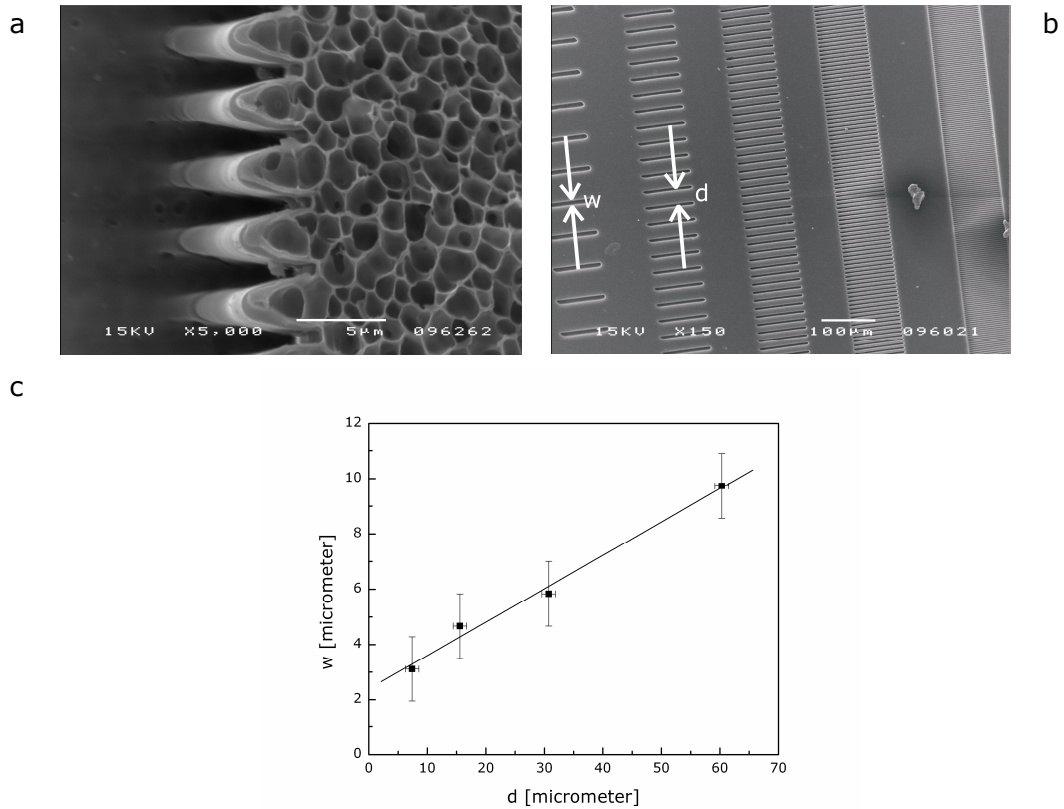
**figure 4** Microstructures illustrating the high uniformity, which is feasible with PS $\mu$ M. The uniformity extends over areas of centimeters squared.

**a** Line pattern of 5 micrometer wide lines with 10 micrometer pitch, made from polyethersulfone.

**b** High aspect ratio microstructure of pillars made from polymethylmethacrylate. The conical shape originates from the conical holes in the mold. Even though the pillars are five times higher than their average width, the structure could be released from the mold without any defects. The polymer is completely dense, and therefore optically transparent.



**figure 5** 150 nm wide lines made of polysulfone. The line pattern on the mold originates from laser interference lithography. A 50 micrometer thick film of a polysulfone solution was applied on the mold, and the phase separation was performed by subsequent immersion in water. The 150 nm line structure illustrates the possibility to fabricate a structure in the far submicron range.



**figure 6** Demonstration of possible deformations in a phase separation recipe, where the polymer displays a large extent of shrinkage.

**a** The mold consisted of a line pattern of equally spaced lines with square angles. The polymer replica of polyethersulfone rounds the corners at the top part of the replica due to the shrinkage. Clearly visible is the dense skin and the underlying porosity.

**b** Replica in polyethersulfone of a mold with a pattern of blocks, all equal in dimensions ( $2 \mu\text{m} \times 100 \mu\text{m}$ ). The spacing between the blocks is doubled every row from right to left, dividing the microstructure density by half every row, and doubling the amount of polymer in between the structures. The replica of the block pattern increases in width every row because of the larger absolute amount of shrinkage in between the blocks.

**c** The width of the replica of the block pattern is plotted as a function of the distance between the blocks.

## chapter 2

<i>Recipe</i>	<i>100 nm</i>	<i>170 nm</i>	<i>330 nm</i>	<i>840 nm</i>
17 wt.-% PES	-	-	+	+
23 wt.-% PES	-	-	+	+
28 wt.-% PES	-	-	+	+
23 wt% PES, 3.5 wt% water	-	-	+	+
23 wt.-% PES, 50:50 s:ns	-	-	+	+
23 wt% PES, 3.5 wt% water, 50:50 s:ns	-	+	+	+
17 wt% PMMA	+	+	+	+

**table 1** *Replication on shallow molds. If the pattern on the mold is replicated successfully in the polymer after PS $\mu$ M, the experiment is marked '+', otherwise the result is marked '-'. The phase separation of solutions of PES in NMP, using water as a non-solvent, yields a relatively high amount of shrinkage (more than 10 percent in the horizontal direction). Addition of non-solvent to the polymer solution and coagulation in a mixture of solvent and non-solvent (in this case 50 wt% of the water was replaced by NMP) improves the replication. The replication does not cause problems in recipes where there is little shrinkage (about 1% or less), for example a solution of high molecular weight ( $M_w=350.000$ ) Polymethylmethacrylate*

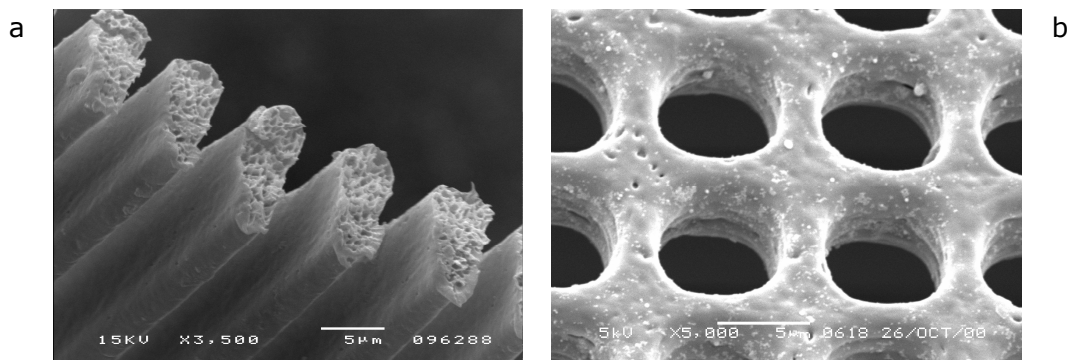
## 2.4 materials

Realizing phase separation can be applied on virtually all soluble polymers, one immediately conceives the enormous amount of polymers which in principle will become accessible for microfabrication. Some of the materials that have been structured by PS $\mu$ M could not be used for microfabrication before. A summary of the recipes described here is given in Table 2.

The phase separation process is most straightforward on uncrosslinked glassy polymers. As long as a good solvent and a miscible non-solvent can be found, the polymer is suitable for liquid induced phase separation and thus for PS $\mu$ M. Amongst the polymers that were processed, were polyimide and polyethersulfone, which have a rather high glass transition temperature and are therefore hard to shape by mechanical processing, like hot embossing. Other amorphous polymers that have been processed by PS $\mu$ M are polyetherimide, polycarbonate, polysulfone, and polystyrene. The latter has been processed both by thermally induced phase separation and liquid induced phase separation, whereas all the other polymers mentioned were processed by liquid induced phase separation. Polymethylmethacrylate has been processed in several different phase separation recipes,

<i>Polymer</i>	<i>Solvent</i>	<i>Wt.-%</i>	<i>Non-solvent</i>
Polyimide Matrimid 5218, Ciba	NMP	13-16	Water
Polyethersulfone Ultrason E6020P, BASF	NMP	14-33	water
Polymethylmethacrylate Polysciences	NMP	16-23	water
Polymethylmethacrylate Polysciences	Acetic acid	30	water
Polyetherimide Ultem 1000, General Electrics	NMP	19	water
Polycarbonate Markrolon CD 2005, Bayer	NMP	13-17	water
Nylon 4.6 Stanyl, DSM	Formic acid	23	water
Polysulfone Ultrason P3500 NTLCD, BASF	THF	25	water
Polysulfone Ultrason P3500 NTLCD, BASF	NMP	30	water
Polystyrene Styron, Dow Chemicals	THF	24	water
Polyvinylidene fluoride Solef, Solvay	NMP	15-30	water
Poly(ethylene-co-vinylalcohol), 60% ethylene Polysciences	DMSO (80 wt.-%), octanol (10 wt.-%)	10	water
Poly(ethyleneoxide) poly(butylene terephthalate) block copolymer Isotis	Chloroform	30	Ethanol, iso propanol
(Styrene-ethylene/butylene-styrene) triblock copolymer, 30 % PS content. Kraton G-1726	THF	17	water
Poly(lactic acid)	Chloroform	32	1-propanol
Polyaniline Emeraldine base ( $M_n = 65.000$ ) Aldrich	NMP (69 wt.-%), Heptamethyleneimine (12 wt.-%)	19	Hexane, water
Polyaniline Emeraldine base ( $M_n = 65.000$ ) Aldrich	NMP (69 wt.-%), Hexamethyleneimine (12 wt.-%)	19	Hexane, water
Polyetherimide / Polyvinylpyrrolidone blend Ultem 1000, General Electric; K90 ( $M_r =$ 360.000), Fluka	NMP	19 PEI, 11 PVP	water

table 2 Recipes used for the preparation of polymeric microstructures by liquid induced  $PS_{\mu}M$ . Abbreviated solvents: NMP (1-methyl-2-pyrrolidinone), THF (tetra hydro furan), DMSO (dimethyl sulfoxide).



**figure 7** Completely open, perforated microstructures fabricated by phase separation micro molding. The liquid induced PS $\mu$ M was realised by vapour exposure and subsequent immersion in water.

**a** Line pattern of 2.5 micrometer wide lines, made of Polyethersulfone (PES) with an aspect ratio of 2.5. The cross section illustrates that the inner structure is porous, while the surface is dense. The perforation is uniform across an area of millimetres squared. The lines span across 100  $\mu$ m length.

**b** Five micrometer wide holes perforated in Polyimide.

including one yielding a non-porous, completely dense configuration (see Figure 4b). Considering the good optical properties of this material it may also be possible to use PS $\mu$ M in integrated optics or photonics.

Crystalline polymers can also be structured by phase separation micro molding. However it is important to take into account that the crystallinity of the polymer can disturb the microstructure in some cases. The microstructure of the crystalline poly(ethylene-co-vinylalcohol) (Figure 8) displays a clear presence of the crystalline structure on the surface, although the structure still exhibits the imprint of the mold. Even so, the crystalline polymer polyvinylidene fluoride was applied in PS $\mu$ M, resulting in a microstructure exhibiting no irregularities due to the crystalline structure (see Figure 2c). Also the crystalline Nylon 4.6 was successfully microstructured by PS $\mu$ M. The formation of crystals depends strongly on the kinetics of phase separation. If the liquid-liquid demixing process is slow, crystallization is favored. Rapid liquid-liquid demixing suppresses crystallization.<sup>31</sup>

Another class of polymers, which can be structured by PS $\mu$ M and has unique and interesting properties, is block copolymers. By PS $\mu$ M a poly(ethyleneoxide) poly(butylene terephthalate) block copolymer (PEO/PBT) and a styrene-ethylene/butylene-



styrene triblock (SEBS) polymer were structured. In Figure 9a a microstructure prepared from SEBS, a thermoplastic elastomer, is depicted.

The properties of the polymeric microstructure are further expanded by the possibility to apply PS $\mu$ M on polymer blends. As an example, addition of polyvinyl pyrrolidone to the slightly hydrophobic polyetherimide results in a more hydrophilic polymer product. Hydrophilicity can be advantageous for example to promote wetting of a microfluidic structure or polymeric microsieve (see Chapter 5). A polymer blend can also form interesting morphologies due to the demixing of the two polymers. When one component can be selectively removed afterwards, this can lead to very open morphologies.

The wide range of polymers that are accessible for PS $\mu$ M also contains materials, which have a specific functionality. For example biodegradable or biocompatible materials have been structured, like polylactic acid and the block copolymer PEO/PBT mentioned earlier. A microstructure prepared from poly(lactic acid) is shown in Figure 9b. The easy process conditions, especially in combination with the possibility to introduce porosity as mentioned earlier, make it very tempting to use PS $\mu$ M for biomedical applications.

Another example of a polymer with a specific functionality is the conductive polymer polyaniline, which has also been structured by PS $\mu$ M. Figure 9c gives an example of a microstructure prepared of polyaniline. A complication in the dissolution of polyaniline is its tendency to form a gel easily.<sup>32</sup> Therefore the solution can normally only be very dilute.

However, polyaniline can be dissolved in the emeraldine base form by addition of gel inhibitors. The preparation procedure of the microstructure from the solution does not require special measures. Thus PS $\mu$ M offers a simple way to structure a polymer, which is electrically conductive after doping.

Being able to process virtually any soluble polymer, PS $\mu$ M addresses already a large class of material properties, which can now be microstructured. Using an additional post processing step, the range of materials can even be further expanded. The polymer product, which results after PS $\mu$ M, can be a precursor for a pyrolysis step. If a suitable polymer has been chosen, for example a polyimide, and the pyrolysis is performed at an adequate temperature under a nitrogen atmosphere, the polymeric precursor will be converted into carbon.<sup>33,34,35</sup> An example of a carbon microstructure is depicted in Figure 10a.

Pyrolysis as a process step subsequent to PS $\mu$ M also gives access to the microfabrication of ceramic and metallic microstructures.<sup>36,37</sup> For example for the pyrolysis to yield an alumina microstructure, aluminum hydroxide powder was suspended into a

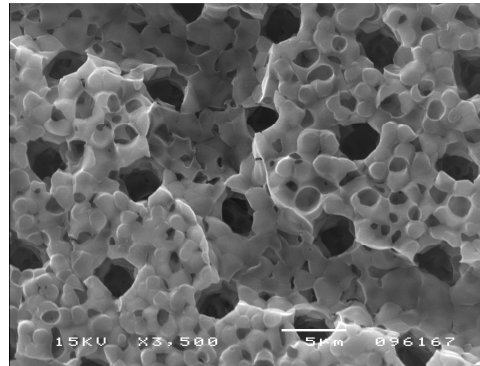


figure 8 *Microstructure of the crystalline poly(ethylene-co-vinylalcohol). The recipe results in a porous configuration where the crystalline structure of the polymer is clearly influencing the microstructure. The phenomenon is not always present in crystalline materials, for example a good replica with a smooth surface was made from polyvinylidene fluoride (see Figure 2c).*

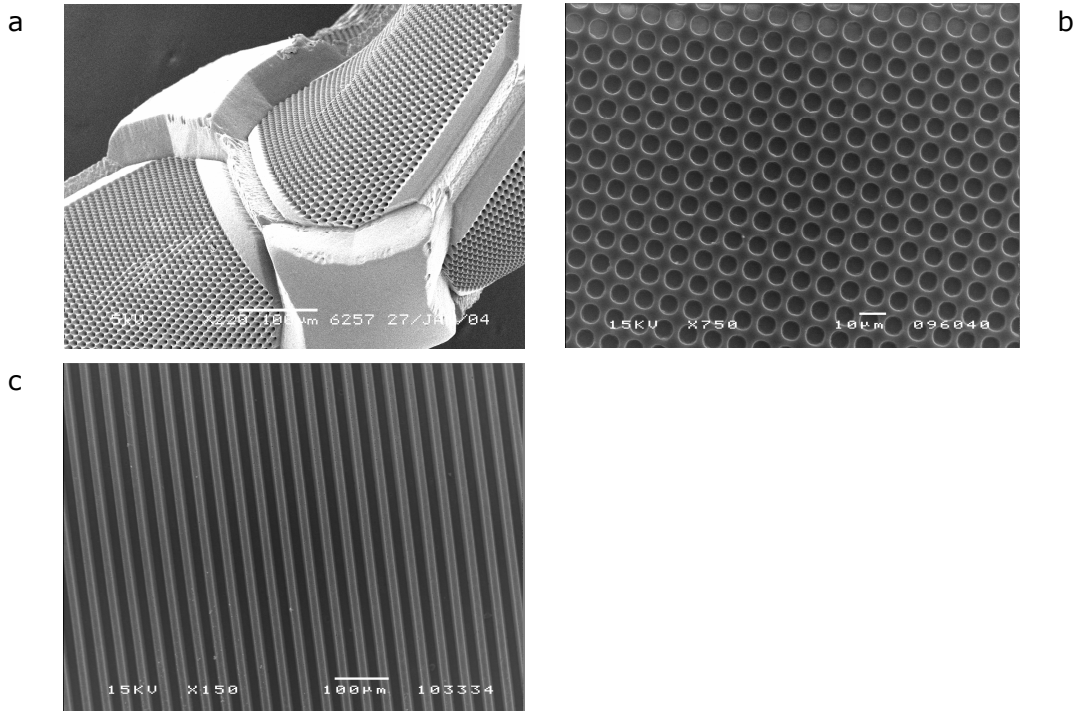


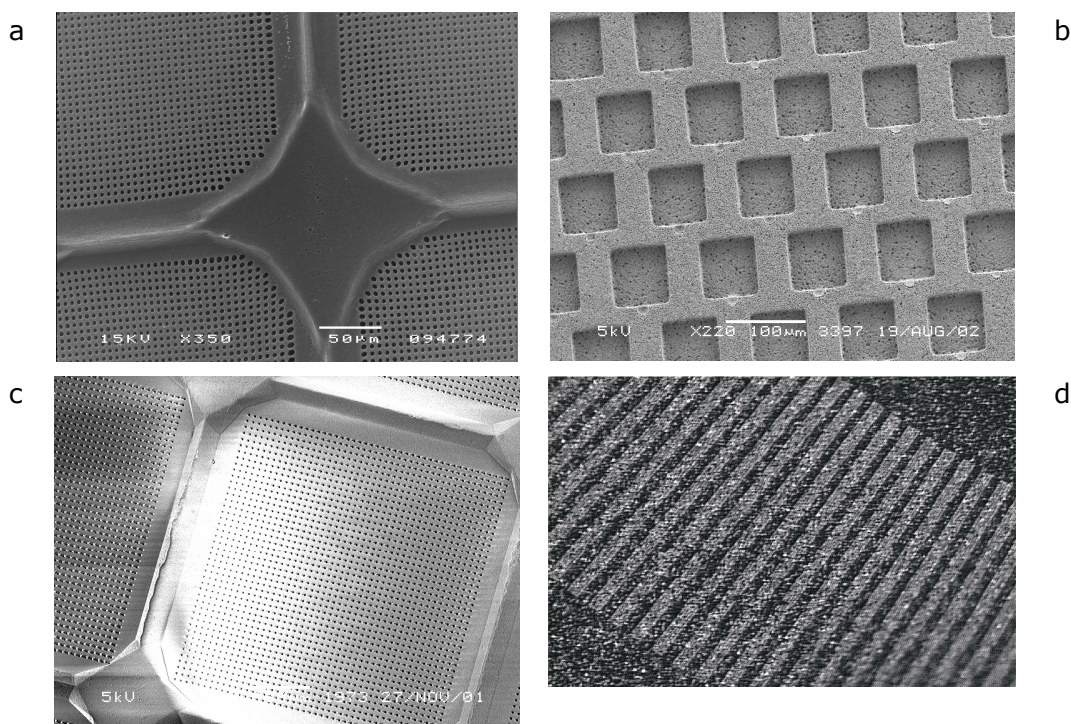
figure 9a *Microstructure prepared from a styrene-ethylene/butylene-styrene triblock (SEBS) polymer.*  
b *Microstructure of the biodegradable polymer poly(lactic acid).*  
c *Microstructure of the electrically conductive polymer polyaniline.*

polymer solution. When the suspension is spread on a mold and phase separated, a precursor of ceramic particles in a polymer matrix is shaped into the microstructure on the mold. The polymer functions as a particle binder. The mechanical properties of the precursor still resemble the mechanical properties of the polymer, which makes it easy to release the precursor from the mold. In this way the brittle nature of ceramics is avoided during the structuring of the material. Subsequently the precursor is subjected to pyrolysis, heating up slowly to a temperature at which the particles start sintering. During the sintering the precursor is exposed to a controlled flow of oxygen. While the particles sinter to form a ceramic microstructure, the polymer is oxidized and removed slowly. In the example of the alumina hydroxide, the particles simultaneously dehydrate to form an alumina microstructure.

A prerequisite for the sintering process is the contact between the ceramic particles in the polymer matrix. Therefore the amount of particles in the solution has to be relatively high, depending also on the size of the particles. As a rule of thumb the weight percentage of the particles has to exceed at least 50 percent in order for the sintering to be successful. Metallic microstructures are prepared similarly, by dispersing metallic particles in the solution prior to PS $\mu$ M and pyrolyzing under optimized conditions afterwards. The ceramic and metallic microstructures, which were fabricated by PS $\mu$ M combined with pyrolysis, resembled the microstructure on the mold. However the size of the particles sets a limitation of the feature size of the microstructures that can be fabricated, and can influence the smoothness of the surface of the microstructure. Figure 10b and 10c depict ceramic microstructures, while Figure 10d depicts a metallic microstructure.

## 2.5 conclusion

Phase separation micromolding is a novel technique for the fabrication of microstructures from an unprecedented broad spectrum of polymers. By additional processing PS $\mu$ M can also yield microstructures from inorganic materials, namely carbon, ceramics and metals. Virtually any soluble polymer can be applied in phase separation, including both amorphous and crystalline polymers, block copolymers, and polymer blends. Also biodegradable polymers and a conductive polymer were applied in PS $\mu$ M, giving the opportunity to fabricate a microstructure of polymers with these specific functionalities. By combination of PS $\mu$ M with a pyrolysis step the range of materials can be expanded to



**figure 10** *Microstructures of inorganic materials, prepared by an extra post-processing step.*

**a** *Glassy carbon structure prepared from a polyimide precursor after pyrolysis.*

**b** *Ceramic, alumina microstructure prepared from a polyethersulfone –  $Al(OH)_3$  precursor after pyrolysis in presence of air. The structure was sintered at 1200 °C.*

**c** *Alumina structure prepared according to the same recipe as the structure in Figure b, sintered at 600 °C.*

**d** *Optical microscope image of a Silver microstructure prepared from a polyethersulfone – silver precursor after pyrolysis in air. The bright reflection of the light on some spots still reveals the regions that were formed from grains in the precursor in the sintering process. The image depicts an area of 1.58 mm x 1.05 mm.*

inorganic materials as well. The process is straightforward, cost effective, and does not require cleanroom conditions. Intrinsic shrinkage of the polymer during phase separation facilitates the release of the microstructure from the mold. PS $\mu$ M therefore gives access to reliable, large-scale fabrication of highly uniform microstructures, even where high aspect ratios are required. Furthermore shrinkage provides a simple method to fabricate perforated, completely open microstructures. However, in recipes with a large amount of shrinkage the replica sometimes exhibits deformations caused by the shrinkage. Also replication of

relatively shallow molds is hindered when the polymer displays a very large extent of shrinkage during the phase separation.

The possibility to introduce porosity in a microstructure gives access to yet unknown functionalities. The intrinsic porosity in microstructures prepared by PS $\mu$ M can be tuned by adjustment of the phase separation recipe.

Methods are described to suppress the formation of macrovoids or skin formation, which are phenomena occurring in fast demixing solutions.

The large amount of materials that can be applied and the yet unknown functionalities that can be addressed in a microstructure, make that PS $\mu$ M complements the present spectrum of microfabrication technologies well. Due to its scope and simplicity, phase separation micromolding is a promising technique with applications in virtually all fields where micron and submicron structuring is required.

## 2.6 experimental

The molds were made by silicon micro machining. On a flat, polished single crystalline <100>-silicon wafer a thin layer of photo resist (OLIN Resist, 907/12) was spun. After exposure to the desired pattern the photo resist was developed and baked for one hour at 150°C. The silicon is then being etched in an Oxford ICP 100 deep reactive ion etcher with a gas mixture of SF<sub>6</sub>:O<sub>2</sub>=100:7 at a temperature of -125°C, Power=600W. When an additional deeper structure is wanted, like the mold used to fabricate the structures in Figure 7b, 9a, 10a and 10c, subsequently the complete wafer is covered with silicon dioxide using a wet oxidation process and subsequently covered with a thick layer of photo resist (OLIN resist 908/35). The photo resist is exposed to an other mask pattern and after development the oxide layer is being etched in a buffered HF-etchant with the photo resist as mask. Finally the additional structure is being etched using an an-isotropic etchant, KOH 25 wt.% at 70°C. To investigate the influence of the surface of the mold on the PS $\mu$ M process a mold was covered by silicon nitride in a chemical vapor deposition process, another mold was covered by silicon oxide in a wet oxidation process and a mold was covered by a thin gold layer by sputtering.

In the mold used for the microstructure depicted in Figure 5 the 150 nm wide lines originate from Laser Interference Lithography. The exposure was performed on a thin layer of Olin 907/12 photo resist, thinned with ethyl-3-ethoxypropionate and methyl-3-methoxypropionate. Reactive ion etching transferred the line pattern into the underlying siliconnitride.

The polymer solutions were applied on the molds by casting using a casting knife blade with adjustable height. A set-up was built in which the mold was clamped, with the surface of the mold leveled with a polished stainless steel reference plane. The casting knife was mounted in an aluminum housing, where the relative height of the blade to the housing was adjustable by high-precision adjustment screws with an accuracy of one micrometer (Newport). The housing in which the casting knife was mounted had a polished gliding area, which could be placed and moved on the stainless steel reference plane, ensuring the height of the casting knife relative to the mold with micrometer accuracy. The thickness of the layers, which were applied on the mold, relative to the top level of the mold, varied in between 5 micrometer and 50 micrometer for the preparation of completely open 'through' microstructures by perforation, and in between 50 and 500 micrometer for the preparation of imprinted polymer films.

Table 2 gives an overview of all the polymers used for PS $\mu$ M, summarizing the solvent and non-solvent and the weight percentage of the polymer in the solution. The suppliers of the different polymers are also mentioned in Table 2. The polymers were dissolved, while stirring, at ambient room temperature, unless stated otherwise. The solvents, which were used, were NMP (1-methyl-2-pyrrolidinone (99%), Acros Organics), THF (tetrahydrofuran, Merck), acetic acid (100%, Merck), formic acid (98-100%, Merck), DMSO (Dimethyl sulfoxide, Merck) or chloroform (Merck). In some cases additives were used, namely 1-

## chapter 2

octanol (Fluka), acetone (Merck), heptamethyleneimine (Fluka), and hexamethyleneimine (99%, Acros Organics). The non-solvents, which were used, were tap water, ethanol (Merck), iso-propanol (Merck), 1-propanol (Merck) and n-hexane (Merck).

Polyaniline, emeraldine base, was dissolved at a temperature of 32°C, while stirring in NMP with an appropriate gel inhibitor (heptamethyleneimine or hexamethyleneimine) for half an hour. Some of the polymer is still undissolved and left time to precipitate. The precipitate is removed, and the solution is applied on the mold. The solution is immersed in a hexane non-solvent bath, where it is left for 5 hours. Subsequently the membrane is rinsed in water.

A PS $\mu$ M experiment based on thermally induced phase separation was performed by dissolving polystyrene in diisodecylphthalate (Merck) at 120°C. After application of the hot solution on a mold, the solution is quenched in ice water ( $T=0^{\circ}\text{C}$ ).

The completely porous structure depicted in Figure 2b was prepared by dissolving polyetherimide (19 wt.-%) and polyvinylpyrrolidone with a high molecular weight ( $M_w=360.000$ ) in NMP. The coagulation is performed in water.

The optically transparent PMMA microstructure depicted in Figure 4b was prepared by dissolving high molecular weight PMMA (200 micron beads powder,  $M_w=350.000$ ) in NMP at 16.7 wt.-%. The thickness of the layer, which was spread on the mold, was below 200 micrometer. The coagulation was performed in water.

The completely open microstructure in Figure 7a was prepared by casting a solution containing polyethersulfone (9.8 wt%), NMP (49 wt%), acetone (39.2 wt%) and a surfactant (Span 80, Fluka, 2.0 wt%) 10 micrometer above the mold features. The mold and solution are exposed to a nitrogen environment, almost saturated with water vapor ( $T=30^{\circ}\text{C}$ , and a relative humidity of 80%) for half a minute. The solution becomes completely turbid. Subsequently the mold and solution are immersed in water. The completely open microstructure shown in figure 7b was prepared

by casting a solution of polyimide (7.7 wt.-%), NMP (51.3 wt.-%) and acetone (41.0 wt.-%) on top of a mold with 5 micrometer wide pillars. The height of the pillars was 20 micrometer and in between the fields of pillars were 50 micron wide trenches of 35 micrometer depth. The solution was applied at 50 micrometer above the top of the pillars, thus preventing damage of the mold by the application of the solvent. The mold and solution are exposed to a nitrogen environment, almost saturated with water vapor ( $T=30^{\circ}\text{C}$ , and a relative humidity of 80%) for half a minute. The solution becomes completely turbid. Subsequently the mold and solution are immersed in water.

The carbon structure in Figure 10a was fabricated, starting with a structure similar to the structure depicted in figure 7b. The polyimide microstructure was used as a precursor, and was heated up to a temperature of 700°C under a constant nitrogen flow (1 l min<sup>-1</sup>).

The ceramic structure depicted in Figure 10b was prepared by dispersing Al(OH)<sub>3</sub> powder with a grain size of 0.4 micrometer (58.8 wt.-%) in a solution containing PES (5.8 wt.-%), NMP (19.8 wt.-%), and acetone (15.6 wt.-%). The precursor, which was easily released from the mold, was sintered at a temperature of 1200°C for two hours in air. A temperature ramp of 1°C min<sup>-1</sup> was chosen in both the heating and the cooling step. The precursor for the ceramic structure in Figure 10c was prepared from a similar recipe, however a different sintering procedure was exploited. The imprinted hybrid precursor was heated up to a temperature of 600°C with a speed of 35°C/min, under a constant airflow of 1 l/min. After two hours at 600°C the film was gradually cooled down to room temperature.

The silver structure in Figure 10d was made by including silver powder, with a grain size between 0.7 and 1.2 micrometer (Chempur) into a 23wt.-% PES solution. The weight percentage of the powder in the suspension was 50%. The hybrid material structure resulting from PS $\mu$ M was sintered at 850°C under a constant airflow.

## references

- <sup>1</sup> L. Vogelaar, R. G. H. Lammertink, J. N. Barsema, W. Nijdam, L. A. M. Bolhuis-Versteeg, C. J. M. van Rijn, M. Wessling, *Small* **2005**, *1*, 645.
- <sup>2</sup> L. Vogelaar, J. N. Barsema, W. Nijdam, C. J. M. van Rijn, M. Wessling, *Adv. Mater.* **2003**, *15*, 1385.
- <sup>3</sup> M. J. Madou, *Fundamentals of Microfabrication*, CRC Press, Boca Raton, U.S. **2002**.
- <sup>4</sup> M. A. Burns *et al.*, *Science* **1998**, *282*, 484.
- <sup>5</sup> T.A. Desai, D.J. Hansford and M. Ferrari, *Biomol. Eng.* **2000**, *17*, 23.
- <sup>6</sup> L. Vogelaar, W. Nijdam, *et al.*, *Adv. Mater.* **2001**, *13*, 1551.
- <sup>7</sup> K. D. Wise and K. Najafi, *Science* **1991**, *254*, 1335.
- <sup>8</sup> C. M. Agrawal and R. B. Ray, *J. Biomed. Mater. Res.* **2001**, *55*, 141.
- <sup>9</sup> S. A. Soper, A. C. Henry, B. Vaidya, M. Galloway, M. Wabuyele, R. L. McCarley, *Anal. Chim. Acta* **2002**, *470*, 87.
- <sup>10</sup> T. Thorsen, S.J. Maerkl, S.R. Quake, *Science* **2002**, *298*, 580.
- <sup>11</sup> Y. Xia and G. M. Whitesides, *Angew. Chem. Int. Ed.* **1998**, *37*, 550.
- <sup>12</sup> S. R. Quake and A. Scherer, *Science* **2000**, *290*, 1536.
- <sup>13</sup> M. Hecke and W. K. Schomburg, *J. Micromech. Microeng.* **2004**, *14*, R1.
- <sup>14</sup> H. Becker and U. Heim, *Sensor Actuat. A-phys.* **2000**, *83*, 130.
- <sup>15</sup> S. Y. Chou, P. R. Krauss and P. J. Renstrom, *Science* **1996**, *272*, 85.
- <sup>16</sup> U. P. Schonholzer, R. Hummel and L. J. Gauckler, *Adv. Mater.* **2000**, *12*, 1261.
- <sup>17</sup> J.E. Smay, G.M. Gratson, R.F. Shepherd, J. Cesarano, J.A. Lewis, *Adv. Mater.* **2002**, *14*, 1279.
- <sup>18</sup> M. Mulder, *Basic principles of membrane technology*, Kluwer academic publishers, Dordrecht, the Netherlands **1996**.
- <sup>19</sup> R. W. Baker, *Membrane technology and research*, Mc Graw-Hill, New York, U.S. **2000**.
- <sup>20</sup> T. A. Desai, *Med. Eng. Phys.* **2000**, *22*, 595.
- <sup>21</sup> D. W. Huttmacher, *Biomaterials* **2000**, *21*, 2529.
- <sup>22</sup> H. Matsuyama, S. Berghmans, M. T. Batarseh, D. R. Lloyd, *J. Membr. Sci.* **1998**, *142*, 27.
- <sup>23</sup> S.-G. Li, Th. Van den Boomgaard, C. A. Smolders, H. Strathmann, *Macromolecules* **1996**, *29*, 2053.
- <sup>24</sup> H. Matsuyama, M. Teramoto, R. Nakatani, T. Maki, *J. Appl. Pol. Sci.* **1999**, *74*, 171.
- <sup>25</sup> H. Park, J. M. Hong, S. Y. Ha, Y. S. Kang, K. H. Ahn, *J. Ind. Eng. Chem.* **1998**, *4*, 31.
- <sup>26</sup> T. H. Young, Y. H. Huang, Y. S. Huang, *J. Membr. Sci.* **2000**, *171*, 197.
- <sup>27</sup> L. J. Zeman, A. L. Zydney, *Microfiltration and ultrafiltration*, Marcel Dekker inc., New York, U.S. **1996**.
- <sup>28</sup> R. M. Boom, I. M. Wienk, Th. Van den Boomgaard, C. A. Smolders, *J. Membr. Sci.* **1992**, *73*, 277.
- <sup>29</sup> R. W. Jaszewski, H. Schiff, B. Schnyder, A. Schneuwley and P. Groning, *Microelectron. Eng.* **1997**, *35*, 381.
- <sup>30</sup> C. Stropnik, V. Musil, M. Brumen, *Polymer* **2000**, *41*, 9227.
- <sup>31</sup> A. M. W. Bulte, M. H. V. Mulder, C. A. Smolders, H. Strathmann, *J. Membr. Sci.* **1996**, *121*, 51.
- <sup>32</sup> J. M. Sansinena, J. Gao, H. L. Wang, *Adv. Func. Mater.* **2003**, *13*, 703.
- <sup>33</sup> O. J. A. Schueller, S. T. Benjamin, G. M. Whitesides, *Sens. Act. A-Phys.* **1999**, *72*, 125.
- <sup>34</sup> J. N. Barsema, N. F. van der Vegt, G. H. Koops, M. Wessling, *J. Membr. Sci.* **2002**, *205*, 239.
- <sup>35</sup> H. V. Shah *et al.*, *Chem. Mater.* **1999**, *11*, 2623.
- <sup>36</sup> N. W. Androff, L. F. Francis, B. V. Velamakanni, *AICHE J.* **1997**, *43*, 2878.
- <sup>37</sup> J. de Jong, N. E. Benes, G. H. Koops, M. Wessling, *J. Membr. Sci.* **2004**, *239*, 265.





A grayscale scanning electron micrograph showing a dense array of interconnected, porous, spherical microstructures. Each structure has a complex, multi-faceted surface with numerous small openings, creating a highly porous, lattice-like appearance.

## chapter 3 freestanding microstructures

prepared by phase separation micro molding

*L. Vogelaar*

*R. G. H. Lammertink*

*M. Wessling*

This chapter describes the fabrication of freestanding microstructures using Phase Separation Micro Molding (PS $\mu$ M). When Phase Separation Micro Molding is performed on a mold having a relief pattern of polygonal holes, freestanding microstructures can be fabricated in a single step. The microstructures are the result of air entrapment inside the hole. Capillary corner flow causes the polymer solution to fill the hole, and thus replace the air. Freestanding microstructures result from the filling process of different polygonal holes. These structures are compared to a model, describing the flow behavior of a fluid in an interior corner.

# 3

*Above: Freestanding microstructures.*

# 3

## 3.1 introduction

Microfabrication processes often have a top down character. Different layers are deposited and selectively removed, building up the microstructure step by step.<sup>1</sup> As a consequence, fabrication of microstructures that are three-dimensionally freestanding is a very tedious and difficult process.<sup>2</sup> With the conventional combination of lithography and etching, such structures can only be fabricated with multiple etching and deposition steps, e.g. via underetching of layers. Simplification of the fabrication process would ease the accessibility of freestanding configurations for applications. An example of a process, which is able to fabricate freestanding configurations of metals is nano transfer technology.<sup>3,4,5</sup>

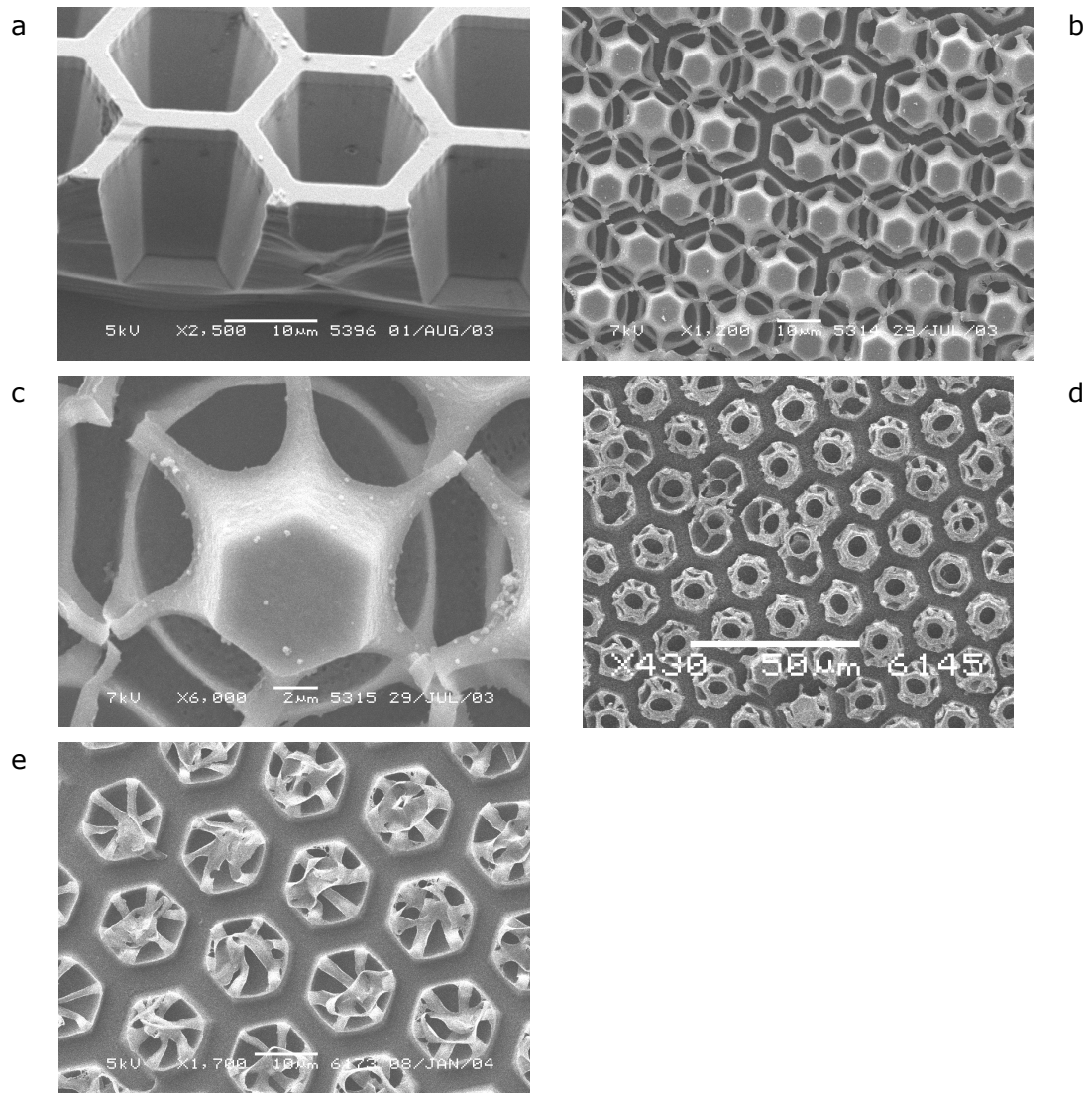
We will show that phase separation micro molding (PS $\mu$ M) is able to fabricate freestanding microstructures from several polymers in a single step. This chapter describes the preparation of freestanding microstructures by PS $\mu$ M, and studies the influence of different parameters on the formation of the structures.

We hypothesize that the formation process of freestanding microstructures relies on capillary flow in a corner. The configuration of liquid flowing in a corner as a result of capillary force has been described theoretically. The equilibrium shape of the liquid and bubble in a polygonal channel can be calculated.<sup>6</sup> Additionally the kinetics of the corner flow process is covered by a model.<sup>7</sup> The experimental results of the formation of freestanding structures are compared to theory.

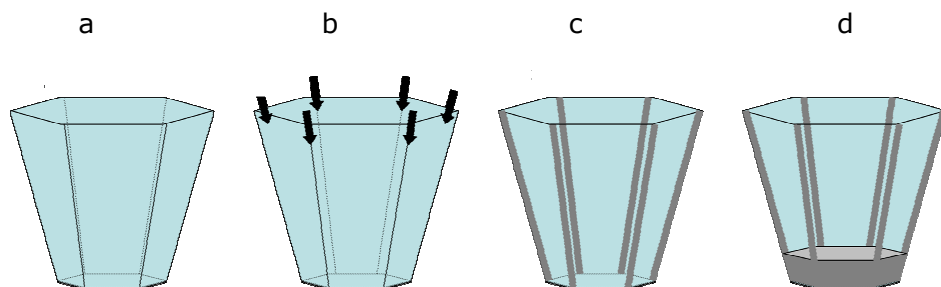
## 3.2 experimental findings

In phase separation micro molding (PS $\mu$ M), a thin layer of polymer solution is cast on a mold. Immersion in a non-solvent causes demixing and phase separation of the solution, during which the polymer rich part of the demixed solution solidifies. The solid polymer assimilates the relief profile on the surface of the mold.<sup>8,9</sup>

Figure 1 displays examples of freestanding microstructures prepared by PS $\mu$ M. These structures are formed on a mold, of which the surface is microstructured with a pattern of polygonal holes. The resulting microstructures consist of a freestanding top part, which is connected with thin ribs to the underlying polymer film. The shape of the microstructures suggests that the freestanding configuration results from entrapment of air bubbles in the polymer solution. The film of polymer solution encloses the holes during the casting. The air



**figure 1** Freestanding microstructures prepared on a mold (a) having honeycomb shaped holes on its surface. Typical examples of a freestanding microstructures prepared from a 13wt% PI solution (b and c), a 16.7 wt% PI solution having an approximately 5 times higher viscosity (d) and a 20 wt% PI solution having an approximately 25 times higher viscosity (e). All microstructures were prepared by immersion immediately after application of the solution.



**figure 2** Schematic representation of the filling process by corner flow (b,c and d) in a finite polygonal hole (a) and the resulting shape of the solution, which will form a freestanding microstructure if solidified by phase separation (d).

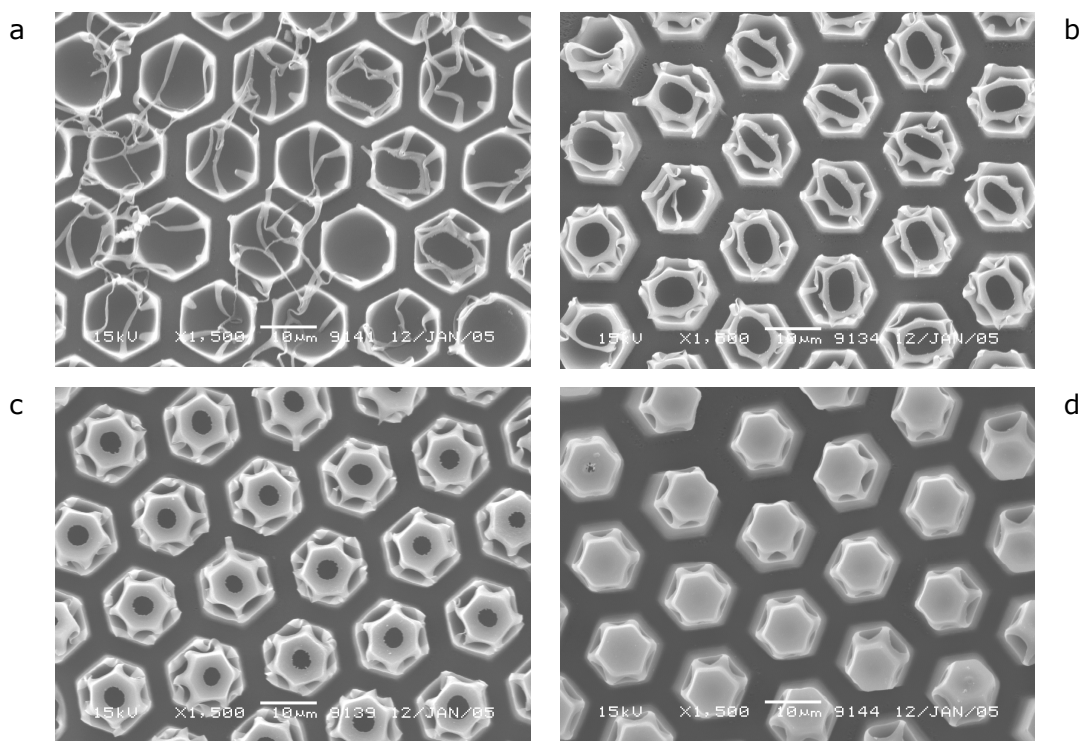
in the hole is slowly replaced by the polymer solution, which starts flowing through the corners of the polygon. A schematic representation of the filling of the polygonal hole is depicted in Figure 2. The immersion in non-solvent and subsequent phase separation of the solution fixates the shape of the flowing polymer solution. The polymer solution demixes in a polymer-lean and a polymer-rich part. The polymer-rich part solidifies simultaneously, and immediately arrests the configuration of the polymer solution.<sup>10</sup>

The fabrication of polymeric microstructures in a freestanding configuration requires only a single step, which is a unique aspect of the PS $\mu$ M process. The interplay between air and fluid evades the top down character that limits other microfabrication methods. The unrivaled simplicity of this fabrication process and the exceptional freestanding shape arises interest in the formation mechanism. The possibility to immediately freeze the shape provides insight in the behavior of a polymer solution, while flowing through a corner.<sup>11</sup>

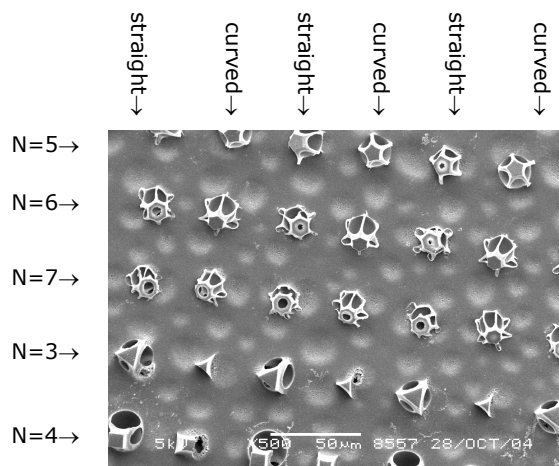
Freestanding microstructures have been prepared from a wide range of polymers, namely poly(imide), poly(methyl methacrylate), poly(vinyl chloride) and poly(sulfone). Table 1 contains parameters describing some fluid characteristics of two poly(imide) (PI) solutions. Figure 1 displays freestanding microstructures prepared from PI solutions of different weight percentages. As is expected from the increase in viscosity, a solution with a higher polymer concentration displays a slower filling process.

<i>Solution</i>	<i>Viscosity [Pa.s]</i>	<i>Surface tension [mN/m]</i>	<i>Contact angle [degrees]</i>
PI-NMP 13 wt%	42	42.5	17.1
PI-NMP 20 wt%	550	47.9	23.4

**table 1** *Viscosity, surface tension and contact angle for two solutions having different concentrations of poly(imide) dissolved in NMP.*



**figure 3** *Evolution of the filling process visualized by microstructures prepared from a 20 wt% PI-NMP solution. The delay time between application of the solution and immersion was 0 (a), 20 (b), 40 (c) and 120 (d) seconds.*

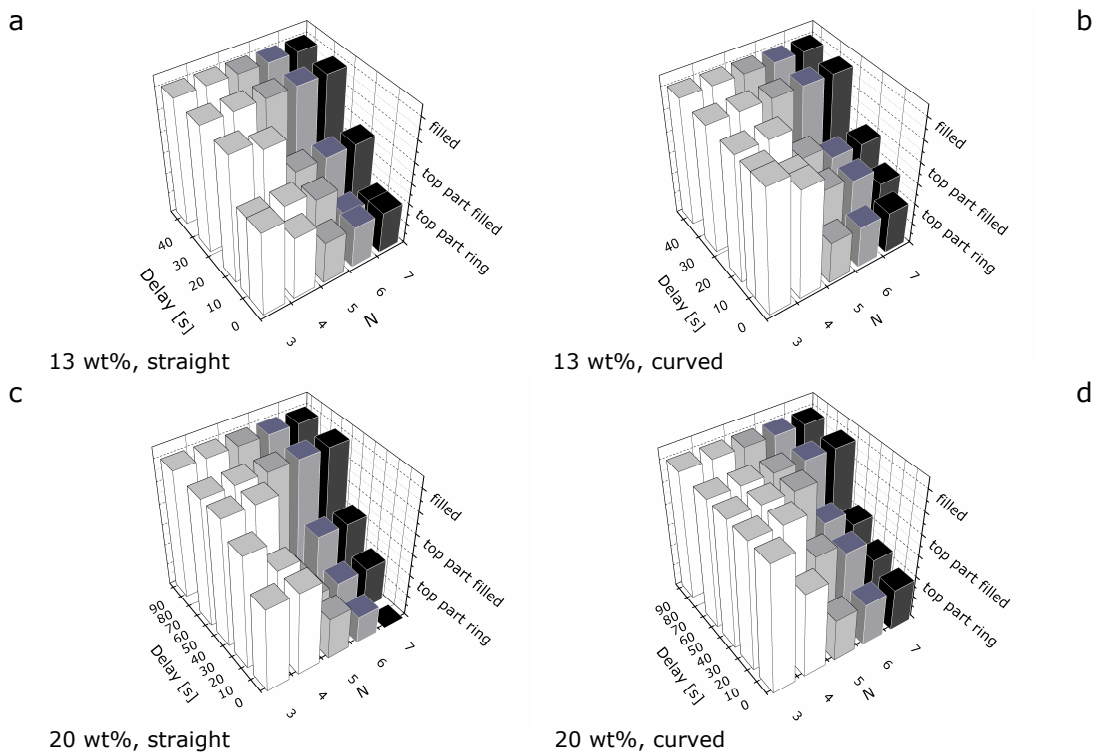


**figure 4** Freestanding microstructures having three to seven ribs prepared from a 13 wt% PI-NMP solution. On the mold, in one direction (the horizontal direction on the picture) the amount of corners is varied. In the other direction (the vertical direction in the picture) the holes had in turn straight walls or curved walls, decreasing the width of the corner while preserving the amount of corners.

The solution flows through the corners of the polygonal hole, and replaces the air. This so-called corner flow is a well-known phenomenon in liquid displacement through non-circular geometries. By delaying the time between application of the solution on the mold and immersion in non-solvent, the corner flow process can be followed in time. The different stages of the filling process are revealed by the shape of the freestanding structure. Such a time lapse is displayed in Figure 3. Eventually, the polymer will replace the air bubble and fill the hole completely.

The filling rate strongly depends on the angle of the corners in the polygonal hole. The dependence is demonstrated in Figure 4. The width of the corners was varied in two different ways. First, the amount of corners per hole was varied. Additionally, polygonal holes with curved walls were present on the mold, which reduces the corner angle while maintaining the amount of corners. To exclude geometric effects other than the corner angle, the cross-sectional area and depth of all the polygonal holes was similar. The diagrams in Figure 5 give an impression of filling kinetics as a function of amount of corners, both for straight-walled holes and holes with curved walls.

From Figure 5 it is clear that a sharper corner increases the filling rate. The angular dependence of the velocity of the flowing liquid through the corners, as well as the shape of the freestanding microstructures, is strongly suggestive of corner flow driven by minimization of the surface energy. Therefore in the next paragraph the shape of the freestanding microstructures and time scales on which they are formed are compared to a theoretical model, describing fluid flow through a corner.



**figure 5** Impression of the stage of filling of the polygonal holes as a function of time and amount of corners for two different PI solutions (13 wt% (a and b) and 20 wt% (c and d) and either straight-walled holes (a and c) or holes with curved walls (b and d). The three different stages indicate if the top part has a ring shape, if the top part is fully filled, or if the entire hole is filled. Intermediate values indicate the percentage of freestanding structures that is in the next stage.

### 3.3 corner flow model

We hypothesize that the only mechanism for the displacement of air and polymer solution is the capillary force. In other words, the only reason the movement takes place is that the surface energy of the entire system is decreased. This excludes possible effects of other forces like buoyancy and gravity. To determine whether the buoyancy played an important role in the formation of the freestanding structures, experiments were performed in which the mold was turned up side down between application of the solution and immersion in non-solvent. In this case the solution also fills the hole, suggesting that buoyancy does not play a significant role.

The model also assumes the volume of the air bubble to be constant. Thus the air is considered not to dissolve in the polymer solution. If these circumstances apply, a model of fluid flowing through the corners of a capillary can be implemented. First the width of the ribs of the freestanding structures is calculated according to a model, describing the equilibrium shape of a bubble in a polygonal hole.<sup>6</sup> Subsequently the kinetics of the corner flow leading to the formation of the microstructure is compared to a model.<sup>7</sup>

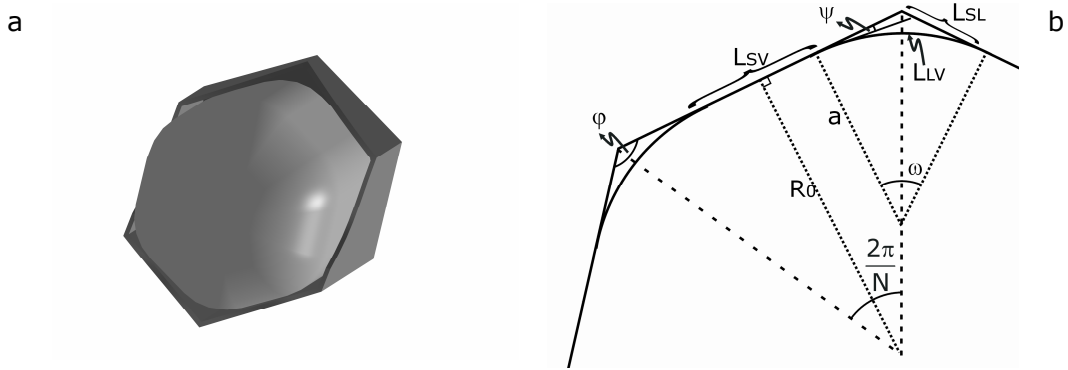
While the solution is flowing into the hole, the air bubble is pushed in opposite direction. The length of the polygonal holes is longer than the diameter of the cross-sectional area. Part of the model is therefore derived from the description of the shape of long bubbles in polygonal capillaries.<sup>12,13</sup> However, the goal of the calculations is not a complete description of the shape of the bubble, but to understand the mechanism of the formation of the freestanding structure. To achieve this, the width of the ribs as a characteristic dimension of the model is compared to the size measured for the freestanding structures. Therefore, entrance effects are not considered and the description will focus on the middle part of the bubble away from the front and rear edge.

The capillary pressure in the case of a non-wetting medium in a non-circular pore of arbitrary shape is derived by Mayer *et al.*<sup>14</sup> Here, the non-wetting medium is the vapor phase (air), whereas the wetting phase (the polymer solution) arranges in the corners. The capillary pressure then is expressed as:

$$P_c A = \gamma_{LV} (L_{LV,tot} + L_{SV,tot} \cos \psi), \quad [3.1]$$

where  $P_c$  is the total capillary pressure of the configuration,  $A$  is the area occupied by the non-wetting phase (the vapor),  $\gamma_{LV}$  is the surface tension of the liquid in air,  $L_{LV,tot}$  is the total





**figure 6a** Illustration of the shape of an air bubble in a polygonal channel. For illustrative purposes the channel is cut open and only part of the polygonal capillary is depicted.

**b** Schematic representation of a fluid meniscus in a polygonal hole, in the middle of the bubble, illustrating the different parameters in the corner flow model.

perimeter of the liquid-vapor interface,  $L_{SV, tot}$  is the total perimeter of the solid-vapor interface, and  $\psi$  is the contact angle of the liquid on the solid.

Figure 6 illustrates the shape of the fluid meniscus in the corner of a polygon. The curvature of the meniscus in the corner is fully determined by the geometry of the hole, the surface tension of the fluid and the contact angle between the liquid and the walls. The following derivation is analogous to the description by Ransohoff *et al.*, who described the problem for an equilateral triangular hole and an arbitrary contact angle.<sup>6</sup> Similar derivations are available for square capillaries or other triangular configurations.<sup>15,16</sup> The problem of a completely wetting liquid (contact angle zero) in a polygonal hole of arbitrary number of corners is also described.<sup>12,17</sup> Using the following expressions, the configuration can be found that minimizes the capillary pressure for any amount of corners and arbitrary contact angle. Although the geometry for corner flow in a polygonal hole is also described by others,<sup>7,18</sup> the derivation according to Ransohoff *et al.* is conceptually simpler, and allows a more straightforward calculation of the lengths of the different perimeters in the cornerflow problem.<sup>6</sup>

In a polygonal of  $N$  sides and corners, each corner has an inner angle,  $\phi$ , given by

$$\phi = \pi - \frac{2\pi}{N} \quad [3.2]$$

### chapter 3

From triangle geometry the angle  $\omega$ , which confines the liquid in the corner (see Figure 6), is derived as:

$$\omega = \pi - \varphi - 2\psi \quad [3.3]$$

and is therefore dependant only on the polygonal shape and the contact angle of the liquid. The total perimeters of the interfaces ( $L_{LV,tot}$  and  $L_{SV,tot}$ ) are found by multiplying the expressions for  $L_{LV}$  and  $L_{SV}$  that are illustrated in Figure 6 by the amount of corners,  $N$ . The total perimeter of the curved liquid-gas interface can thus be expressed as

$$L_{LV,tot} = N\omega a \quad [3.4]$$

The perimeters of the solid-liquid interface and the total solid-vapor interface are

$$L_{SL} = a \frac{\sin(\omega/2)}{\sin(\varphi/2)} \quad [3.5]$$

$$L_{SV,tot} = N(2R_0 \tan(\pi/N) - 2L_{SL}), \quad [3.6]$$

in which  $R_0$  is the radius of the inscribed circle of the polygon. The expression for the area covered by the vapor phase consists of three contributions, the first one expressing the total area of the polygon, the other two determining the area covered by the liquid phase:

$$A = N(R_0^2 \tan(\pi/N) - \frac{1}{2} L_{SL}^2 \sin \varphi + \frac{1}{2} a^2 (\omega - \sin \omega)) \quad [3.7]$$

N	$R_0$ [ $\mu\text{m}$ ]	13 wt% PI solution			20wt% PI solution		
		a [ $\mu\text{m}$ ]	Projection $L_{LV}$ [ $\mu\text{m}$ ]	Width [ $\mu\text{m}$ ]	a [ $\mu\text{m}$ ]	Projection $L_{LV}$ [ $\mu\text{m}$ ]	Width [ $\mu\text{m}$ ]
3	6.94	4.02	5.46	3.6	4.14	4.92	3.0
4	7.91	4.32	4.03	2.5	4.45	3.26	2.5
5	8.30	4.43	2.86	1.3	4.58	1.98	2.0
6	8.50	4.49	1.99	1.0	4.65	1.05	1.7
7	8.61	4.53	1.34	0.8	4.70	0.36	1.4

**table 2** Calculation of the interfacial radius of curvature  $a$ , the projected length of the perimeter of the liquid-vapor interface (equal to  $2L_{SL} \sin(\varphi/2)$ ) and measurement of the width of the ribs in the freestanding structures for different polygonal holes and two different PI solutions.

The interfacial radius of curvature,  $a$ , that minimizes the expression for the capillary pressure given in formula 1, is calculated numerically, using the expressions in formulas 2-7.

Knowing the interfacial radius of curvature, the complete equilibrium configuration of the wetted corner is determined. The calculated dimensions can be compared to the sizes that are measured from the freestanding microstructures. The width of the ribs of the freestanding microstructures is approximated by the length  $L_{LV}$ . Table 2 lists the calculated curvature  $a$  and the projected width of the interfacial perimeter  $L_{LV}$  for two PI solutions, in comparison to the measured width of the ribs.

Evidently, the measured width of the ribs is much smaller than the size predicted by the calculation. One explanation may be the shrinkage of the polymer during the phase separation, which can reduce the width of the rib in comparison to the width of the flowing solution. Another explanation can be that the assumption of the air bubble having its equilibrium shape at the moment of solidification is not correct. Although the polymer solution flowing through the corners already fills the bottom of the hole, the equilibrium width of the wetted corner might not yet be achieved.

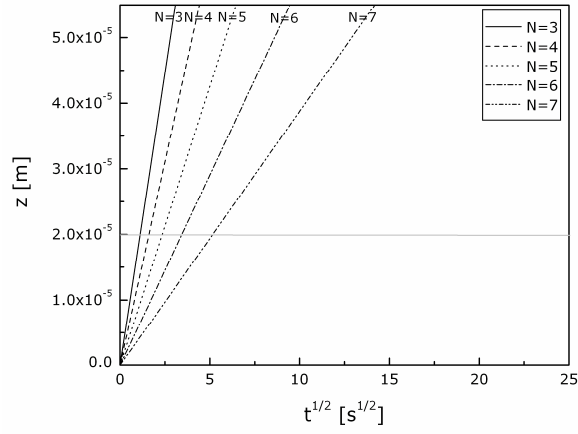
The evolution of the fluid meniscus in time, while flowing through an interior corner (not necessarily being part of a polygonal hole), is described by Weislogel *et al.*<sup>7</sup> In the case of flow through a corner of a polygon, the meniscus of the flowing fluid will rise until it reaches a certain height, marked by Weislogel *et al.* as the constant height condition. In that case, they derived for the final height of the meniscus in a polygon of  $N$  corners:

$$H = \frac{d}{2f} \frac{\sin\left(\frac{\varphi}{2} + \delta\right)}{F_a} \left[ 1 - \left( 1 - \frac{F_a \cot\left(\frac{\pi}{N}\right)}{\sin^2\left(\frac{\varphi}{2} + \delta\right)} \right)^{\frac{1}{2}} \right], \text{ in which} \quad [3.8]$$

$$\delta = \frac{\pi}{N} - \psi, \quad f = \left( \frac{\cos \psi}{\sin\left(\frac{\varphi}{2}\right)} - 1 \right)^{-1} \quad \text{and} \quad F_a = \frac{\sin^2 \delta}{\tan\left(\frac{\varphi}{2}\right)} + \sin \delta \cos \delta - \delta \quad [3.9]$$

$H$  is the height of the fluid meniscus measured from the corner, while  $d$  is the width of the sides of the polygon. The distance, which the propagating tip of the flow has traveled through the corner is dependent on the final height of the solution  $H$ , the interfacial tension  $\gamma_{LV}$ , the dynamic viscosity  $\mu$ , and a flow resistance  $F_i$ , and is given by:

a



b

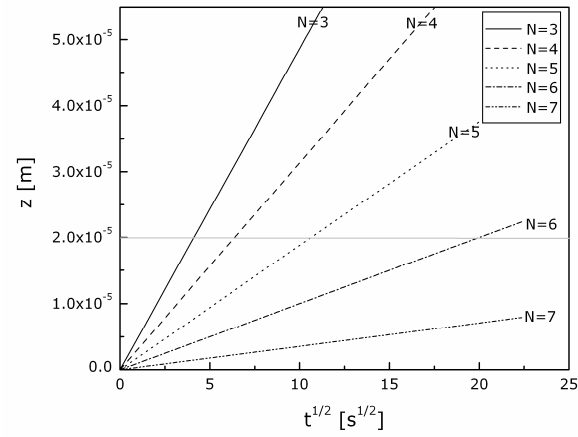


figure 7 Calculation of the position of the tip of a 13wt% (a) and a 20 wt% (b) PI solution as a function of time and amount of corners. The gray line indicates where the tip has reached the bottom of the holes (20  $\mu\text{m}$ ).

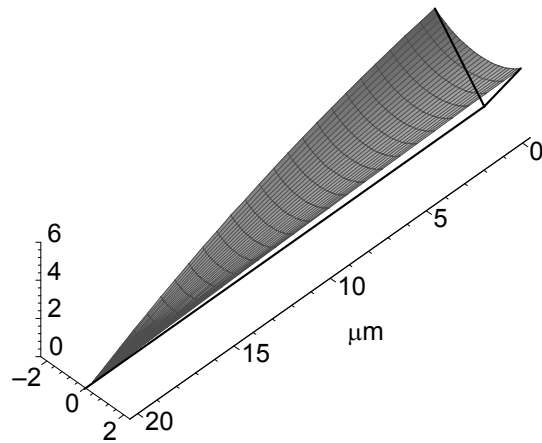
$N$	$t_{\text{down}} [s]$	$t_{\text{down}} [s]$
	13wt% PI solution	20wt% PI solution
3	1.3	16.9
4	2.6	40.7
5	5.5	113
6	11.8	400
7	26.6	3182

table 3 Calculated time after which the polymer solutions have reached the bottom of the polygonal hole as a function of amount of corners for two different PI solutions.

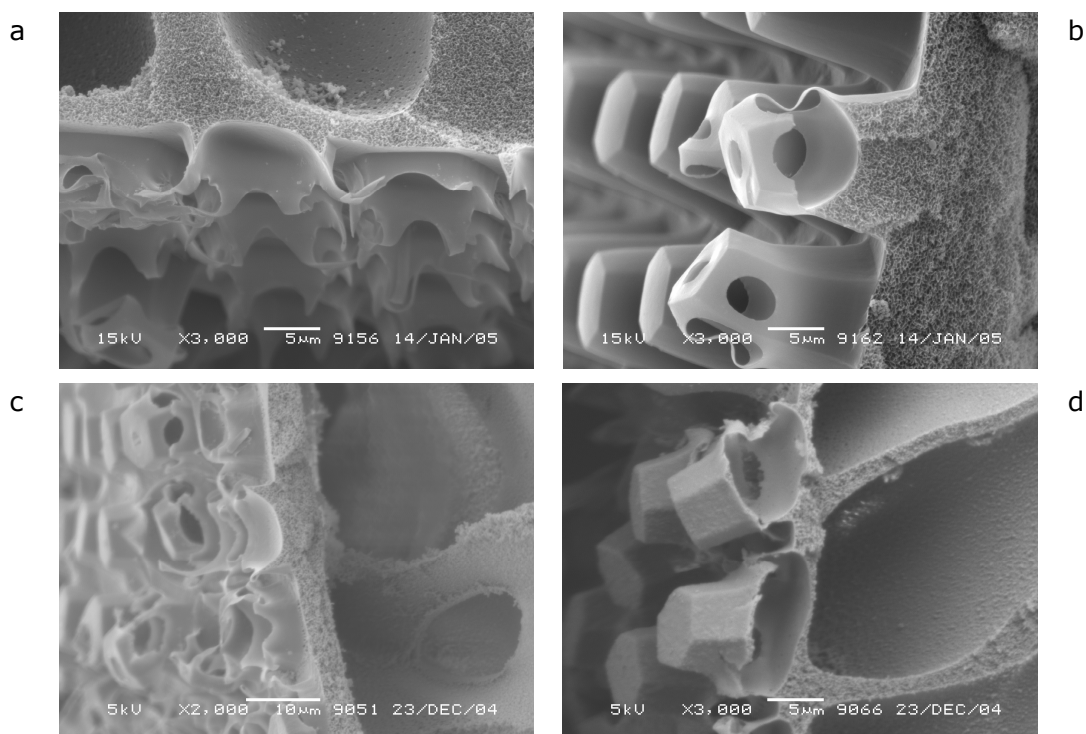
$$z(t) = 1.702 \left( \frac{\gamma_{LV} F_i \sin^2 \left( \frac{\phi}{2} \right)}{\mu f} \right)^{\frac{1}{2}} H^{\frac{1}{2}} t^{\frac{1}{2}} \quad [3.10]$$

The flow resistance  $F_i$  varies only slightly as a function of corner geometry and contact angle. Therefore the flow resistance is approximated by an intermediate constant value of  $F_i \approx 0.13$  for all geometries and contact angles considered here. This approximate value is based on a corner angle between 60 and 130 degrees for an almost wetting fluid.<sup>7,19</sup> The distance of the tip of the polymer solution as a function of time and number of corners for two different polyimide solutions is depicted in Figure 7. Table 3 resumes the calculated time required for the polymer solution to reach the bottom of the hole. To give an impression of the shape of the flowing solution, the calculated geometry of a corner flow is depicted in Figure 8 (60° corner angle).

From the calculations in Figure 7 and Table 3, it is concluded that the corner flow predicted by the model is much slower than the actual formation process (see Figure 5). The following section reflects on possible explanations for the mismatch between the corner flow model and the results.



**figure 8** Example of the geometry of a polymer solution while flowing through the corner of a polygonal hole, calculated for a triangular hole and a 13wt% PI solution at the moment the tip of the flowing solution has just reached the bottom of the hole.



**figure 9** *Cross-section of freestanding microstructures prepared from PI solutions of 20wt% (a and b) or 13 wt% (c and d) without a delay time (a and c) or with such a delay time that the microstructures reveal an advanced stage of the filling process (90 seconds for Figure 9b and 20 seconds for Figure 9d).*

### 3.4 reflection on results and model

The shape of the freestanding microstructures shows significant differences compared to the shape that is expected theoretically. As mentioned earlier, the calculated width of the liquid-vapor perimeter does not match the width of the ribs of the freestanding structure. A possible explanation is found in the shrinkage of the polymer upon solidification, or in the fact that the shape of the corner flow and the bubble might not yet have reached equilibrium.

The volume of the air bubble during the formation process is not constant, as was assumed in the calculation. Figure 9a shows a cross section of a freestanding microstructure

prepared from the highly concentrated PI solution, where the filling is almost complete. The size of the bubble is clearly reduced in comparison to the initial size (depicted in Figure 9b). Dissolution will take place to minimize the surface area of the bubble with the surrounding medium. The dissolution rate depends on the initial size of the bubble, and will be higher for smaller bubbles. For the volumes of the air bubbles discussed here, dissolution of air can account for the observed change in volume. The displacement of the boundary of the air bubble as a consequence of dissolution of air is estimated to be in the order of  $10^{-7}$  m.s<sup>-1</sup>, based on the decrease in radius of unrestricted air bubbles.<sup>20,21</sup> Indeed on the timescales on which the freestanding structures are formed, the displacement as a result of dissolution would be significant. The assumption that there is no significant change in the air volume during the filling process is therefore not correct, at least for the more concentrated polymer solution.

Another interesting aspect of the filling process is revealed when these cross sections are compared with the cross section of the structures prepared from the solution with a lower concentration (Figure 9c and 9d). The solution having the lower polymer concentration fills the hole from the bottom, pushing the air bubble upwards. The higher concentrated solution hardly moves the bubble. The bottom part of the structure, formed in the top of the hole, expands, while the top part does not show significant changes. The expansion of the bottom part of the structure is on cost of the volume of the air bubble. A possible explanation is that part of the air dissolves in the polymer solution, which becomes more apparent on the longer timescale of the more viscous polymer solution.

In some cases, the time scale, on which the freestanding microstructures form is much shorter than predicted by the cornerflow model. The calculated time deviates the most for the highly viscous solution in combination with six or seven corners. In the regime where the contact angle approaches the complementary angle ( $\psi \approx 90^\circ - \phi/2$ ), the corner flow model behaves asymptotically. The model represents a physically impossible situation for these contact angles, and therefore the model generates highly unstable predictions. In the case of the highly viscous solution, for six and seven corners the contact angle of the solution is within the unstable area of the corner flow model. In that case, small fluctuations in any variable lead to tremendous changes in the calculated time as well as the projected width of the ribs. Therefore the model is considered to be inadequate to describe the situation for the highly viscous solution and six or seven corners.

Possibly the description of the filling process needs a more advanced description, which takes into account other driving forces besides the capillary force. For instance, the

small inclination of the sidewalls of the holes was neglected. This inclination results in an asymmetric bubble, with higher curvature near the bottom of the hole. The asymmetry leads to a driving force that displaces the bubble out of the hole.

Apparently the corner flow model as it was described here does not fully match the flowing behavior of the polymer solutions. A discrepancy may be the no-slip boundary condition on which the corner flow model is founded. For polymer solutions it is reported that, as a result of the molecular behavior of non-absorptive polymers, a depletion layer may form close to a surface. In this layer the polymer chains are effectively absent. This influences the local viscosity and shear rates close to the surface, which may explain why the polymer solution flows faster than predicted for a model liquid.<sup>22</sup>

To study if the phenomenon of mismatch in timescales also applies in a less complicated system, corner flow in an open channel is studied. The use of an open channel excludes effects related to the curvature of the air bubble, gravitational and buoyancy related effects (since the channel is placed horizontally) and effects that might be caused by finite capillary length. The flow rate of the polymer solution in the corners of the square channel is determined from optical microscopy. Within 3 s the corner flow of the 13 wt% solution has travelled 500  $\mu\text{m}$ , whereas the corner flow model predicts a travelling time of 2.6 s for only 20  $\mu\text{m}$  (see table 3). Similarly, the 20 wt% solution traverses 375  $\mu\text{m}$  within 17 s, opposed to a prediction of 20  $\mu\text{m}$  in 40.7 seconds. Apparently, also in the simplified system there is a mismatch between the timescales predicted by the corner flow model and the measurements.

Although the quantitative predictions of the corner flow model are incorrect, similar trends are observed between theory and experiments for the formation of freestanding structures. The width of the ribs decreases with an increasing number of corners, which is also predicted from the corner flow model. However, for the solution of the higher polymer concentration the width of the ribs is calculated to be smaller than in the case of the lower polymer concentrations, which is not always confirmed experimentally. This discrepancy can be explained by different shrinkage of the polymer upon solidification during phase separation. This becomes less, as the polymer concentration in the solution is higher. Due to the difference in shrinkage, comparison of the width of the ribs for the different polymer solutions may be misleading as an indication for the relative width of the fluid menisci in the corner prior to phase separation.

Considering the timescales of the corner flow, the experiments confirm the trends predicted in theory. A wider angle will decrease the corner flow, as will a higher polymer concentration in the solution. In view of the qualitative similarities, it is plausible that corner



flow driven by capillary force plays an important role in the formation mechanism of the freestanding structures.

### 3.5 conclusions

Freestanding microstructures in different configurations have been prepared in a single step process by PS $\mu$ M. The evolution of the microstructures as a function of time is related to the process of fluid flow in a polygonal capillary. The shape of the freestanding microstructures and the timescale on which they evolve are compared to a theoretical model describing fluid flow in an interior corner. The corner flow model correctly predicts qualitative trends of the formation process. A smaller angle of the corner leads to a larger width of the ribs of the structure, and a faster filling of the polygonal hole. A more viscous polymer solution will slow down the filling process. However, there is a mismatch between the quantitative predictions by the corner flow model and the experimental observations. Therefore the description of the formation process of the freestanding structures requires a more advanced model. Cornerflow is a phenomenon to consider when utilizing the PS $\mu$ M process. Nevertheless, the PS $\mu$ M can be utilized for fabrication of microstructures in different freestanding configurations from several polymers in a single process step. The simplicity of the fabrication of such freestanding microstructures particularly distinguishes PS $\mu$ M from other microfabrication processes.

### 3.6 experimental

*Materials and Substrates.* The molds were prepared from silicon by standard photolithography and etching techniques. Photoresist was spun on a silicon wafer. The photoresist was exposed and developed. Subsequently the photoresist was post-baked and the underlying silicon was etched by Deep Reactive Ion Etching.

The polymers that were used for the preparation of freestanding microstructures were Polyimide (PI) (Matrimid 5218, Ciba), Polysulfone (PSf) (Ultrason P3500 NTLCD, BASF), and Polymethylmethacrylate (PMMA) ( $M_w = 350,000$ , Polysciences). However, the results mentioned here display only freestanding structures prepared from PI. The polymers were dissolved in NMP (1-methyl-2-pyrrolidinone (99%), Acros Organics) in weight percentages of 13 wt% for PI, 18.3 wt% for PSf, and 16.7 wt% for PMMA. To investigate the effect of viscosity on the formation process additionally PI

solutions of 9.1 wt%, 16.7 wt% and 20 wt% were prepared. The polymers were dissolved while stirring at ambient room temperatures (20-25 °C).

*Instrumentations.* The SEM observations were performed on a JEOL 5600 LV electron microscope. An acceleration voltage of 5 kV was applied. Previous to imaging the polymeric samples were coated with a thin layer of platinum (approximately 25 nm thick) to avoid charging of the samples. To prepare the cross-sections, the polymer was immersed in ethanol, subsequently frozen in liquid nitrogen and broken.

Contact angle measurements were performed on a Goniometer from Dataphysics (OCA 15+). Viscosity measurements were performed on a Brabender Viscotron 8024. The surface tension of the polymer solutions was determined using the Wilhelmi plate method on a Krüss Tensiometer K12.

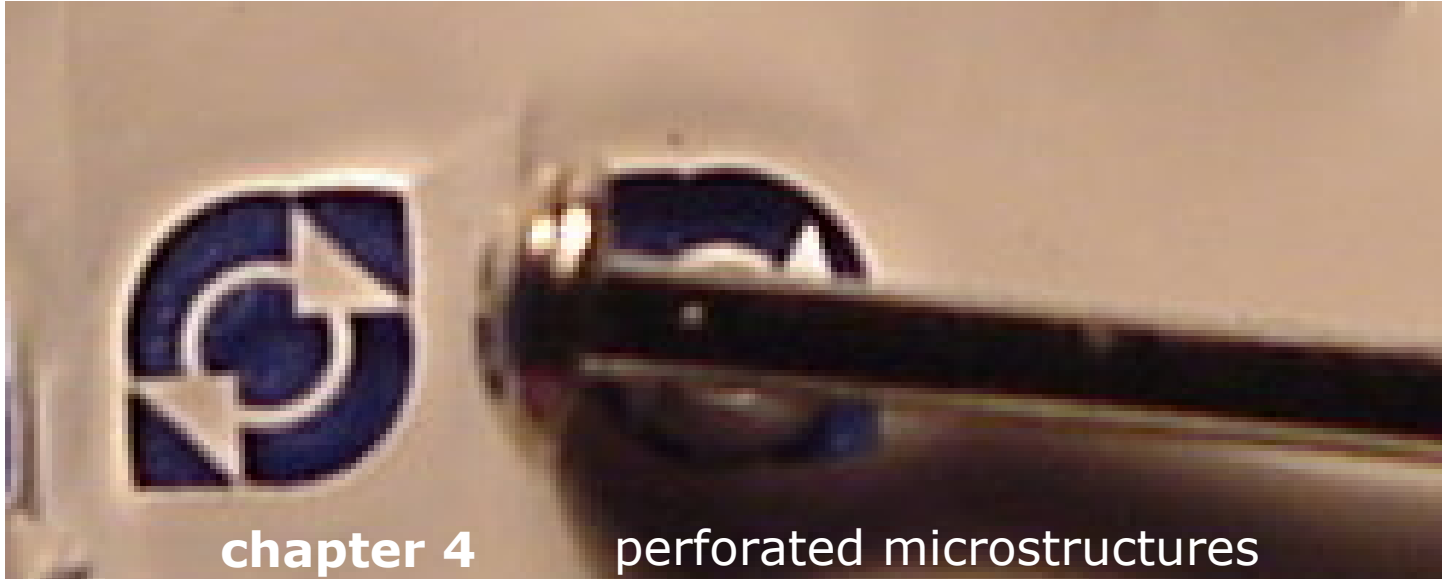
*PSUM*. The molds that were utilized for the preparation of the freestanding microstructures contained a pattern of polygonal holes. In all cases the area of the holes was kept constant, namely 250 micron squared, while the amount of corners was varied. All the molds were etched to a depth of approximately 20 micron. Due to the etching process, the sidewalls of the holes have a small inclination of approximately seven degrees.

The polymer solutions were spread out in a thin film on top of the mold using a casting knife. The casting knife was mounted in a set-up, in which the height of the blade relative to the mold could be adjusted.<sup>9</sup> The films of polymer solution were casted at a thickness of 200 micrometer. Subsequently the mold, covered with the film of polymer solution, is immersed

in tap water. Due to the exchange of solvent and non-solvent the solution phase separates and the polymer rich part solidifies. For NMP based solutions, having polymer concentrations around the values that were used here in combination with water, very fast precipitation of the polymer occurs, typically less than a second for a film thickness of 200  $\mu\text{m}$ .<sup>10</sup> The polymeric microstructured film releases from the mold after a few minutes. Then the film is kept in water for approximately 30 minutes, and dried in air. All experiments were performed in duplo.

## references

- <sup>1</sup> M. J. Madou, *Fundamentals of Microfabrication*, CRC Press, Boca Raton, U.S. **2002**.
- <sup>2</sup> Q. Xu, I. Tonks, M. J. Fuerstman, J. C. Love, G. M. Whitesides, *Nanolett*. 2004, 4, 2509.
- <sup>3</sup> S. Jeon, E. Menard, J. U. Park, J. Maria, M. Meitl, J. Zaumseil, J. A. Rogers, *Adv. Mater.* **2004**, 16, 1369.
- <sup>4</sup> E. Menard, L. Bilhaut, J. Zaumseil, J. A. Rogers, *Langmuir* **2004**, 6871.
- <sup>5</sup> J. Zaumseil, M. A. Meitl, J. W. P. Hsu, B. R. Acharya, K. W. Baldwin, Y. L. Loo, J. A. Rogers, *nano Lett.* 2003, 3, 1233.
- <sup>6</sup> T. C. Ransohoff, P. A. Gauglitz, C. J. Radke, *AIChE J.* **1987**, 33, 753.
- <sup>7</sup> M. M. Weislogel, S. Lichter, *J. Fluid Mech.* **1998**, 373, 349.
- <sup>8</sup> L. Vogelaar, J. N. Barsema, W. Nijdam, C. J. M. van Rijn, M. Wessling, *Adv. Mater.* **2003**, 15, 1385.
- <sup>9</sup> L. Vogelaar, R. G. H. Lammertink, J. N. Barsema, W. Nijdam, L. A. M. Bolhuis-Versteeg, C. J. M. van Rijn, M. Wessling, *Small* **2005**, 1, 645.
- <sup>10</sup> For similar solutions, using NMP as a solvent and water as a non-solvent, the precipitation time is determined to be less than a second. See G. R. Fernandes, J. C. Pinto, R. Nobrega, *J. Appl. Pol. Sci.* 2001, 82, 3036. On the timescale of the formation of the freestanding microstructures, the precipitation is therefore considered instantaneous.
- <sup>11</sup> Another example of insight in imbibition behavior by microfabrication: E. Kim, G. M. Whitesides, *J. Phys. Chem. B* **1997**, 101, 855, in combination with: De Gennes, P. G. In *Liquids at Interfaces*; Charvolin, J.; Joanny, J. F.; Zinn-Justin, J., Eds.; North Holland: Amsterdam, 1990; p 311.
- <sup>12</sup> H. Wong, C. J. Radke, S. Morris, *J. Fluid Mech.* 1995, 292, 71.
- <sup>13</sup> H. Wong, C. J. Radke, S. Morris, *J. Fluid Mech.* 1995, 292, 95.
- <sup>14</sup> R. P. Mayer, R. A. Stowe, *J. Colloid Interface Sci.* **1965**, 20, 893.
- <sup>15</sup> B. J. Legait, *Colloid Interface Sci.* **1983**, 96, 28.
- <sup>16</sup> G. Mason, N. R. Morrow, *J. Colloid Interface Sci* **1991**, 141, 262.
- <sup>17</sup> A. Mazouchi, G. M. Homsy, *Phys. Fluids* **2001**, 13, 1594.
- <sup>18</sup> K. Rejmer, S. Dietrich, M. Napiorkowski, *Phys. Rev. E* **1999**, 60, 4027.
- <sup>19</sup> T. C. Ransohoff, C. J. Radke, *J. Colloid Interface Sci.* **1988**, 121, 392.
- <sup>20</sup> W. S. Chen, T. J. Matula, L. A. Crum, *Ultrasound Med. Biol.* **2002**, 28, 793.
- <sup>21</sup> P. S. Epstein, M. S. Plesset, *J. Chem. Physics* **1950**, 18, 1505.
- <sup>22</sup> R. Tuinier, T. Taniguchi, *J. Phys. Condens. Matter* **2005**, 17, L9.



## chapter 4      perforated microstructures

prepared by phase separation micro molding:  
application as polymeric microsieves and  
free standing polymeric etch and deposition masks

*L. Vogelaar*

*R. G. H. Lammertink*

*J. N. Barsema*

*C. J. M. van Rijn*

*M. Wessling*

Perforated polymer microstructures can be realized by PS $\mu$ M as a consequence of the shrinkage, which takes place during the solidification. Perforation is promoted by the inclusion of volatile additives and the inclusion of a lipophilic surfactant. PS $\mu$ M was exploited to fabricate a polymeric microsieve, a microfiltration membrane with very sharp size discrimination and very high fluxes (approximately two orders of magnitude higher than comparable microfiltration membranes). Furthermore the use of perforated microstructures as free standing etch and deposition masks is demonstrated. An additional heat treatment, causing collapse of the intrinsic porosity and further uniform shrinkage, enables progress to feature sizes, which are substantially smaller than previously demonstrated for free standing masks.

*Parts of this chapter have been published previously in Small and Advanced Materials.<sup>1,2</sup>  
Above: perforated microstructure having the size of the head of the pin next to it.*

# 4

## 4.1 introduction

A wide variety of microscale replication methods have been described in recent years (see also chapter 1).<sup>3,4</sup> These technologies include for example hot embossing,<sup>5</sup> nano imprint and soft lithography.<sup>6,7</sup> Replication can provide economic advantages, and the variety in choice of materials is greatly expanded. One recently reported replication method is phase separation micromolding (PS $\mu$ M) (see also chapter 2).<sup>1,2</sup> The method relies on phase separation of a polymer solution in contact with a microstructured mold when exposed to a non-solvent.

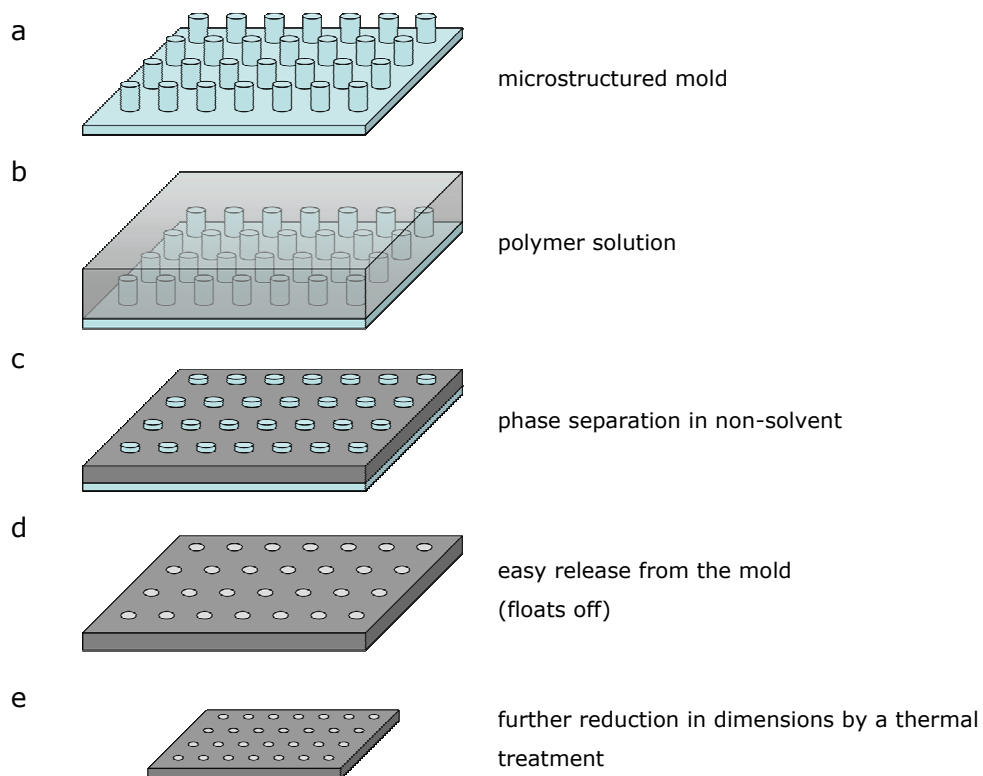
A major advantage of phase separation micromolding over existing replication methods is that it immensely expands the diversity in materials to choose from. Furthermore, PS $\mu$ M enables fabrication of porous, microstructured films, which was previously inaccessible in microfabrication. Another benefit of this method is the simple release of the material from the mold after phase separation, due to a small amount of intrinsic shrinkage. Often the polymer films simply float off, allowing the preparation of very thin structured films. Preparation of perforated structures was demonstrated using this method as well.<sup>1</sup>

This chapter will go into detail on the preparation of perforated microstructures. Furthermore, the application of such perforated (completely open or ‘through’) microstructures is illustrated on the hand of two examples: polymeric microsieves and freestanding polymeric etch and deposition mask. Furthermore a heat treatment of a porous, microstructured film can lead to uniform size reduction of the microstructures.

## 4.2 perforation process

As mentioned earlier, the shrinkage in PS $\mu$ M is responsible for the very easy fabrication of perforated structures (see chapter 2). During the phase separation the polymer contracts and pulls itself in the direction of the mold features. When the layer of polymer solution is applied just above the mold features, the mold can perforate the polymer, creating the through structure.

Figure 1a-d depicts a schematic representation of the preparation of a perforated microstructure by phase separation micro molding. A layer of polymer solution is applied on the mold, so that the highest features of the mold are just submerged. The solution is immersed in a non-solvent, where the exchange of solvent and non-solvent causes the



**figure 1** Schematic representation of the phase separation micromolding process, with additional isotropic shrinkage.

**a** Microstructured mold containing pillars.

**b** A polymer solution is cast onto the substrate.

**c** The substrate with the polymer solution is placed in a non-solvent bath, during which the polymer phase separates and shrinks. The mold perforates the polymer.

**d** The perforated polymer film is easily released from the mold.

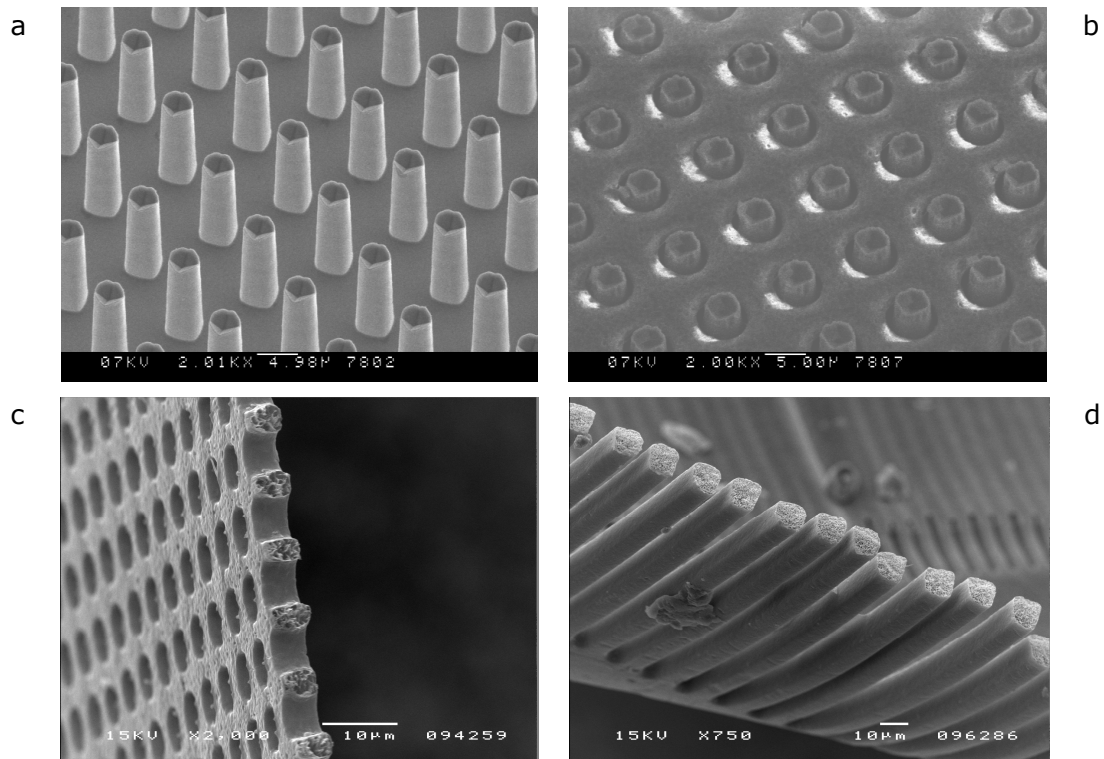
**e** Additional heating results in isotropic shrinkage of the polymer film, while maintaining the shape of the microstructures.

polymer to solidify, i.e. subjected to liquid induced phase separation. During the phase separation the polymer shrinks, mainly in the direction normal to the substrate surface.<sup>8</sup> Control of the casting thickness and amount of shrinkage allows perforation of the polymer film, creating a freestanding, completely open, ‘through’ microstructure. The very easy release conditions of the polymeric replica from the mold are also attributed to the shrinkage, taking place during the solidification.<sup>1,2</sup>

PS $\mu$ M gives rise to very facile fabrication of perforated microstructures. When using photolithography and etching the fabrication of such structures requires multiple lithographic steps,<sup>9,10,11</sup> boosting the fabrication costs. When soft lithography is applied the structure needs to be peeled off the mold, setting high demands on the mechanical strength.<sup>12,13</sup> Therefore the structured film cannot be too thin (typically not thinner than five micrometer) and the minimal dimension of the perforation pattern is restricted (approximately 5 micrometer).<sup>13</sup> Consequently, it takes a very high aspect ratio of the mold structure when a thick film is required in combination with a small perforation feature size. In PS $\mu$ M the structure is already loose from the mold, so hardly any force is needed and thus the thickness of the film is less restricted. As exhibited in Figure 2, a perforated structure can be fabricated in a film of only a few micrometer thickness. Figure 2 a-c also depict how the structure is formed on the mold.

In the case of a very fast demixing process, a skin is formed at the interface between non-solvent and polymer when the polymer solution is submerged in the non-solvent bath. The skin can hinder the perforation by the mold. Nevertheless, if the phase separation is performed in a two-step process of vapor induced phase separation and subsequent liquid induced phase separation, similar to the process described to prevent macrovoid formation in chapter 2, the formation of a skin can be reduced and a perforated structure can be created.

To fabricate a perforated microstructure, the highest mold features should only be submerged by a few micrometers of polymer solution. For this, accurate positioning of the casting knife is required. Accordingly, contact with the fragile mold features is not necessary. The risk of damaging the mold is of course higher when the solution is applied nearer to the mold features. To avoid this risk and still be able to perforate the microstructure, the solution can be applied at greater distance from the mold features when a volatile component is included. The casting knife then spreads the layer of polymer solution at a higher level, thus preventing possible damage of the mold e.g. by particles which are dragged into the solution. After the solution is applied on the mold, the volatile additive is left some time to evaporate prior to the immersion in the non-solvent bath. The level of the



**figure 2** *Fabrication and two examples of a perforated microstructure by PS $\mu$ M.*

**a** *Mold with a 5 micrometer wide and 20 micrometer high pillar pattern on its surface.*

**b** *The polymeric replica on the mold, after phase separation and prior to release. Because of the shrinkage of the polymer layer towards the mold during the phase separation the pillars have perforated the polymer.*

**c** *Perforated polyimide microstructure after release from the mold. The cross section was made for illustrative purpose.*

**d** *Example of a perforated microstructure of lines, prepared from polyethersulfone. The cross section is for illustrative purpose.*

solution will lower during this evaporation. The shrinkage during the phase separation will finally make the free surface of the polymer sink below the top level of the mold, resulting in a perforated structure. Due to observation of edges of tearing of solid polymer in partly successful perforations by SEM we ascribe the formation of open microstructures to perforation of the solidifying polymer. Optical microscope inspection proves that evaporation of a volatile solvent only is not sufficient to fabricate perforated microstructures.

Only the combination of evaporation and subsequent liquid induced phase separation causes the perforation of the polymer.<sup>2</sup>

We observed that the addition of the lipophilic surfactant Span-80 improves the perforation of the film by the mold, even at very low weight percentages of the surfactant. Addition of Span-80 suppresses macrovoid formation<sup>14</sup> and yields a more compact membrane structure, leading to an increase in mechanical strength.<sup>15</sup>

### 4.2 polymeric microsieve

The perforated polymeric thin film, which is depicted in Figure 2c, can readily be used as a polymeric microsieve. A microsieve is a thin filtration membrane with a regularly distributed pore pattern.<sup>9,10,16</sup> It combines accurate size discrimination with high fluxes. Since the selective layer is very thin (approximately 1-5 micron) and highly porous, the clean water flux of the microsieve depicted in Figure 2c is measured to be one million l/(h.bar.m<sup>2</sup>), which is two orders of magnitude higher than comparable microfiltration membranes currently used. Until now this device is fabricated out of silicon-based materials by multiple lithographic steps and subsequent etching, and is therefore expensive in comparison to other microfiltration membranes. A 'ready to use' polymeric microsieve can be fabricated at once by applying PS $\mu$ M, in combination with the earlier mentioned evaporation step of a volatile additive. The costs of the microsieve produced with PS $\mu$ M in a mass fabrication process will hardly differ from the costs of normal microfiltration membranes. For the fabrication of microsieves PS $\mu$ M is clearly a good, yet cheap alternative to the costly present fabrication process. Moreover PS $\mu$ M expands the range of materials from which the microsieve can be prepared. The material can then be selected and optimised for the filtration process.

### 4.3 freestanding etch and deposition mask

Here we report on the application of phase separation micromolding to prepare perforated polymer films that are subsequently exploited as dry etch masks and lift-off masks. As an additional feature, we demonstrate that a heat treatment of a porous microstructured film causes additional isotropic shrinkage of the polymer film, which allows one to prepare structures with dimensions more than twice as small as the original mask.



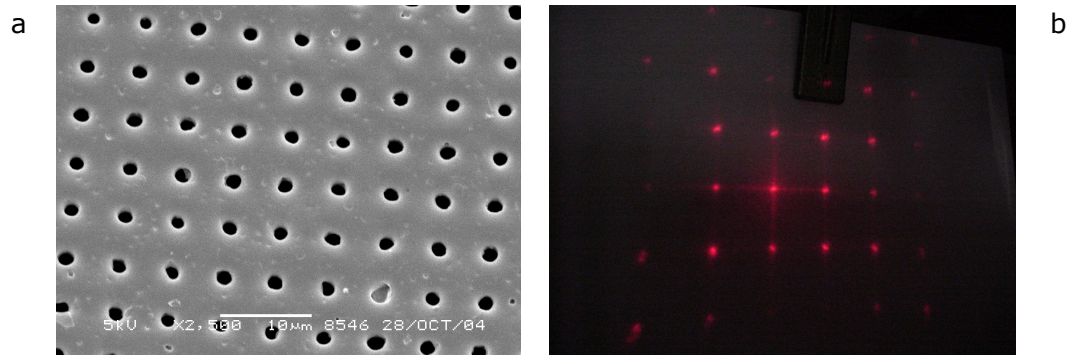
Previously, elastomeric membranes containing well-defined structures have been prepared and used as shadow masks.<sup>17</sup> Their fabrication includes spincoating of a prepolymer mixture on a microstructured substrate, followed by curing. After curing, the resulting elastomer can be carefully peeled off the substrate. This method has been successfully used to fabricate masks that, amongst others, were employed for selective deposition of catalyst and electrode materials on a PEM fuel cell membrane.<sup>18</sup> Although this is a powerful process to create a perforated elastomeric film that can serve as an etch resist or shadow mask, the limited mechanical stability, especially for films thinner than 50  $\mu\text{m}$ , is a major drawback concerning the release from the mold. Thicker films of course will enhance the mechanical stability but will, consequently, put more stringent requirements on the mold design. Smaller features and thicker films mean higher aspect ratios of the microstructured mold, which is not always possible due to limitations in the mold fabrication process. Moreover, high aspect ratio structures make the mold more fragile. In PS $\mu\text{M}$  the easy release from the mold ensures that hardly any force is needed and thus the thickness of the film is less restricted.

Decal transfer microlithography (DTM), was described by Nuzzo *et al.* to pattern a substrate by releasing a thin PDMS membrane mask from a patterned PDMS decal stamp.<sup>19</sup> This release could either be performed by cohesive mechanical failure, where the masks were physically torn from the decal, or by selective pattern release, in which case the release properties of the decal were adjusted by incorporation of a “No Stick” interface. Although this method allows generation of features at a smaller length scale, the process is more complicated than other methods to prepare polymeric shadow-masks.

Another approach to fabricate a polymeric shadow-mask membrane is the application of SU-8 based photoplastic resist.<sup>20</sup> The composition of this formulation was adapted in order to reduce the stress that is generated during the crosslinking step. For thin and fragile membranes, a sacrificial layer had to be used in order to successfully remove the membrane from its support. It must be noted that this method still requires UV exposure of the SU-8 layer to define the structure and can therefore not be considered as a replication method.

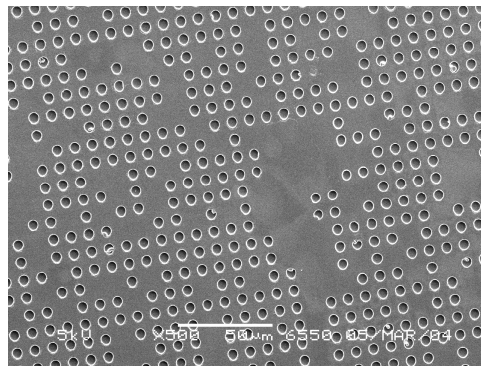
Nanostencils prepared by silicon micro machining are also used as a dry resist for direct patterning by deposition.<sup>21</sup> Although the deposition is accurate even on a scale of several hundred nanometers, the nanostencils have a few limitations in comparison to polymeric masks. Due to their high fabrication costs the nanostencils have to be reused to make the process economically feasible. Furthermore, direct conformal contact between the stencil and the substrate is not possible, which complicates the process.

## chapter 4



**figure 3a** SEM image of a dense perforated film, formed after a heating program. The untreated film had a pattern of holes with a width of 4 micron and a spacing of 9.5 micron, while the dimensions of the film after the heat treatment are 1.3 micron and 5 micron respectively. Due to the heat treatment the previously turbid film has become transparent, indicating that the pores in the film have collapsed.

**b** Photograph of optical diffraction of monochromatic red light through the structure depicted in Figure 3a. The diffraction reveals that the overall periodicity of the structure is maintained throughout the entire film, and therefore the reduction in size by the heat treatment is uniform. The overall shrinkage is determined from the pattern to be as high as 47%. However, the holes in the film are reduced in size even further, as can be observed in Figure 3a.

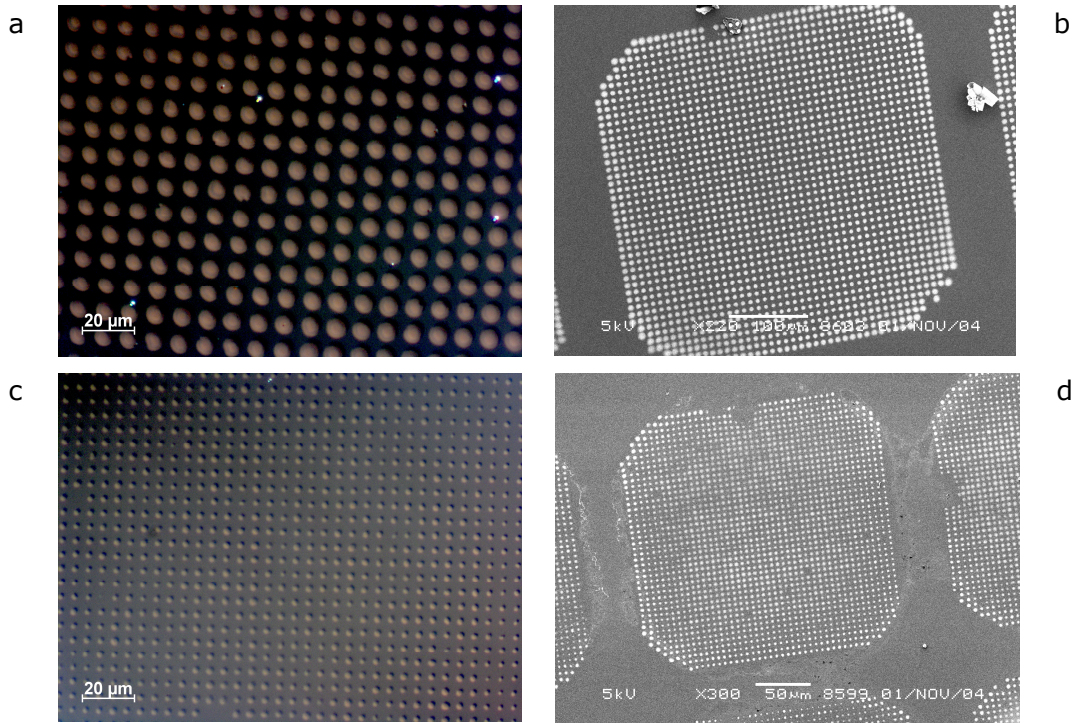


**figure 4** SEM images of a dry etched silicon substrate using a Polyimide etch mask. The mask consisted of an arbitrary hole pattern.

Using phase separation micromolding, the free-standing microstructured films can be prepared out of a wide range of materials. Depending on the parameters of the phase separation process (e.g. composition of the solution and non-solvent), it is possible to prepare microstructures with an intrinsic porosity. The presence of porosity can be seen visually by the turbidity of the film and is also illustrated by SEM images in figure 2. The phase separation process allows one to control the porosity of the polymer film. An example is the incorporation of a non-solvent vapor prior to immersion in non-solvent, as mentioned before.

When we expose a porous polymer film to a controlled heat program, a reduction in porosity can be obtained, eventually leading to a dense film. A schematic representation is depicted in Figure 1e. A typical result is illustrated in Figure 3a. When the polymer microstructure is subjected to a temperature slightly above the glass transition temperature, the polymer becomes increasingly mobile and the interior submicrometer pores collapse. Collapse of the porous interior of the microstructured film precedes the collapsing of the actual microstructure. This is a direct consequence of the curvature of the porous interior, which is evidently higher than the curvature of the microstructure. Due to the high homogeneity of the pore distribution in the interior of the film, the deformation accompanying the pore collapse is very uniform. Therefore, the film dimensions shrink isotropically during densification, while keeping the microstructure in tact. This procedure is clearly beneficial to obtain even smaller perforated structured films. Depending on the heat treatment the reduction in size of the perforations in the film can be even higher than the overall shrinkage of the film, as is demonstrated in figure 3. Although the overall shrinkage of the film is 47%, the perforations are reduced in size by approximately 65%. A possible explanation is that once all the interior pores have collapsed, the polymer, which is still mobile, will continue to minimize the surface area by reducing the size of the microstructures. Nevertheless, the shrinkage of the perforations was also uniform and the shape of the microstructures was not disrupted by the heat treatment. A similar heat treatment in the case of the polymeric microsieve would mean a reduction of the pore size, shifting the filtration cut-off towards smaller sizes.

To prove that the shrinkage in the heat treatment is uniform across the entire film, we reduced a structure with a periodic hole pattern almost a factor 2 in size. As a consequence of the periodicity of the pattern, it is possible to detect non-uniformity on a larger scale by optical diffraction. If the shrinkage is non-uniform, the large-scale periodicity is not maintained, which will be revealed by a change in the optical diffraction of the



**figure 5** *Optical microscope images (a and c) and SEM images (b and d) of gold patterns on a silicon substrate obtained by evaporation using a Polyethersulfone lift-off mask. The mask used in figure 5c (same sample as 5d) was a similar mask as used in figure 5a (same sample as 5b), subjected to a heat treatment in which an overall shrinkage of 47% was realized. The resulting dots have a width of 2 micron.*

structure. However the diffraction pattern, as depicted in Figure 3b, was similar throughout the entire surface of the microstructure, which extended over an area of a few centimeters squared. The reduction in size does not involve unwanted deformations of the periodicity of the microstructure on a larger scale. On a smaller scale, observations by SEM and optical microscopy do also not reveal any defects or deformation of the structure.

The perforated microstructures were applied on silicon to serve as a mask for deposition or etching. The application of the mask on the silicon substrate is optimized by wetting the polymer, e.g. with water or ethanol. The mask is dried while clamped in between the silicon and a flat non-sticking material, e.g. a glass or Teflon coated slide (depending on the material of the mask), to enhance the contact between the polymer and the silicon.

After the polymer is applied on the substrate, it can directly be used as a shadow

mask for etching or deposition. Etching of silicon, underlying such a shadow mask, was demonstrated in a dry etching process (see Figure 4). Two materials were used as an etch mask, namely Polyethersulfone and Polyimide. The masks withstand the etching reasonably well, while only the top layer showed considerable damage. Also the adherence of the masks on the silicon during the etching does not decay. Afterwards the masks could easily be peeled off the substrate. In the case of the dry etching of silicon, the least damage was observed for the Polyimide mask. Since PS $\mu$ M is applicable on several materials, the etch mask can be selected on the resistance against a specific etching process.

Deposition of materials through the microstructures was performed as well. Figure 5a depicts a pattern of gold dots, deposited on silicon by sputtering through a Polyethersulfone mask. The width of the dots is as small as 5 micrometer, which is already comparable with the minimum feature size that can be achieved using a PDMS shadow mask.<sup>13</sup> When the mask is subjected to a heat treatment, the width of the dots of the sputtered pattern reduces to 2 micrometer as observed by SEM and optical microscopy (see Figure 5b).

## 4.4 conclusion

PS $\mu$ M proves to be an easy and reliable method to fabricate perforated, ‘through’ polymer microstructures. The fabrication of a polymeric microsieve was demonstrated. Freestanding polymeric masks were also prepared by PS $\mu$ M and utilized for etching and deposition. PS $\mu$ M allows a large freedom in choice of the material, and therefore enables tailoring of the mask material to either the filtration process in the case of the microsieve, or the etching or deposition process in the case of the masks. The easy release of the films from the mold makes the demands on mechanical strength and therefore thickness of the microstructured films less stringent. This possibility facilitates the fabrication of perforated microstructures with smaller feature sizes (e.g. 5 micron holes).

Controlled collapse of the inner porosity in an additional heat treatment of the polymer results in a uniform shrinkage. A size reduction of the microstructure up to 65% was demonstrated. As a final remark, it should be noted that even though the minimum feature sizes reported here (namely 1.3 micron) are already below the limits of comparable polymeric etch and deposition masks, the boundaries of PS $\mu$ M considering perforated films have not fully been explored yet. Therefore it might well be possible to reduce the dimensions even further, below the micrometer regime.

## 4.5 experimental

Preparation of porous microstructured films was realized on molds, which were prepared by photolithography and silicon micro machining. For details on the mold preparation see reference 1 and chapter 2. The masks were prepared either from Polyimide (Matrimid 5218, Ciba) or Polyethersulfone (Ultrason E6020 P, BASF). The solutions consisted from polymer, NMP (1-methyl-2-pyrrolidinone (99%), Acros) as a solvent, acetone (Merck) as a volatile additive and a surfactant (Span 80, Fluka) in a ratio of 9.8 wt%, 49 wt%, 39.2 wt% and 2.0 wt% respectively for the Polyethersulfone solution, and 7.7 wt%, 51.3 wt%, 41.0 wt% and 0.0 wt% for Polyimide. After application of the solution on a mold the volatile additive was allowed to evaporate for 1 minute. Meanwhile the solution was exposed to a water vapor saturated nitrogen environment (temperature of 30 °C and a relative humidity of 90%) to improve the homogeneity of the resulting pore morphology, in which the solution became turbid. Subsequently the mold and solution were immersed in a water non-solvent bath, and the microstructured polymer mask could be easily released from the mold after a few minutes.

To attach the polymer masks to silicon substrates, the films were wetted in ethanol or water and clamped between the silicon surface and a glass slide (for dense polyethersulfone) or a Teflon coated slide (for porous Polyethersulfone and Polyimide). The ethanol or water was allowed to evaporate for 2 to 3 hours at room temperature, after which the slides were removed.

Densification of porous microstructured films of Polyethersulfone was performed by heating up to 250 °C, starting from room temperature. For this purpose a Carbolite ® TZF 12/100 high temperature tube furnace, mounted with an Eurotherm 2408CP temperature controller was used. Initially, the polymer was heated up with a speed of 50 °C/min, until a

temperature of 150 °C was reached. The polymer was kept at 150 °C for 15 minutes, after which the heating was resumed at a speed of 5 °C/min. After the polymer was kept at 250 °C for 30 minutes, it was quenched to room temperature. The heat treatment was performed in an N<sub>2</sub> atmosphere with an N<sub>2</sub> flow of 10 cm<sup>3</sup>/min.

Dry etching was performed using an Elektrotech PF 340 system. The substrate temperature was set to 10 °C and the chamber pressure was maintained at 75 mTorr. A gas mixture of SF<sub>6</sub> (30 sccm), CHF<sub>3</sub> (25 sccm), and O<sub>2</sub> (20 sccm) was used for the plasma, which was generated using 60W power. Under these conditions, the silicon is etched at a rate of approximately 450 nm/min. The etching was performed for 10 minutes, using a Polyethersulfone or a Polyimide mask.

Gold evaporation was performed on a Balzers SCD 040 coater. The sputtering was performed at a current of 15 mA for 40 minutes, resulting in an approximate gold layer thickness of 500 nm.

SEM experiments were performed on a Jeol JSM 5600 LV. An operation voltage of 5kV was used.

Optical microscope images were taken on a Zeiss Axiovert 40 MAT Optical microscope. Differential interference contrast (DIC) was used to enhance the visibility of the gold dot pattern depicted in Figure 5.

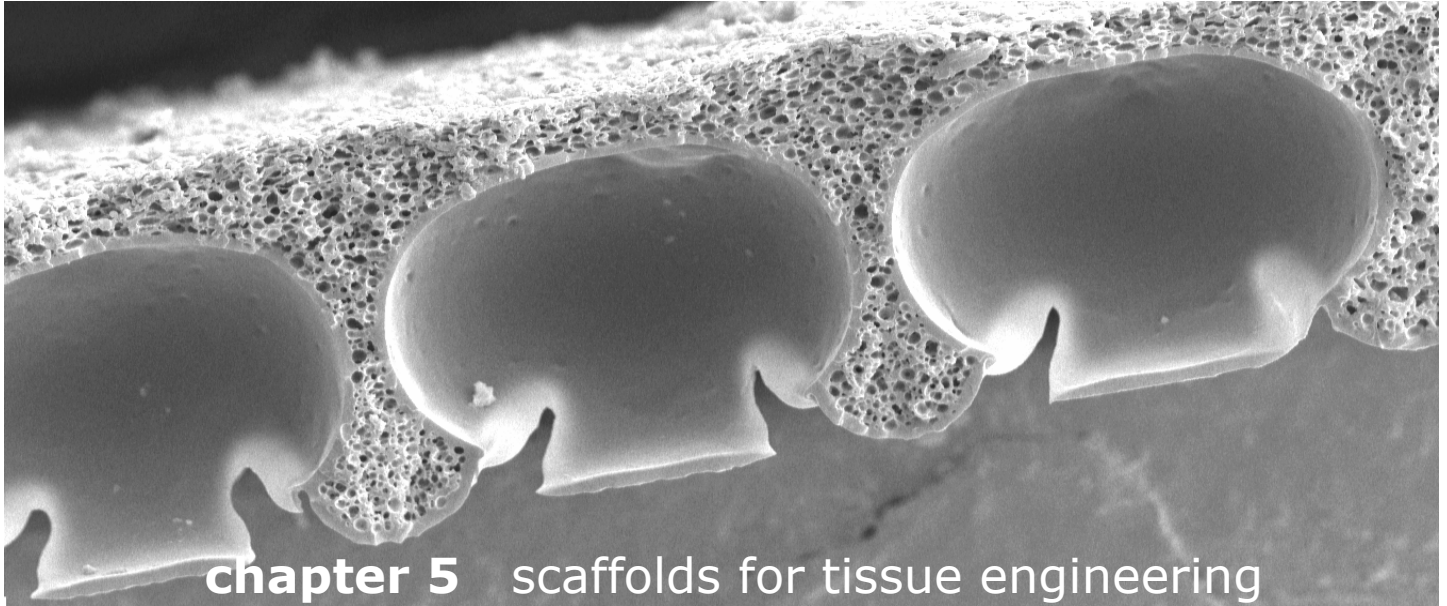
The set-up for optical diffraction consisted of a laser pointer (wavelength in between 645-665 nm), which was pointed on a Polyethersulfone microstructure having a periodic hole pattern. The diffraction pattern was projected on a white screen placed at a distance of 22.8 cm from the microstructure. From the distance between the maxima of the pattern (1.6 cm for a structure, which was not subjected to a heat treatment and 3.0 cm for a treated structure) the overall shrinkage of the polymer in the heat treatment was calculated to be 47 %.

## references

- <sup>1</sup> L. Vogelaar, R. G. H. Lammertink, J. N. Barsema, W. Nijdam, L. A. M. Bolhuis-Versteeg, C. J. M. van Rijn, M. Wessling, *Small* **2005**, *1*, 645.
- <sup>2</sup> L. Vogelaar, J. N. Barsema, W. Nijdam, C. J. M. van Rijn, M. Wessling, *Adv. Mater.* **2003**, *15*, 1385.
- <sup>3</sup> Y. Xia, J. A. Rogers, K. E. Paul, G. M. Whitesides, *Chem. Rev.* **1999**, *99*, 1823
- <sup>4</sup> M. Geissler, Y. Xia, *Adv. Mater.* **2004**, *16*, 1249
- <sup>5</sup> M. Hecke, W. K. Schomburg, *J. Micromech. Microeng.* **2003**, *14*, R1
- <sup>6</sup> S. R. Quake, A. Scherer, *Science* **2000**, *290*, 1536
- <sup>7</sup> Y. Xia, G. M. Whitesides, *Angew. Chem. Int. Ed.* **1998**, *37*, 550
- <sup>8</sup> C. Stropnik, V. Musil, M. Brumen, *Polymer* **2000**, *41*, 9227.
- <sup>9</sup> S. Kuiper, C. J. M. van Rijn, W. Nijdam, M. C. Elwenspoek, *J. Membr. Sci.* **1998**, *150*, 1.
- <sup>10</sup> C. J. M. van Rijn, G. J. Veldhuis, S. Kuiper, *Nanotechnology* **1998**, *9*, 343.
- <sup>11</sup> L. Leoni, T. A. Desai, *IEEE Trans. Biomed. Eng.* **2001**, *48*, 1335.
- <sup>12</sup> E. Ostuni, R. Kane, C. S. Chen, D. E. Ingber, G. M. Whitesides, *Langmuir* **2000**, *16*, 7811.
- <sup>13</sup> R. J. Jackman, D. C. Duffy, O. Cherniavskaya, G. M. Whitesides, *Langmuir* **1999**, *15*, 2973.
- <sup>14</sup> D. M. Wang, F. C. Lin, T. T. Wu, J. Y. Lai, *J. Membr. Sci.* **1998**, *142*, 191.
- <sup>15</sup> H. A. Tsai, D. H. Huang, R. C. Ruan, J. Y. Lai, *Ind. Eng. Chem. Res.* **2001**, *40*, 5917.
- <sup>16</sup> C. J. M. van Rijn, W. Nijdam, S. Kuiper *et al.*, *J. Micromech. Microeng.* **1999**, *9*, 170
- <sup>17</sup> D. C. Duffy, R. J. Jackman, K. M. Vaeth, K. F. Jensen, G. M. Whitesides, *Adv. Mater.* **1999**, *11*, 546.
- <sup>18</sup> K. Shah, W. C. Shin, R. S. Besser, *J. Power Sources* **2003**, *123*, 172.
- <sup>19</sup> W. R. Childs, R. G. Nuzzo, *J. Am. Chem. Soc.* **2002**, *124*, 13583.
- <sup>20</sup> G. Kim, B. Kim, J. Brugger, *Sens. Act. A* **2003**, *107*, 132.
- <sup>21</sup> M. Kölbl, R. W. Tjerkstra, G. Kim, J. Brugger, C. J. M. van Rijn, W. Nijdam, J. Huskens, D. N. Reinhoudt, *Adv. Funct. Mater.* **2003**, *13*, 219.







## chapter 5 scaffolds for tissue engineering

prepared by phase separation micro molding

*L. Vogelaar*

*B. J. Papenburg*

*A. A. Poot*

*D. W. Grijpma*

*R. G. H. Lammertink*

*D. Stamatialis*

*M. Wessling*

In a tissue engineering scaffold, porous microstructures prepared from a biodegradable polymer can combine the possibility of directional cell growth with sufficient transport of nutrients. Using Phase Separation Micro Molding (PS $\mu$ M) highly porous microstructures are prepared from poly(lactic acid). Diffusion of glucose through the microstructures is measured. Cell culturing experiments reveal that cells proliferate well on the microstructures. The cells have a slight tendency to grow in the channels of the microstructures, which is promising for directional growth. The microstructures prepared by PS $\mu$ M are suitable candidates for tissue engineering provided the interconnectivity of the pores is increased.

*Above: Air bubbles encapsulated in a microstructure of poly(lactic acid).*

# 5

## 5.1 introduction

In tissue engineering, life sciences and engineering are combined to understand and develop biological replacements to restore, maintain or improve tissue functions.<sup>1</sup> Engineered tissues presently reported are e.g. skin, cartilage and arteries. Tissue engineering focuses on construction of replacements in vitro. A tissue replacement is grown under optimized conditions from autogenic tissue, herewith providing a transplant stemming from the patients own cell material. Such a transplant could be advantageous compared to allogenic tissue (stemming from a donor), because of absence of problems like rejection and pathogen transmission.

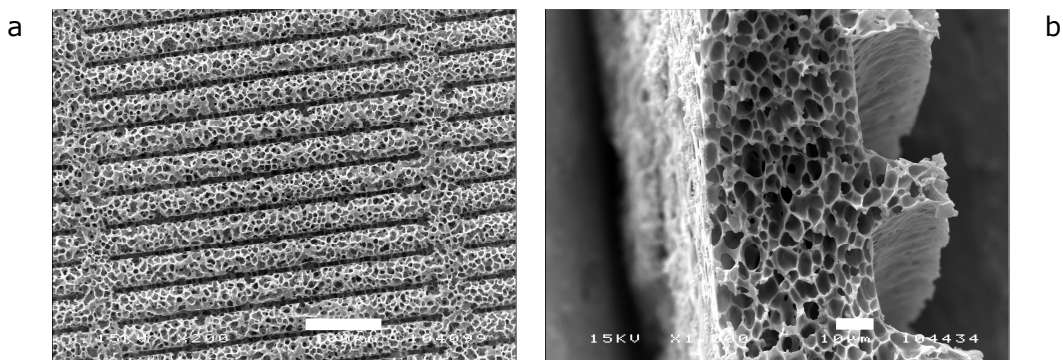
Cells of the desired type are isolated from living tissue and cultured on a scaffold: an open, porous structure prepared from a natural or synthetic material. The scaffold mimics the extracellular matrix, a mesh-like substance between the cells, which promotes proliferation and provides a supporting structure to which cells adhere in natural tissue. The scaffold containing the cells is preserved in vitro under optimized conditions until the cells have multiplied to a certain amount. Subsequently the construct is transplanted.

To prevent an inflammatory response after transplantation, the scaffold should be prepared from a biocompatible material. Construction of the scaffold from a material that is in addition biodegradable allows the cells to build their own extracellular matrix while the scaffolds degrades, which is preferable over a permanent scaffold. For the cells to proliferate it is very important that nutrients and oxygen can be transported through the scaffold towards the cells.<sup>2</sup> In return, carbon dioxide and other secretion products must find their way out of the scaffold. A high porosity of the scaffold material, which can guarantee sufficient transport, is therefore essential. Eventually, the scaffold should provide the possibility of blood vessel growth (angiogenesis) to accommodate permanent nutrient supply. In addition, the expanding cell culture in the scaffold should not block the transport of nutrients in the long term. Techniques that are presently most in use to achieve highly porous scaffolds from biomaterials for the purpose of tissue engineering are e.g. salt particulate leaching, thermally induced phase separation, solution casting, high pressure gas foaming and direct printing.<sup>3,4,5</sup>

In the engineering of tissues that host multiple cell types and require precisely defined cell-cell and cell-substrate interactions, it is vital to have control over the spatial organization of cells.<sup>6,7,8</sup> Examples of tissues where the adequate functioning of the tissue depends on controlled orientation are retinal, nerve, cardiac and vascular tissues.<sup>9,10,11</sup>

Essential is that the controlled *in vitro* conditions simulate the *in vivo* environment. Directional growth can be achieved by spatial patterning of the scaffold material, with a resolution typically in the micrometer scale.<sup>12</sup> Microfabrication techniques like soft lithography, injection molding or photolithography have been applied to achieve this spatial control over cell growth.<sup>13,14,15,16,17</sup>

Combining the above-mentioned requirements, for the engineering of certain types of tissues it would be ideal to have a scaffold, prepared from a biocompatible, biodegradable material, that can combine directional growth with sufficient nutrient transport. The techniques that are normally used for the preparation of scaffolds, which are porous and therefore allow nutrient transport, do currently not incorporate microfabrication, which is necessary for directional growth. Meanwhile soft lithography and photolithography are applicable on a limited amount of materials, which are generally not biodegradable.<sup>18</sup> Moreover these techniques yield dense substrates, that will retain nutrients when used as a scaffold in a three dimensional configuration.



**figure 1** *Examples of highly porous microstructures prepared from PLLA.*

**a** *Structured side of a microstructure prepared from a 5 wt% solution of PLLA in dioxane. Coagulation was performed in ethanol. The bar indicates 100  $\mu\text{m}$ .*

**b** *Cross-section of a microstructure prepared from a 7.5 wt% solution of PLLA in dioxane. Coagulation was performed in propanol. The bar indicates 10  $\mu\text{m}$ .*

In Phase Separation Micro Molding (PS $\mu$ M), in principle, any polymer for which a suitable solvent is available can be used for microfabrication (see chapter 2).<sup>19,20</sup> This very broad range of polymers includes several biocompatible or biodegradable polymers. Therefore PS $\mu$ M is an obvious candidate for preparing microstructured scaffolds, which can enable directional growth. Moreover PS $\mu$ M can yield microstructures with an intrinsic porosity throughout the material, allowing the necessary transport through the scaffolds towards and from the cells. To our knowledge, besides direct writing methods that can be time consuming, PS $\mu$ M is the sole option for preparing porous microstructured biodegradable scaffolds.

Ideally, porous microstructured sheets are stacked, forming a three-dimensional scaffold, where the cells grow in the microstructures and the porosity provides supply of nutrients and elimination of secretion products like carbon dioxide. The expanding cell culture is constricted to the microstructures and cannot enter the pores. Therefore blocking the transport through the scaffold by the cells is avoided. The concept of stacking sheets can also exploit the possibility of seeding different types of cells on the individual sheets, which expands the possibilities for the composition of the tissue.<sup>21</sup> The tissue could largely benefit from the creation of a scaffold containing different kinds of cells, since different types of functions can be integrated.

This chapter describes the preparation and optimization of microstructured porous films from biodegradable polymers. Their possible use as a scaffold for tissue engineering is evaluated by determination of the pore morphology, diffusion measurements and finally cell culturing experiments.

## 5.2 results and discussion

### 5.2.1 materials and ps $\mu$ m process

After screening on biocompatibility, biodegradability and mechanical stability, two types of poly(lactic acid) (PLA) and poly( $\epsilon$ -caprolactone) (PCL)<sup>22,23</sup> were selected for scaffold preparation by PS $\mu$ M.<sup>24,25,26,27,28</sup> The influence of two different solvents (chloroform and dioxane) on the pore morphology was studied. Well-formed porous microstructures were found when alcohols were used as non-solvents. Alcohols of increasing chain length, namely methanol, ethanol, isopropanol, isobutanol and isopentanol, were examined as the

coagulation medium. Replication of a microstructured mold using PS $\mu$ M succeeded without noticeable difficulties for each of the polymers. Some of the above-mentioned recipes yielded highly porous microstructures (figure 1).

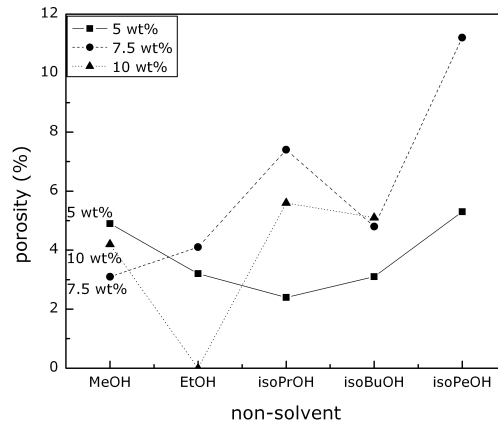
To optimize the pore morphology, the polymer solutions were prepared at different concentrations between five and ten weight percent. The non-solvents were varied as well, while all other conditions, like temperature, substrate and thickness of the polymer film, were kept constant. The pore morphologies of the resulting microstructures were studied by SEM to quantify porosity and determine the minimum and maximum pore size. In general, the highest porosity was obtained using solutions of poly (L-lactic acid) (PLLA) in dioxane (see Figure 1). The graphs in Figure 2a - c present the porosity of the microstructures prepared using various PLLA-dioxane solutions of different concentrations as a function of the alcohol that was used as a non-solvent. The graphs in Figure 2d - f depict the corresponding values for the pore size.

The error in the determination of the porosity is rather high because of inaccuracy in the conversion of the gray scale electron microscopic image into black and white. Nevertheless the trends (Figure 2a - c) match the impression regarding porosity that is visually perceived from the SEM observations. Although the values of the porosity in the cross section and the structured side of the microstructure are rather high, the surface on the unstructured side can be fairly dense. The porosity on the unstructured side is influenced mainly by solvent evaporation during the application of the polymer solution on the mold, and the kinetics of the exchange between solvent and non-solvent. The concentration of the solution influences the porosity throughout the entire polymer film after phase separation. As expected, from Figure 2 it generally stands for all evaluated solution – non-solvent combinations that the lower the concentration, the higher the porosity.

From Figure 2 it appears that generally the use of methanol as a non-solvent results in a low porosity, where on the other hand the size of the scarce pores is quite large. Use of higher alcohols leads to a higher porosity and smaller pore sizes. Similarly, the pores on the unstructured side of the polymer appear to be larger than the pores in the cross-section and structured side. Conversely, the pores on the unstructured side are very scarce, causing the porosity to be lower on this side. A more rapid exchange of solvent and non-solvent occurs on the unstructured side in comparison with the rest of the polymer. Use of lower alcohols as a non-solvent also promotes the exchange. In this case the decrease in porosity is expected, although usually the lower porosity is accompanied by a decrease in pore size. In that aspect the phase separation recipe behaves extraordinary.

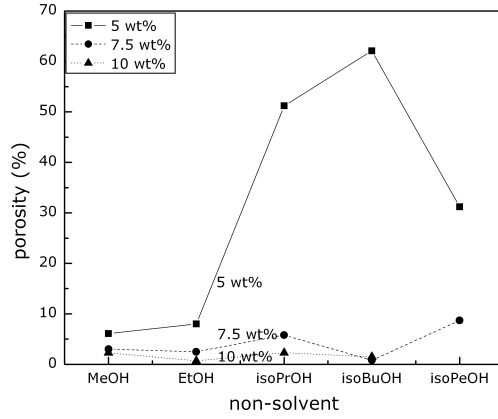
a

unstructured side



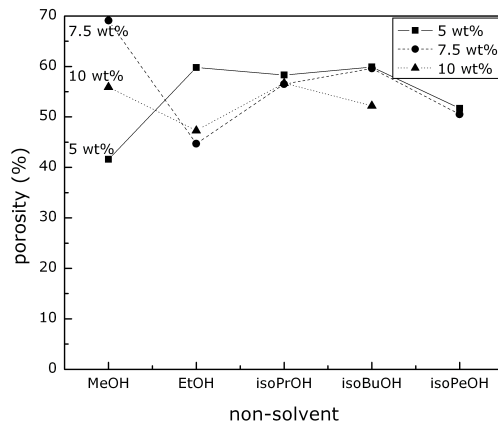
b

structured side

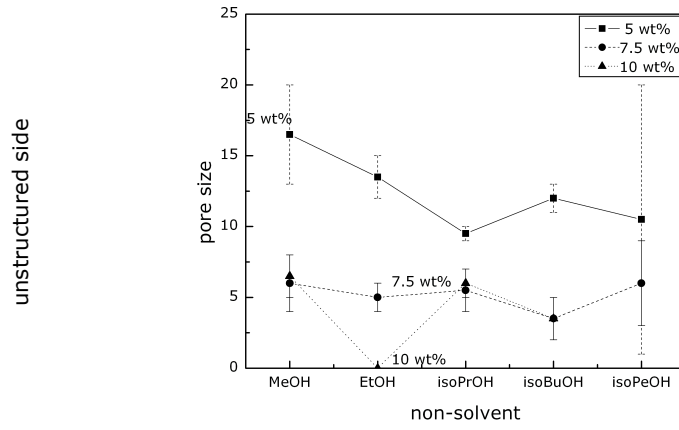


c

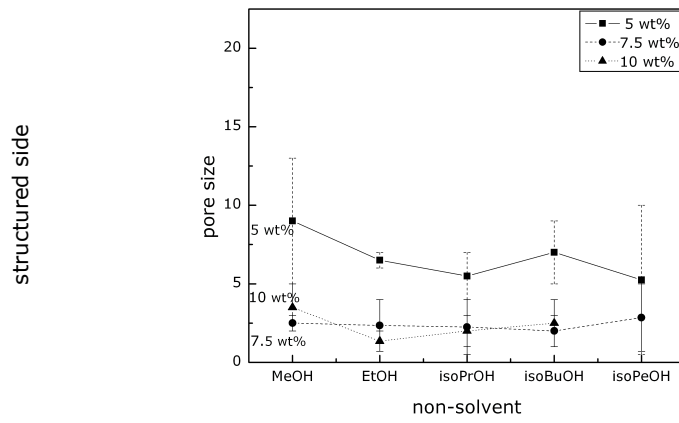
cross section



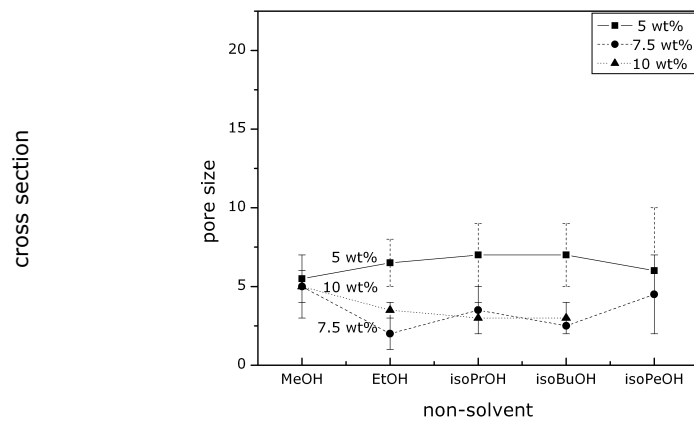
d



e



f



**figure 2 (previous pages)** *Porosity and pore size of microstructures prepared from PLLA in dioxane as a function of the chain length of the alcohol used as a non-solvent and the concentration of the solution. a) Porosity of the unstructured side. b) Porosity of the structured side. c) Porosity of the cross-section. d) Pore size measurement of the unstructured side. e) Pore size measurement of the structured side. f) Pore size measurement of the cross-section. The bars in the graphs of the pore size indicate the pore size range, and therefore indicate the minimum and maximum pore size within one microstructure.*

Isobutanol and isopentanol have a disadvantage for application in tissue engineering because of their toxicity in combination with their slow mixing behavior with dioxane and low evaporation rates. Therefore the use of these alcohols involves the risk that during culturing the cells will come into contact with traces of the toxic non-solvent that are left in the scaffold material. Concerning the optimal pore size for a scaffold, there is an upper limit considering the fact that the cells should be retained in the channels of the microstructure, in order not to block the pores. Consequently, the pores on the microstructured side should not be larger than the minimal dimensions of the cell, which is approximately 10  $\mu\text{m}$ . As can be seen in Figure 2d - f, for the phase separation of a solution of PLLA in dioxane this criterion is obeyed except when using isopentanol or methanol as the non-solvent.

From the graphs in Figure 2 and the above-mentioned considerations it is concluded that the most successful recipe in view of pore morphology for the preparation of tissue engineering scaffolds is a 5 wt% solution of PLLA in dioxane, using either ethanol or propanol as the non-solvent.

To further improve the porosity of the skin layer formed on the unstructured side of the microstructures, scaffolds are also prepared in an environment of air, saturated with solvent vapor. The presence of the vapor is expected to reduce evaporation of the solvent from the air side of the polymer solution film, thereby increasing the porosity of the unstructured side. However, SEM observations reveal no evident increase of the porosity of the skin layer.



## 5.2.2 glucose diffusion experiments

Further characterization of the transport properties of the membranes is provided by measurements of glucose diffusion through the microstructure. The microstructure is clamped between two compartments. One compartment contains clean water while the other contains a 5.7 mM glucose solution. The concentration of the solution mimics the content of glucose in blood or culturing medium. The glucose concentration of both compartments is measured as a function of time. A typical result of a diffusion experiment is depicted in Figure 3. As a measure for the glucose diffusion, Table 1 presents the overall glucose delivery through the microstructure after 30 hours. The deliveries in Table 1 are determined for microstructures prepared from four different recipes. From Figure 3 and Table 1, it can be seen that transport of glucose through the microstructures is possible. Yet, the delivery is very low, especially considering the high porosities that were observed by SEM. Probably the interconnectivity of the pores is still limited, and requires further optimization. The mass balance of glucose on both compartments shows that there is no significant accumulation of glucose inside the membrane.

From Table 1 a higher delivery is observed when propanol is used as a non-solvent in comparison with ethanol. Moreover the delivery shows an increase when the microstructure is prepared in a solvent saturated environment opposed to preparation in air. The effect of the solvent saturated environment is surprising, since there was no difference observed by SEM. Apparently the interconnectivity is promoted by the preparation in the solvent saturated environment.

<i>Non-solvent</i>	<i>Solvent environment</i>	<i>Delivery after 30 hr [mg.cm<sup>-2</sup>]</i>
Ethanol	no	1.4
isopropanol	no	2.1
Ethanol	yes	3.3
isopropanol	yes	4.4

**table 1** *Delivery of glucose after 30 hours for porous microstructures of PLLA using different preparation routes. The microstructures were all prepared from a 5 wt% PLLA solution in dioxane. The values for the delivery are averages over multiple microstructures.*

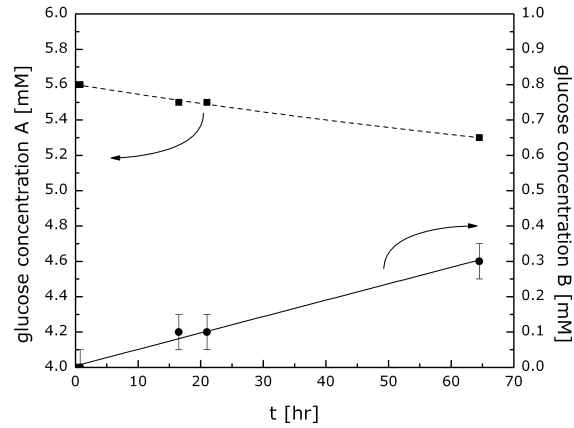
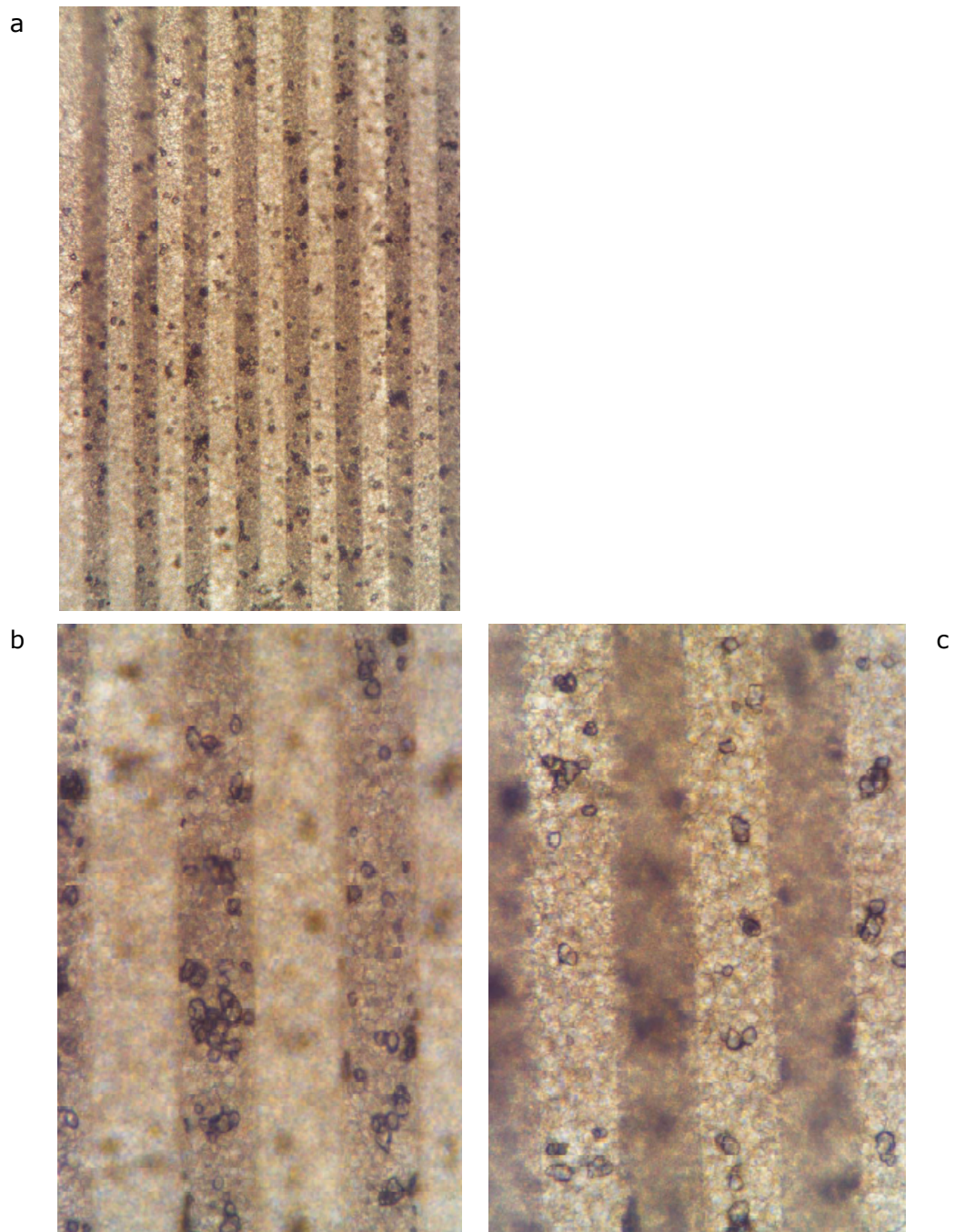


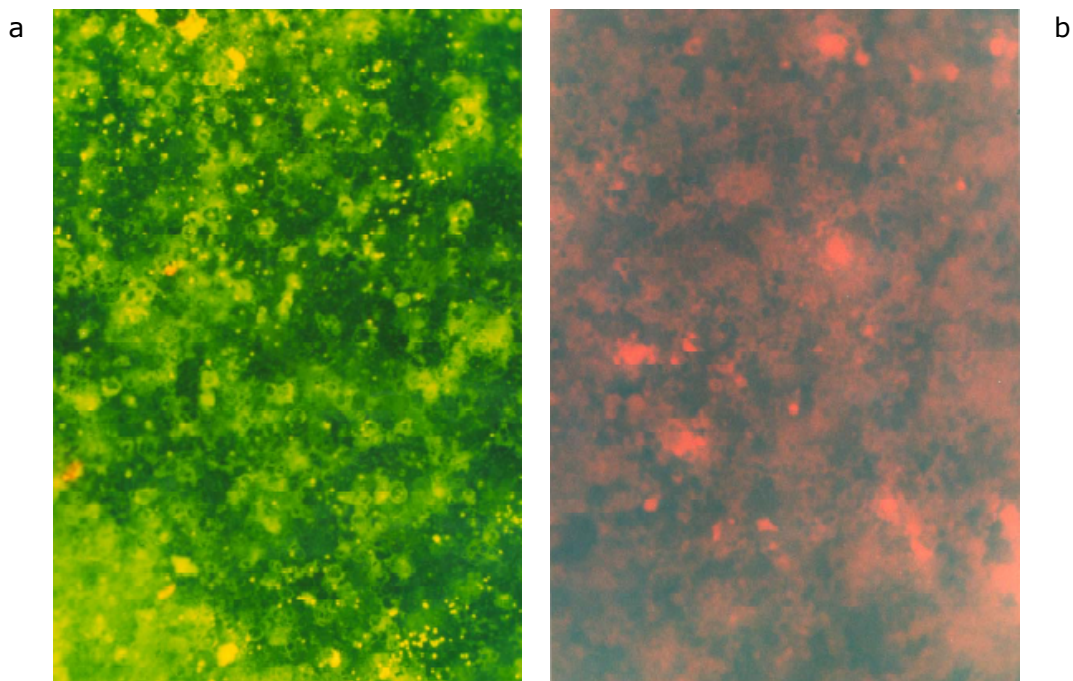
figure 3 Example of diffusion of glucose through a porous PLLA microstructure as a function of time. The upper line illustrates the glucose concentration of the initially glucose containing compartment (compartment A). The lower line describes the glucose content of the initially glucose free compartment (compartment B).

### 5.2.3 cell culturing experiments

Finally, cell-culturing experiments are performed to evaluate if the scaffolds prepared from PLLA by PS $\mu$ M are suitable for growth of cells. The experiments were performed on the microstructures that displayed the highest porosity, prepared from a 5 wt% solution. Human Microvascular Endothelial Cells (HMEC) are seeded on the structured side of the microstructure with a density of 20.000 cells cm<sup>-2</sup>. The culturing medium is refreshed every two days. During the entire culturing period, the cells are kept in an incubator. The gradual change of color of the culturing medium as a result of a change in pH visualized by an indicator shows that the cells proliferate on the microstructures. During microscopic observations, no distinct differences are distinguished between the microstructures prepared from the different recipes. However, since the microstructures are not stacked, there is no need for transport of nutrients through the microstructure. Since the difference between the microstructures from the different recipes is mainly in the pore morphology, a distinction in cell growth is not expected.



**figure 4** Typical example of HMEC cells on a porous PLLA microstructure with 50 micron wide channels (dark gray) after two days of culturing. a) Overview over the entire area at a magnification of 50x. b) Cells in the channels of the microstructure at a magnification of 100x. c) Cells in between the channels of the microstructure at a magnification of 100x.



**figure 5** *Example of a fluorescence microscopic image of a) living cells (stained by acridin orange, and b) dead cells (stained by propidium iodide). Small bright dots indicate the presence of cells. Magnification 50x.*

A typical example of cells growing on a microstructure after two days of culturing is displayed in Figure 4. Although during the experiment no effort is made to promote directional growth, a slight tendency is observed for the cells to grow inside the deeper part of the microstructure, i.e. in the microchannels instead of on top of the rims. This tendency is observed especially close to the walls of the channel, and probably indicates that the cells prefer to maximize contact to the scaffold material. With longer culturing times (after 4 and 7 days) the distinction between growth in the lower or the upper parts of the microstructure disappears. The cells gradually form a monolayer across the entire microstructure. Therefore if the microstructures would be stacked in a three-dimensional scaffold configuration, the stacking ought to be performed during the first stage of culturing, preferably before the formation of a monolayer takes place.

After seven days of culturing, the cells are examined using fluorescence microscopy. A typical example of a fluorescence image of living and dead cells is given in figure 5. Just before the photos in Figure 5 are taken, optical microscopy has already revealed the presence of the cells on the studied area of the microstructure. The fluorescence microscopy shows that most of the cells are alive, indicating that the cells proliferate well on the microstructure.

### 5.3 conclusions

Porous microstructures have been prepared from various biocompatible and biodegradable polymers. The microstructures may serve as scaffolds for tissue engineering, in which the cells can grow. The microstructure provides possibilities for directional growth. The porosity of the polymer enables transport, which is necessary for continuous supply of nutrients and oxygen to the cells and removal of carbon dioxide. The optimal recipe in terms of pore morphology and applicability as a scaffold was found for a 5wt% solution of PLLA in dioxane, in combination with ethanol or propanol as a non-solvent.

Diffusion driven transport of glucose through the microstructures was measured. The highest diffusion was measured for a microstructure prepared in an environment of air saturated with solvent vapor, where propanol was used as a non-solvent. The relatively low glucose diffusion indicates that the interconnectivity of the pore morphology still requires further optimization.

HMEC cells were cultured on the microstructures. Even though it was not stimulated in any way, the cells exhibit a slight tendency to grow in the channels of the microstructure, which should provide the opportunity for allow directional growth. After longer culturing times a monolayer of cells is formed on top of the microstructure. Fluorescence microscopy reveals that the cells proliferate well on the microstructure.

### 5.4 experimental

*Preparation of microstructures.* The mold was prepared from silicon by lithography and deep reactive ion etching. The microstructure on the mold consisted of lines, 500  $\mu\text{m}$  in length, having a width and height of 50  $\mu\text{m}$ . The lines were spaced at a distance of 50  $\mu\text{m}$ .

The polymers that were used were poly(L-lactic acid) (PLLA) having a high molecular weight (approximately between 100.000 and 300.000  $\text{g}\cdot\text{mol}^{-1}$ ),

poly(DL-lactic acid) (PDLLA, Polysciences) having a high molecular weight (approximately between 330.000 and 600.000  $\text{g}\cdot\text{mol}^{-1}$ ) and poly( $\epsilon$ -caprolactone) (PCL, Solvay CAPA 680,  $M_w \approx 80.000 \text{ g}\cdot\text{mol}^{-1}$ ). Solutions of PLA were prepared using chloroform as well as dioxane as solvents, while only chloroform was used to dissolve the PCL.<sup>23,29</sup> Chloroform and dioxane, both of analytical quality, were acquired from Merck. As non-solvents methanol, ethanol, isopropanol,

isobutanol (all acquired from Merck, analytical quality) and isopentanol (Acros, analytical quality) were used. All polymers were dissolved under constant stirring at ambient conditions.

The polymer solutions were cast on the mold using a Gardner blade with adjustable height (see experimental section of chapter 2). The solution was cast at a thickness of 300 micrometer. Additionally, some of the microstructures were prepared in an environment of air saturated with solvent vapor. This environment was created by a closed box, in which the solvent had been placed before for several hours. The box had two small openings, which were only opened during the short time in which the casting procedure and immersion was performed.

Subsequently, the mold and polymer solution were immersed in the non-solvent, where the microstructure was released from the mold within a few minutes. In some cases, water was used to facilitate the release. Next, the microstructure was rinsed in the non-solvent for 24 hours. The microstructures were dried for at least 24 hours. If the microstructures were applied for cell culturing, the drying was performed in a sterile environment.

*Microscopy.* Scanning Electron microscopy was performed on a JEOL T220, at an acceleration voltage of 15 kV. The magnifications were between 500 and 3500x, depending on the pore morphology. Before characterization by SEM, the samples were coated with a 15 nm thin layer of gold, using a Balzers SCD 040 coater. To give a quantitative measure of the porosity, the grey-scale SEM-images were converted into black and white, where the percentage of black in the image is a measure for the porosity.

Optical and fluorescence microscopy was performed using a Leica Laborlux microscope. Prior to fluorescence microscopy the cells were labelled with a fluorescent dye consisting of 12  $\mu$ l acridin orange (AO) solution (1 mg/ml AO dissolved in water), 40  $\mu$ l propidium iodide (PI) solution (1 mg/ml PI dissolved in water) and 8 ml phosphate-buffered saline (PBS). This solution was incubated on the structures and cells for approximately 5 minutes. In the fluorescence microscope a mercury lamp was used for excitation. To detect the living cells, stained with AO, an excitation filter for blue light (450-490 nm) was incorporated, whereas to detect the dead cells, stained with PI, a filter for green light (530-560 nm) was incorporated. For the emission, filters of 515 nm for AO (green light) and 580 nm for PI (red light) were used.

*Glucose diffusion.* The microstructure (diameter 17 mm) was clamped in between two glass compartments. Glucose (Sigma, SigmaUltra, D-(+)-glucose, 99.5% glucose content) was dissolved in milli-Q water to a concentration of 1 g/l or 5.7 mM,

which equals the glucose content in blood. One compartment was initially filled with the glucose solution, the other compartment contained milli-Q water. Over time, several samples were taken from both compartments. The glucose content of these samples was determined employing an enzymatic method using hexokinase followed by absorbance photometry using a spectrophotometer (Roch COBAS Integra 800).

*Cell culturing.* The microstructures that were used for cell culturing were prepared from a 5 wt% solution of PLLA in dioxane, using either ethanol or propanol as a non-solvent, with or without a solvent saturated environment. The microstructures consisted of long channels, having a width of 50  $\mu$ m, spaced at a period of 100  $\mu$ m. The width of the channels is chosen slightly broader than the average size of the cells.

A 24 well cluster plate (Corning incorporated, costar 3526) was used for the cell culturing. Before placement into the well plate, the microstructures were sterilized by rinsing in a 70% ethanol solution, followed by a 96% ethanol solution, after which they were rinsed twice in pure water. Once the microstructures were placed in the well plate, 500  $\mu$ l of culture medium was added per well and left to incubate overnight (constant temperature of 37°C and CO<sub>2</sub> concentration of 5%). The culture medium consisted of RPMI1640/M199 (1:1) supplemented with 1% penicillin/streptomycin, 1% glutamax and 20% human serum. To check the pH of the medium during the cell culturing a pH indicator (phenol red) was added. The pH of the fresh plasma medium was 7.4 and decreased to approximately 6.8 during the culturing experiment as a consequence of the cells metabolising medium.

Human microvascular endothelial cells (HMEC) were released from the bottom of a culturing flask using 2 ml of trypsin/EDTA solution (0.05%/0.02%) in PBS. Before adding the trypsin, the culture medium was removed from the dish and the cells were briefly rinsed with PBS. One or two minutes after addition of the cell detachment solution, the trypsin was inactivated by adding fresh culture medium. Fifty microliters of the cell suspension was placed in a counting-chamber (Bürker SV190). The cell suspension was diluted with culture medium to a density of approximately 40.000 cells per 500  $\mu$ l. The culture medium in the well plate was then replaced with 500 $\mu$ l of cell suspension per well. The well plate was kept in the incubator during the entire culturing experiment. Every two to three days the medium was refreshed. After 2, 4 and 7 days of culturing the cells were studied by light microscopy.

## references

- <sup>1</sup> R. P. Lanza, R. Langer, J. Vacanti (eds.), *Principles of tissue engineering*, Academic Press, San Diego, U.S. **2000**.
- <sup>2</sup> D. W. Huttmacher, *Biomaterials* **2000**, *21*, 2529.
- <sup>3</sup> D. W. Huttmacher, *J. Biomater. Sci. Polymer Edn.* **2001**, *12*, 107.
- <sup>4</sup> C. M. Agrawal, R. B. Ray, *J. Biomed. Mater. Res.* **2001**, *55*, 141.
- <sup>5</sup> H. P. Hentze, M. Antonietti, *reviews in Biotechnology* **2002**, *90*, 27.
- <sup>6</sup> T. A. Desai, *Med. Eng. Phys.* **2000**, *22*, 595.
- <sup>7</sup> J. Deutsch Snyder, T. A. Desai, *Biomed. Microdevices* **2001**, *3*, 293.
- <sup>8</sup> S. Kaihara, J. Borenstein, R. Koka, S. Lalan, E. R. Ochoa, M. Ravens, H. Pien, B. Cunningham, J. P. Vacanti, *Tissue Eng.* **2000**, *6*, 105.
- <sup>9</sup> C. J. Lee, M. S. Blumenkranz, H. A. Fishman, S. F. Bent, *Langmuir* **2004**, *20*, 4155.
- <sup>10</sup> S. Sarkar, M. Dadhania, P. Rourke, T. A. Desai, J. Y. Wong, *Acta Biomaterialia* **2005**, *1*, 93.
- <sup>11</sup> J. Deutsch, D. Motlagh, B. Russell, T. A. Desai, *J. Biomed. Mater. Res.* **2000**, *53*, 267.
- <sup>12</sup> R. Thakar, F. Ho, N. F. Huang, D. Liepmann, S. Li, *Biochem. Bioph. Res. Co.* **2003**, *307*, 883.
- <sup>13</sup> G. M. Whitesides, E. Ostuni, S. Takayama, X. Y. Jiang, D. E. Ingber, *Annu. Rev. Biomed. Eng.* **2001**, *3*, 335.
- <sup>14</sup> T. H. Park, M. L. Shuler, *Biotechnol. Prog.* **2003**, *19*, 243.
- <sup>15</sup> G. Kumar, Y. C. Wang, C. Co, C. C. Ho, *Langmuir* **2003**, *19*, 10550.
- <sup>16</sup> R. Kapur, B. J. Spargo, M. S. Chen, J. M. Calvert, A. S. Rudolph, *J. Biomed. Mater. Res.* **1996**, *33*, 205.
- <sup>17</sup> K. R. King, C. C. J. Wang, M. R. Kaazempur-Mofrad, J. P. Vacanti, J. T. Borenstein, *Adv. Mater.* **2004**, *16*, 2007.
- <sup>18</sup> Y. Lu, S. C. Chen, *Adv. Drug Deliver. Rev.* **2004**, *56*, 1621.
- <sup>19</sup> L. Vogelaar, J. N. Barsema, W. Nijdam, C. J. M. van Rijn, M. Wessling, *Adv. Mater.* **2003**, *15*, 1385.
- <sup>20</sup> L. Vogelaar, R. G. H. Lammertink, J. N. Barsema, W. Nijdam, L. A. M. Bolhuis-Versteeg, C. J. M. van Rijn, M. Wessling, *Small* **2005**, *1*, 645.
- <sup>21</sup> T. Okano, 8<sup>th</sup> European Symposium on Controlled Drug Delivery, April **2004**, 23.
- <sup>22</sup> K. A. Athanasiou, G. G. Niederauer, C. M. Agrawal, *Biomaterials* **1996**, *17*, 93.
- <sup>23</sup> R. A. Zoppi, S. Contant, E. A. R. Duek, F. R. Marques, M. L. F. Wada, S. P. Nunes, *Polymer* **1999**, *40*, 3275.
- <sup>24</sup> P. A. Gunatillake, R. Adhikari, *Eur. Cells Mater.* **2003**, *5*, 1.
- <sup>25</sup> M. Vert, P. Christel, F. Chabot, J. Leray, G. W. Hastings, P. Duchenne (eds.), *Macromolecular Biomaterials*, CRC Press, Boca Raton, U.S. **1984**.
- <sup>26</sup> A. G. A. Coombes, S. C. Rizzi, M. Williamson, J. E. Barralet, S. Dopwnes, W. A. Wallace, *Biomaterials* **2004**, *25*, 315.
- <sup>27</sup> Q. Hou, D. W. Grijpma, J. Feijen, *Macromol. Rapid. Commun.* **2002**, *23*, 247.
- <sup>28</sup> S. Ramakrishna, J. Mayer, E. Wintermantel, K. W. Leong, *Compos. Sci. Technol.* **2001**, *61*, 1189.
- <sup>29</sup> P. van de Witte, *Poly lactide Microstructures*, PhD Thesis, University of Twente, Enschede, the Netherlands, **1994**.







## chapter 6

## self cleaning surfaces: phase separation micro molding as a route to superhydrophobicity

*L. Vogelaar*

*R. G. H. Lammertink*

*M. Wessling*

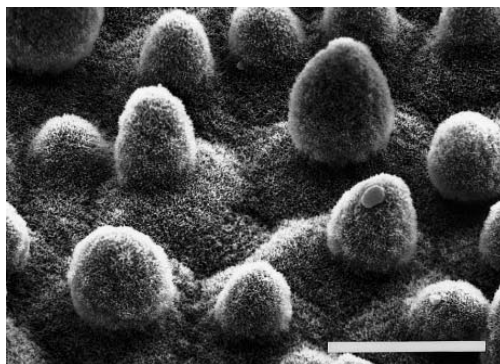
Phase Separation Micro Molding is utilized to prepare surfaces of a hydrophobic material with a hierarchical roughness, mimicking the self-cleaning properties of the lotus plant leaves. First of all, the microstructure increases the roughness of the surface, and additionally the porosity of the microstructure superimposes a roughness on a smaller length scale. The hydrophobicity of Hyflon® AD was optimized by variation of the patterns of the microstructure and the phase separation process, tuning the roughness on both levels. The optimized surfaces, in terms of hydrophobicity, display water contact angles well above 160 degrees. Due to the very low contact angle hysteresis, water droplet roll-off angles are as low as 0.5 degrees.

*Above: Water drop on the superhydrophobic surface of a plant leaf.*

## 6.1 introduction

In its evolutionary optimization process, nature has established a highly effective way to deal with contaminating particles. The leaves of certain plants (notably the Lotus) and wings of insects exhibit superhydrophobicity.<sup>1,2,3,4,5</sup> On the surface of leaves, the droplets display a contact angle close to the contact angle with air,  $180^\circ$ . Water does not show any affinity for the surface, causing water drops to behave very extraordinary, e.g. by bouncing and rolling instead of sliding.<sup>6,7,8</sup> When water droplets roll off such surfaces, they drag along dirt particles, which explains their self-cleaning character. Wax crystals on the Lotus leaf create a very rough surface structure, which enhances the hydrophobicity. The wax crystals pile up in pillars with micrometer-scale dimensions (see Figure 1). The texture on the leaves consists of a two-fold roughness, originating from the pillar structure and the wax crystals.<sup>1,3</sup> Therefore optimal self-cleaning properties for artificial surfaces can be expected if the double roughness structure of the Lotus-leave is mimicked.<sup>9,10</sup>

Synthetic surfaces that display a self-cleaning effect can find use in applications like microfluidics, but also on macroscale applications as an antifouling layer. Superhydrophobic antifouling coatings are already commercialized.<sup>11</sup> Surfaces with more or less random roughness structures have been fabricated out of a very wide diversity of materials. Among them are PTFE surfaces roughened in various ways,<sup>12,13,14,15</sup> polypropylene after thermally induced phase separation,<sup>16</sup> fractal surfaces of alkylketene dimer,<sup>17</sup> several structures of carbon nanotubes,<sup>18,19</sup> some of which were coated with PTFE to enhance the hydrophobicity,<sup>20</sup> nanofibers of poly(vinyl alcohol)<sup>21</sup> and polyacrylonitrile,<sup>22</sup> solutions of polymethylmethacrylate and fluorine-end-capped polyurethane blends that were cast and dried,<sup>23</sup> poly(acrylonitrile co  $\alpha,\alpha$ -dimethyl *meta*-isopropenylbenzyl isocyanate) with perfluorinated linear diol prepared by electrospinning,<sup>24</sup> polystyrene prepared by electrohydrodynamics,<sup>25</sup> phase separated tetraethyl *orthosilicate* coated with fluoroalkylsilane,<sup>26</sup> and aluminum structured in various ways.<sup>27</sup> Another approach to increase the surface area and thus the roughness is microstructuring surfaces. These surfaces have the additional advantage that they are attractive model surfaces, where the regularity of the pattern and the shape of the microstructures is very well defined and controlled. Microfabricated ultrahydrophobic surfaces have been made out of silicon, that was subsequently coated with a hydrophobic material (e.g. a silane),<sup>28,29,30</sup> SU-8 photoresist treated with a hydrophobic coating,<sup>31</sup> or poly(dimethylsiloxane) by means of replica molding.<sup>32,33</sup>



**figure 1** SEM image of the rough surface on the leaves of *Nelumbo nucifera* (lotus). The bar indicates 20  $\mu\text{m}$ . Reproduced from reference 5 (with kind permission of Springer Science and Business Media).

As can be seen from this long, yet incomplete list, the spectrum of materials is diverse, as is the range of fabrication methods used to construct superhydrophobic surfaces. Ultimately, for a superhydrophobic surface to have success in a commercial application simplicity and cost-effectiveness of the fabrication process and accessibility of the materials are desired. Besides, for most uses, the mechanical stability of the surface is also important.<sup>26</sup> However, many of the preparation routes are not very straightforward, e.g. they may require vacuum equipment, many fabrication steps or are time consuming. Additionally, some of the applied materials are rather ‘exotic’ and not commercially available bulk materials.

Phase Separation Micro Molding (PS $\mu$ M) is a microfabrication method, which is especially suitable for preparation of microstructured surfaces that possess an intrinsic porosity.<sup>34</sup> PS $\mu$ M is applicable on virtually any soluble polymer, which opens up a very wide range of materials and, consequently, surface properties.<sup>35</sup> A surface can be prepared from a hydrophobic material with a hierarchical roughness structure, consisting of a microstructure onto which a roughness on a smaller length scale originates from the intrinsic porosity. The fabrication process can thus be used to truly mimic the two-fold roughness structure of the Lotus leaf, and might provide a very simple preparation route to superhydrophobicity in a synthetic surface.

There are a few other preparation processes that yield superhydrophobic surfaces with roughness on multiple length scales.<sup>18,22,23,25</sup> In structures of aligned carbon nanotubes,

the nanotubes form the superimposed roughness.<sup>18,22</sup> Another example is the incorporation of porous microspheres.<sup>25</sup> Surfaces prepared by drying of solutions of polymethylmethacrylate and fluorine-end-capped polyurethane blends arrange the polymer in microstructures having a roughness on the nanometer level.<sup>23</sup> The enhancement of the self-cleaning properties that is predicted by theory is indeed confirmed experimentally for these surfaces.<sup>9,36</sup>

A water drop on a rough hydrophobic surface can show two different kinds of behavior. Both cases are schematically illustrated in Figure 2. In one case the water profile follows the contour of the rough material. The contact angle is in this case predicted by the Wenzel equation:

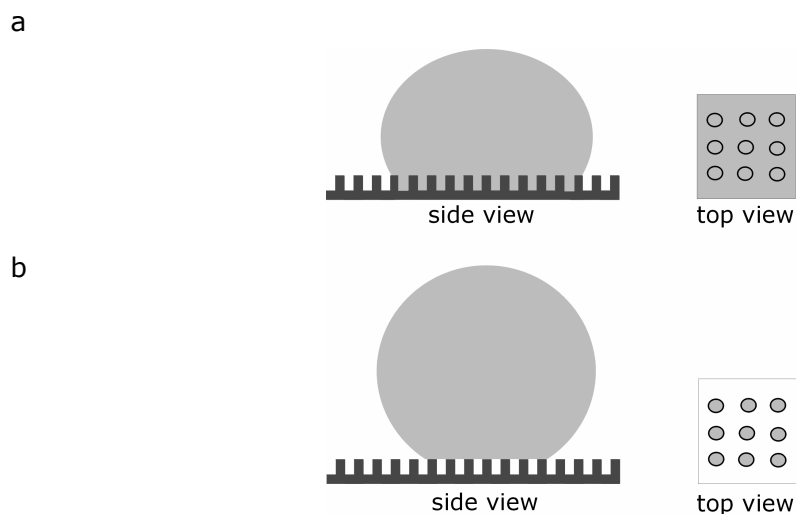
$$\cos \theta_W = r \cos \theta, \quad [6.1]$$

in which  $\theta_W$  is the contact angle measured on the rough surface,  $\theta$  is the contact angle on a smooth surface and  $r$  is the roughness factor; the ratio between the total surface area and the projected surface area. By definition  $r$  is higher than 1, so for behavior according to the Wenzel equation hydrophobic surfaces ( $\theta > 90^\circ$ ) will increase in hydrophobicity, while hydrophilic surfaces ( $\theta < 90^\circ$ ) will become more hydrophilic.

Another possibility is that a water drop on a rough surface prefers not to follow the contour of the roughness, but rather bridges the gap between the protrusions of the rough material. Such ‘fakir’ droplets exhibit a contact angle according to the Cassie-Baxter equation:<sup>37</sup>

$$\cos \theta_{CB} = -1 + \Phi_S (1 + \cos \theta), \quad [6.2]$$

in which  $\theta_{CB}$  is the water contact angle on the rough surface, and  $\Phi_S$  is the surface solid fraction: the contact area between water and material, in other words the ratio between the projected area of the protrusions of the structure and the total projected surface area. This expression of the Cassie-Baxter equation describes only the ideally non-wetting case, as is depicted schematically in Figure 2b. Equation 6.2 does not take into account that the drop might actually wet an area that is slightly larger than the surface solid fraction, because the liquid may partly penetrate into the grooves.<sup>38</sup> A self-cleaning surface generally shows Cassie-Baxter like behavior. Additionally, there is very little hysteresis between advancing and receding contact angle, predicting a low sliding angle: a very small inclination may cause the drop to roll off instantaneously.



**figure 2** Schematic representation of the regime, in which the Wenzel equation applies (a), and the Cassie-Baxter regime (b). In the projected top view the shaded area is the area in contact with water. In the case of the Wenzel equation the roughness factor,  $r$ , is the total wetted area divided by the projected area. In the case of the Cassie-Baxter equation the solid fraction  $\Phi_s$  is the area in contact with the droplet (the projection of the protrusions) divided by the projected area.

## 6.2 results and discussion

In PS $\mu$ M a polymer solution is applied on a mold, which has a micrometer sized relief profile on its surface. Subsequently, mold and solution are immersed in a non-solvent. The non-solvent and solvent exchange, causing the polymer to solidify and assimilate the structure on the mold. PS $\mu$ M is a very reliable, simple and cost effective replication method.<sup>34</sup>

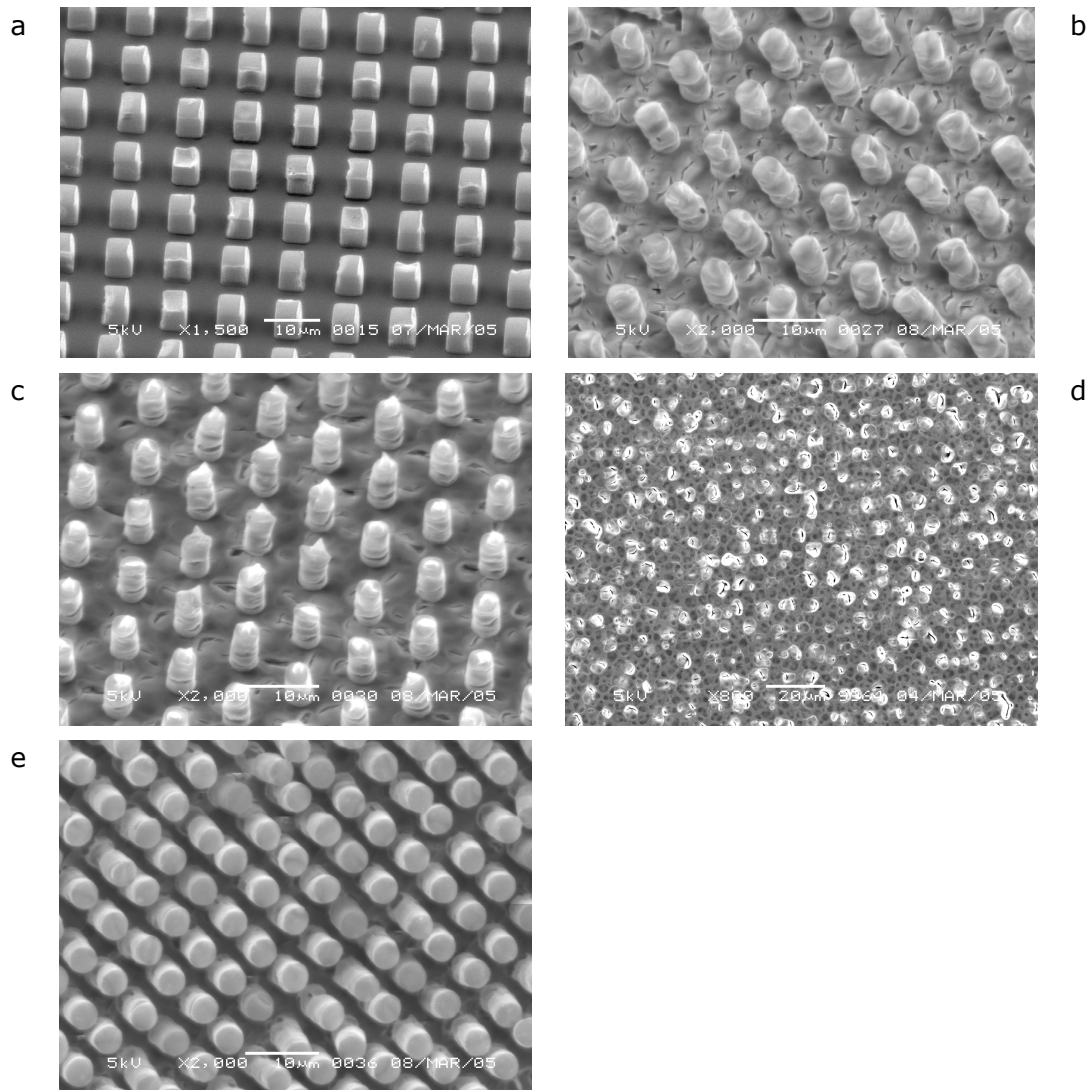
The porosity stems directly from the use of liquid induced phase separation in the process. The polymer solution separates in a polymer-lean and a polymer-rich part. The polymer rich part will form the solid polymer, while the polymer lean part can cluster in the polymer and form pores.<sup>39,40</sup> By adjusting the composition of the solvent and non-solvent, the phase separation process can yield highly porous as well as dense materials. Accordingly, the porosity in a microstructure prepared by PS $\mu$ M can be tailored by tuning the recipe.<sup>35</sup>

The use of microfabrication has the advantage that the design of the microstructure can be chosen in any size or shape. Therefore both roughness levels of the fabricated surface can be adjusted: the microstructure by control over the mold design, and the porosity by control over the phase separation recipe. This aspect distinguishes PS $\mu$ M from the other methods that can achieve a hierarchical roughness, in which the roughness has a more complex correlation to the different process parameters.

Generally, hydrophobic flat surfaces can exhibit contact angles up to 120°. The hydrophobic polymer Hyflon® AD was chosen as a hydrophobic material, which is suitable for processing by PS $\mu$ M. For this material, which is a copolymer of tetrafluoroethylene (TFE) and 2,2,4-trifluoromethoxy-1,3-dioxole (MDO) (empirical formula  $(C_2F_4)_n(C_4F_6O_3)_m$ ), water contact angles up to 120° have been reported.<sup>41,42</sup> Moreover the polymer is well soluble in perfluorinated solvents, and is therefore easily applicable in PS $\mu$ M. Hyflon® AD is one of the few soluble perfluoropolymers. Two types of the polymer were processed, namely Hyflon® AD 60X (composed of 60 mol% MDO and 40 mol% TFE) and Hyflon® AD 80X (composed of 80 mol% MDO and 20 mol% TFE). For simplicity the two types of Hyflon® AD will subsequently be abbreviated by H60 and H80. Although Hyflon is chosen here as an example, we like to emphasize that many more hydrophobic polymers can be processed that may lead to superhydrophobic surfaces.

To study the influence of the microstructure, six different patterns are prepared, each consisting of microstructures with a minimum feature size of five micrometer. The minimum feature size is chosen to mimic the typical size of the microstructures on the leave of the lotus. The microstructures consist of either cylindrical or rectangular pillars. The different mold patterns can be divided in three patterns of which the surface solid fraction  $\Phi_S$  is around 0.5, and three patterns of which the surface solid fraction is approximately 0.2 (see Table 1).

Polymer solutions are prepared in different weight concentrations, in order to vary the intrinsic porosity of the resulting film. To evaluate the effect of the intrinsic porosity introduced by the phase separation on the hydrophobicity, smooth microstructures are prepared by evaporation as well (see Figure 3a). The microstructures prepared by PS $\mu$ M clearly display a superimposed roughness stemming from the phase separation process (Figure 3b and c). AFM measurements confirm that phase separation indeed increases the roughness (Figure 4). Sometimes the pillars of the microstructure even collectively demonstrate the formation of a sharp tip (Figure 3c). The presence of such a tip can further



**figure 3** Surfaces prepared from Hyflon<sup>®</sup> AD 80X. Figure a shows a structure of square pillars prepared by evaporating a 15wt% solution on a mold. Figures b and c show microstructures of pillars, prepared by PS $\mu$ M, illustrating the roughness superimposed on the microstructure. In Figure 1d, the use of a very shallow mold (500 nm) in combination with PS $\mu$ M of a 15 wt% solution demonstrates that the microstructure appears to determine the position of the pores. Figure e displays the protrusions of a microstructure of closely packed pillars, prepared by PS $\mu$ M, with limited superimposed roughness.

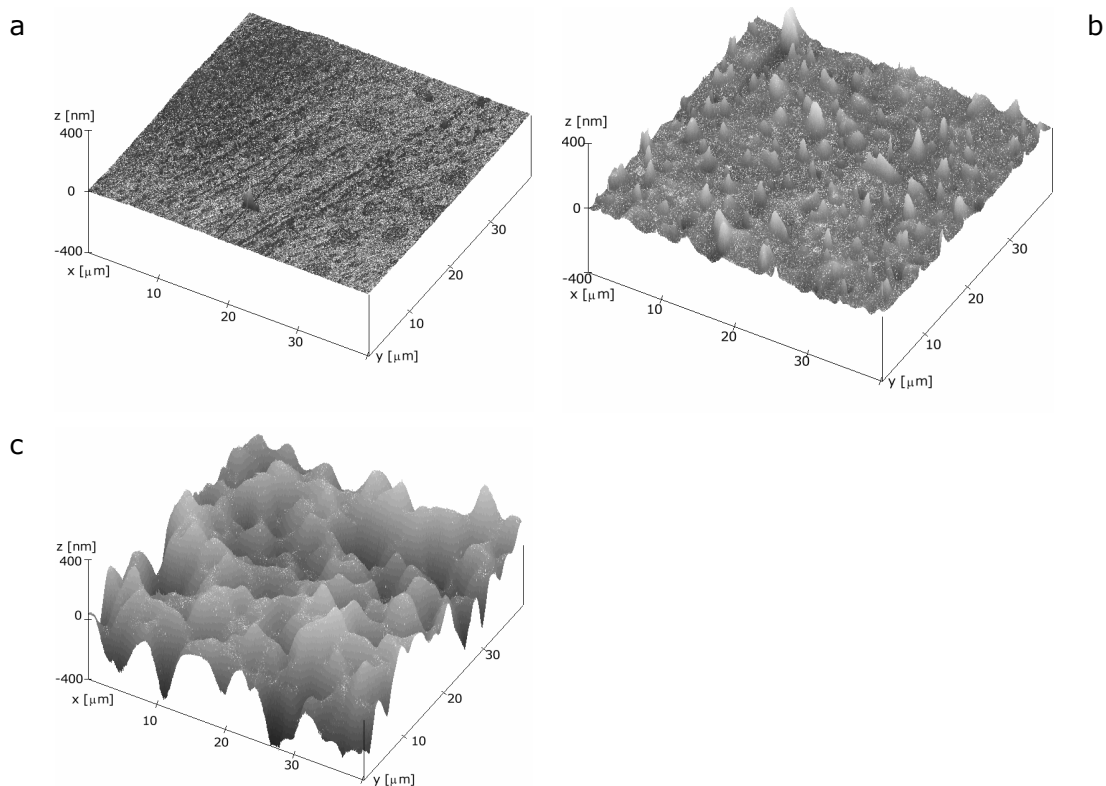


figure 4 Atomic Force Microscopy on Hyflon® AD surfaces.

a H80 surface prepared by evaporation.

b H80 surface prepared by phase separation of a 17.5 wt% solution.

c H60 surface prepared by phase separation of a 17.5 wt% solution.

reduce the contact area of the droplet on the surface and therefore promote superhydrophobicity. Apparently the microstructure influences the porosity. Such collective behavior is also observed on very shallow molds. The pores are placed where all the deeper parts of the mold were before (Figure 3d).

The different surfaces prepared by PS $\mu$ M are initially screened by measuring the static contact angles. Subsequently, for the optimal phase separation recipe advancing and receding contact angles are determined. During the initial screening it appeared that the contact angles measured on H80 surfaces prepared by PS $\mu$ M are generally higher than the



values on H60 surfaces. The better performance of H80 surfaces is unexpected, since a H60 surface prepared by phase separation is rougher than a similar H80 surface (see AFM measurements in Figure 4) Moreover, the contact angles on smooth H60 surfaces are slightly higher than on H80, as expected from the higher fluor content. A possible explanation for the higher contact angle on structured H80 is found when the surfaces are observed by electron microscopy. A clear distinction in the robustness of the surfaces is established. The microstructures of H60 are somewhat damaged, whereas the structured H80 is unaffected by the use for measurements. The inferior mechanical stability of H60 compared to H80 might be an explanation, although also differences in pore morphology within the material may have caused the higher sensitivity to deformations of H60. The presence of such deformations may explain the lower contact angles observed for water drops on H60 surfaces. Nevertheless, for H80 surfaces the results are similar even after clamping them between two glass plates several times, and therefore these surfaces appear to be robust.

Increasing the polymer concentration of the casting solution generally leads to a decrease of the porosity after phase separation, and therefore decreases the roughness. If on the other hand the polymer concentration in the solution is too low, there is insufficient polymer to precisely assimilate the structure on the mold and form a stable microstructure. The optimal polymer solution, consequently, is the solution that contains just enough polymer to form a defect-free microstructure (namely 17.5 wt%).

Table 1 resumes the advancing and receding contact angles for each pattern on H80 surfaces prepared by PS $\mu$ M, in comparison to the values on a H80 surface prepared by evaporation. The expectations based on the Cassie and Baxter equation (equation 2) are calculated (Table 1). The calculation only takes the microstructure into account, and is based on measurements of the contact angles on a smooth H80 surface ( $\theta_a = 116^\circ$ ,  $\theta_r = 104^\circ$ ,  $\theta_s = 110^\circ$ ). Typical examples of drops on a superhydrophobic Hyflon surface are depicted in Figure 5.

From the data in Table 1 it follows that the phase separated microstructures generally provide higher contact angles and reduced hysteresis in comparison to microstructures prepared by evaporation. The improved superhydrophobicity demonstrates that the roughness originating from the phase separation mimics the function of the superimposed roughness on the lotus leaf. The increase in contact angle is much higher for the structures having a  $\Phi_S$  around 0.2 (pattern 1-3) than for the structures having a  $\Phi_S$  of 0.5 (pattern 4-6). In the latter case sometimes there is even no detectable improvement in hydrophobicity. The top part of the protrusions on patterns 4-6 appears to be hardly

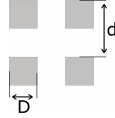
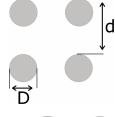
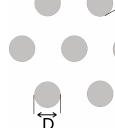
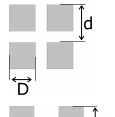
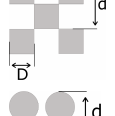

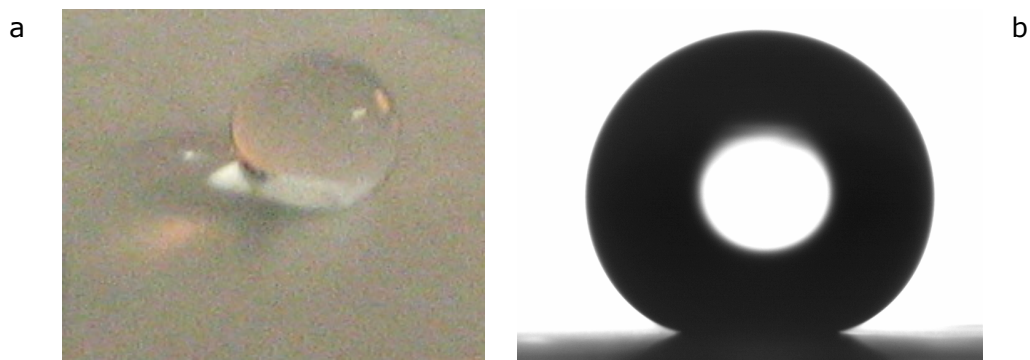
Pattern	Predicted contact angle (Cassie-Baxter)	Advancing and receding contact angle Evaporation	Advancing and receding contact angle PS $\mu$ M
1.  $d = 10 \mu\text{m}$ $\Phi_s = 0.25$	$\theta_{CB} = 147$	$\theta_a = 140$ $\theta_r = 135$	$\theta_a = 160$ $\theta_r = 159$
2.  $d = 10 \mu\text{m}$ $\Phi_s = 0.20$	$\theta_{CB} = 151$	$\theta_a = 146$ $\theta_r = 142$	$\theta_a = 162$ $\theta_r = 150$
3.  $d = 10 \mu\text{m}$ $\Phi_s = 0.23$	$\theta_{CB} = 148$	$\theta_a = 156$ $\theta_r = 153$	$\theta_a = 167$ $\theta_r = 165$
4.  $d = 7.07 \mu\text{m}$ $\Phi_s = 0.50$	$\theta_{CB} = 132$	$\theta_a = 152$ $\theta_r = 145$	$\theta_a = 149$ $\theta_r = 142$
5.  $d = 10 \mu\text{m}$ $\Phi_s = 0.50$	$\theta_{CB} = 132$	$\theta_a = 148$ $\theta_r = 143$	$\theta_a = 154$ $\theta_r = 139$
6.  $d = 6.27 \mu\text{m}$ $\Phi_s = 0.50$	$\theta_{CB} = 132$	$\theta_a = 157$ $\theta_r = 151$	$\theta_a = 156$ $\theta_r = 152$

table 1 Measurements and predictions of advancing and receding contact angles on Hyflon® AD 80X surfaces. The surfaces were either prepared by evaporation or by PS $\mu$ M. The patterns on the microstructures consist of either pillars or square posts in different compositions, with  $D = 5 \mu\text{m}$ . The experimental error in the measurements is approximately three degrees.



**figure 5** *Water drops on a H80 surface patterned by PS $\mu$ M. The water drops display contact angles above 160 degrees.*

**a** *Photograph.*

**b** *Side view from a goniometer measurement.*

influenced by porosity (see Figure 3e). Although it is not yet clear why the roughness on these microstructures differs from similar microstructures in a less closely packed configuration (see Figures 3b and 3c), this phenomenon might explain why there is little influence of the preparation method on the measured contact angles for these patterns.

Considering the contact angles measured on the different patterns, in most cases higher contact angles and less hysteresis are measured for the patterns with  $\Phi_s$  around 0.2, compared to the patterns having a  $\Phi_s$  of 0.5, as was predicted by the Cassie-Baxter equation. However the Cassie-Baxter equation does not always give a correct prediction for the contact angles on the microstructures that were prepared by evaporation. Higher contact angles are measured especially for the three structures having a  $\Phi_s$  of 0.5. Inaccuracy in the fabrication process of the mold can not account for such low values. The deviations towards lower contact angles can be explained if the drop is not completely in the Cassie-Baxter regime, and wets an area larger than merely the tops of the protrusions.

Comparing different patterns with similar  $\Phi_s$ , the hysteresis is clearly influenced by the possible contact lines that the water can form on the patterns, in agreement with theoretical predictions.<sup>14</sup> The shorter the contact lines between the surface and the water the less the hysteresis, since the water is offered hardly any possibility to pin on the surface. In the data in Table 1 such pinning behavior is demonstrated by structure 5. The pattern is

composed of the same pillar structure and additionally has the same  $\Phi_S$  as the pattern in structure 4, but the pillars are arranged differently. The only explanation is that in structure 5 the contact line between the water and the surface is longer, permitting pinning. The pillar pattern in a hexagonal lattice, structure 3, offers the least possibility for the drop to pin on the surface, and indeed the measurements indicate a very low hysteresis.

To check if the low hysteresis and high contact angles correctly predict superhydrophobic behavior, the sliding angle was determined on a surface patterned with structure 3. If the surface was placed under a very small inclination angle of 0.5 degrees, water drops can no longer stay on the surface and immediately roll off. The very low sliding angle confirms the superhydrophobic character of the surface.

### **6.3 conclusions**

Phase Separation Micro Molding is used to prepare superhydrophobic surfaces that can be utilized for self-cleaning purposes. The superhydrophobicity stems from hierarchal roughness, consisting of the microstructure and a superimposed roughness caused by intrinsic porosity. This is concluded from measurements of water contact angles on microstructured surfaces prepared by PS $\mu$ M, in comparison with results of measurements on similar surfaces prepared by evaporation. In PS $\mu$ M, both levels of roughness can be optimized: the microstructure by adjusting the patterns on the mold and the superimposed roughness by adaptation of the phase separation recipe. For the optimized surfaces, water contact angles well above 160 degrees are measured, showing hardly any contact angle hysteresis. If the surface is inclined by only 0.5 degrees, drops can no longer rest on the surface and roll off. PS $\mu$ M therefore proves to be a successful route for the preparation of superhydrophobic surfaces.

### **6.4 experimental**

*Preparation of the surfaces.* Hyflon ® AD 80X and Hyflon ® AD 60X were obtained from Solvay Solexis. Both materials were dissolved in HGalden ZT 130, which was also acquired from Solvay Solexis. The polymers were dissolved in different concentrations between 10 and 20 weight percent, at ambient room temperature under constant stirring.

The mold was prepared from silicon by photolithography and etching. The etching was performed on a Plasmatherm SLR 770, using a standard Bosch process ( $C_4F_8$ ,  $SF_6$  and Ar gas). The silicon substrate was maintained at a temperature of 20 °C. One cycle consisted of 2s of deposition, 2s of removal and 6s of etching. The final depth of the mold was 8 micrometer. The height of the microstructures

from the optimized recipe (see below) is measured to match the 8 micrometer depth of the mold.

The solutions were spread out by casting in a film, having a thickness of 100 micrometer for PS $\mu$ M and 250 micrometer for evaporation. Immersion precipitation was performed in n-pentane (98%, Acros). The polymer was kept on the mold in pentane for approximately half an hour, and subsequently rinsed in ethanol (analytical quality, Merck) for another half hour. Evaporation of solvent succeeded in a nitrogen environment at ambient room temperature for approximately 20 hours. To prevent the polymer films from curling, they were either dried while clamped between glass slides, or were attached on thin glass slides coated with double sided sticky tape. In the latter case, the sticky tape was applied on the backside of the structured polymer film, while the film was floating and spread on water. This way the polymer was completely flat on the glass plate. The films were dried in air.

*Contact angle measurements.* Contact angle measurements were performed on a Goniometer

(Dataphysics OCA 15+). Initially, the surfaces resulting from different PS $\mu$ M recipes were screened by measuring statical contact angles, using drops having a volume of 6  $\mu$ l. Advancing and receding contact angles were determined by placing the needle in the drop, and continuously supplying or withdrawing water. The sliding angle was determined by placing the glass plate, on which the polymer was coated, on a leveled surface. The surface was inclined gradually, placing a drop of 11  $\mu$ l on the surface after each inclination step.

*Electron Microscopy.* The SEM observations were performed on a JEOL 5600 LV electron microscope. An acceleration voltage of 5 kV was applied. Prior to imaging the polymeric samples were coated with a thin layer of platinum (approximately 25 nm thick) to avoid charging of the samples.

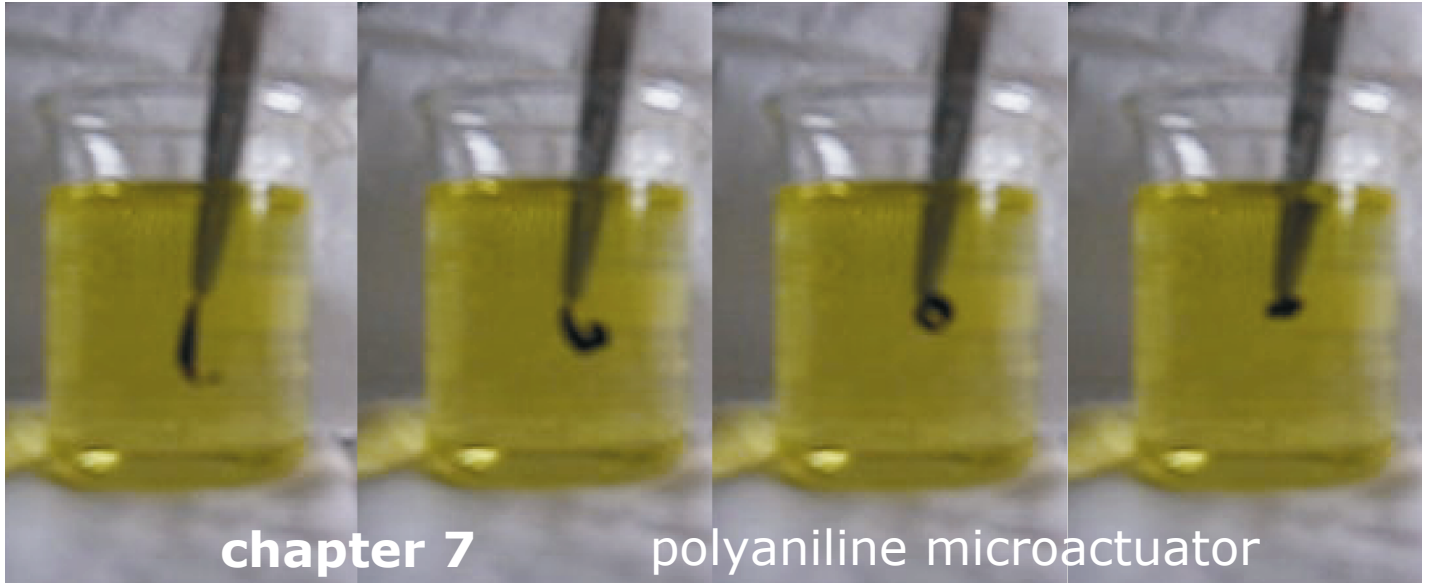
*Atomic Force Microscopy.* The AFM measurements were performed on a Nanoscope III (Digital Instruments) operating in tapping mode.

## references

- <sup>1</sup> C. Neinhuis, W. Barthlott, *Ann. Bot.-London* **1997**, *79*, 667.
- <sup>2</sup> R. Blossey, *Nature Mater.* **2003**, *2*, 301.
- <sup>3</sup> A. Otten, S. Herminghaus, *Langmuir* **2004**, *20*, 2405.
- <sup>4</sup> G. S. Watson, J. A. Watson, *Applied Surface Science* **2004**, *235*, 139
- <sup>5</sup> W. Barthlott, C. Neinhuis, *Planta* **1997**, *202*, 1.
- <sup>6</sup> D. Quéré, *Physica A* **2002**, *313*, 32
- <sup>7</sup> D. Richard, D. Quéré, *Europhys. Lett.* **2000**, *50*, 769.
- <sup>8</sup> D. Richard, D. Quéré, *Europhys. Lett.* **1999**, *48*, 286.
- <sup>9</sup> N. A. Patankar, *Langmuir* **2004**, *20*, 8209
- <sup>10</sup> K. Acatay, E. Simsek, C. Ow-Yang, Y. Z. Menceloglu, *Angew. Chem. Int. Ed.* **2004**, *43*, 5210.
- <sup>11</sup> Examples of commercial products making use of the 'Lotus effect': Tegotop 105, [www.degussa-home-care.com](http://www.degussa-home-care.com), antifouling fabric for jeans: nanocare, [www.mac-mode.nl](http://www.mac-mode.nl).
- <sup>12</sup> S. Minko, M. Mueller, M. Motornov, M. Nitschke, K. Grundke, M. Stamm, *J. Am. Chem. Soc.* **2003**, *125*, 3896.
- <sup>13</sup> S. Veeramasesaneni, J. Drelich, J. D. Miller, G. Yamauchi, *Prog. Org. Coat.* **1997**, *31*, 265.
- <sup>14</sup> W. Chen, A. Y. Fadeev, M. C. Hsieh, D. Oner, J. Youngblood, T. J. McCarthy, *Langmuir* **1999**, *15*, 3395.
- <sup>15</sup> J. Zhang, J. Li, Y. Han, *Macromol. Rapid Comm.* **2004**, *25*, 1105.
- <sup>16</sup> H. Y. Erbil, A. L. Demirel, Y. Avci, O. Mert, *Science* **2003**, *299*, 1377.
- <sup>17</sup> S. Shibuichi, T. Onda, N. Satoh, K. Tsujii, *J. Phys. Chem.* **1996**, *100*, 19512; T. Onda, S. Shibuichi, N. Satoh, K. Tsujii, *Langmuir* **1996**, *12*, 2125.
- <sup>18</sup> S. Li, H. Li, X. Wang, Y. Song, Y. Liu, L. Jiang, D. Zhu, *J. Phys. Chem. B.* **2002**, *106*, 9274.
- <sup>19</sup> H. Li, X. Wang, Y. Song, Y. Liu, Q. Li, L. Jiang, D. Zhu, *Angew. Chem. Int. Ed.* **2001**, *40*, 1743.
- <sup>20</sup> K. K. S. Lau, J. Bico, K. B. K. Teo, M. Chhowalla, G. A. J. Amaratunga, W. I. Milne, G. H. McKinley, K. K. Gleason, *Nano Lett.* **2003**, *3*, 1701.
- <sup>21</sup> L. Feng, Y. Song, J. Zhai, B. Liu, J. Xu, L. Jiang, D. Zhu, *Angew. Chem.* **2003**, *115*, 824.
- <sup>22</sup> L. Feng, S. Li, Y. Li, H. Li, L. Zhang, J. Zhai, Y. Song, B. Liu, L. Jiang, D. Zhu, *Adv. Mater* **2002**, *14*, 1857
- <sup>23</sup> Q. Xie, J. Xu, L. Feng, L. Jiang, W. Tang, X. Luo, C. C. Han, *Adv. Mater.* **2004**, *16*, 302.
- <sup>24</sup> K. Acatay, E. Simsek, C. Ow-Yang, Y. Z. Menceloglu, *Angew. Chem. Int. Ed.* **2004**, *43*, 5210.

## chapter 6

- <sup>25</sup> L. Jiang, Y. Zhao, J. Zhai, *Angew. Chem. Int. Ed.* **2004**, *43*, 4338.
- <sup>26</sup> A. Nakajima, K. Abe, K. Hashimoto, T. Watanabe, *Thin Solid Films* **2000**, *376*, 140.
- <sup>27</sup> M. Thieme, R. Frenzel, S. Schmidt, F. Simon, A. Hennig, H. Worch, K. Lunkwitz, D. Scharnweber, *Adv. Eng. Mater.* **2001**, *3*, 691.
- <sup>28</sup> D. Oner, T. J. McCarthy, *Langmuir* **2000**, *16*, 7777.
- <sup>29</sup> Z. Yoshimitsu, A. Nakajima, T. Watanabe, K. Hashimoto, *Langmuir* **2002**, *18*, 5818.
- <sup>30</sup> J. Bico, C. Marzolin, D. Quere, *Europhys. Lett.* **1999**, *47*, 220.
- <sup>31</sup> N. J. Shirtcliff, S. Aqil, C. Evans, G. McHale, M. I. Newton, C. C. Perry, P. Roach, *J. Micromech. Microeng.* **2004**, *14*, 1384.
- <sup>32</sup> B. He, N. A. Patankar, J. Lee, *Langmuir* **2003**, *19*, 4999.
- <sup>33</sup> J. Jopp, H. Gruell, R. Yerushalmi-Rozen, *Langmuir* **2004**, *20*, 10015.
- <sup>34</sup> L. Vogelaar, J. N. Barsema, C. J. M. van Rijn, W. Nijdam, M. Wessling, *Adv. Mater.* **2003**, *15*, 1385
- <sup>35</sup> L. Vogelaar, R. G. H. Lammertink, J. N. Barsema, W. Nijdam, L. A. M. Bolhuis-Versteeg, C. J. M. van Rijn, M. Wessling, *Small* **2005**, *1*, 645.
- <sup>36</sup> S. Herminghaus, *Europhys. Lett.* **2000**, *52*, 165.
- <sup>37</sup> D. Queré, *Nature Mater.* **2002**, *1*, 14.
- <sup>38</sup> A. Marmur, *Langmuir* **2004**, *20*, 3517.
- <sup>39</sup> M. Mulder, *Basic Principles of Membrane Technology*, Kluwer academic publishers, Dordrecht, the Netherlands **1996**.
- <sup>40</sup> R. W. Baker, *Membrane Technology and Research*, Mc Graw-Hill, New York, U.S. **2000**.
- <sup>41</sup> V. Arcella, P. Colaïanna, P. Maccone, A. Sanguineti, A. Gordano, G. Clarizia, E. Drioli, *J. Membr. Sci.* **1999**, *163*, 203.
- <sup>42</sup> A. Gordano, V. Arcella, E. Drioli, *Desalination* **2004**, *163*, 127.



## fabricated by phase separation micro molding

*L. Vogelaar*

*H. Zhang*

*R. G. H. Lammertink*

*M. Wessling*

Perforated microstructures prepared from polyaniline (PANi) by phase separation micro molding are utilized as microactuators. PANi shows a pH dependant change in volume. Under certain conditions, the phase separation process results in an asymmetric pore morphology within the polymer film. The gradient in material density, resulting from the asymmetry, is responsible for an asymmetric expansion when subjected to a change in pH. The extent of bending is determined by the acid concentration. Elongated PANi microstructures can therefore be used as microactuators. The use of a single layer of material avoids problems related to delamination. The actuation of the device does not require an external power supply.

*Above: polyaniline film bending and curling up in an acidic solution.*

## 7.1 introduction

Microactuators are microdevices that convert a stimulus, for example an electrical potential or the presence of chemical compounds, into a movement. In microfluidics, for example, such microactuators are exploited to pump or direct liquids.<sup>1</sup> Application as artificial muscles in biomedical devices is also demonstrated.<sup>2</sup> The use of polymers for such devices has a few advantages, especially concerning contact with biological samples. Preferably, the device should be inexpensive and suitable for single use, which avoids cross-contamination. Furthermore, the liquid environment in which the devices operate should not affect its function.

Conjugated polymers find use as active layers in microactuator devices.<sup>1,3,4</sup> The volume of the polymer changes in response to a signal. If the polymer is laminated on a non-responsive material, the result is a bending movement of the device. Examples of conjugated polymers that are used to fabricate microactuators are polyaniline and polypyrrole. Another type of microactuator is based on hydrogels, which are able to expand when subjected to a change in pH. An important advantage of hydrogel-based actuators is that they do not require an external power supply for operation.<sup>5</sup>

In order to prepare a microactuator, the responsive material must be available for microstructuring. The hydrogels, for instance, are microstructured photochemically. Microstructuring of conjugated polymers is possible in various ways,<sup>6</sup> e.g. by electrodeposition on patterned electrodes,<sup>1</sup> photochemical patterning,<sup>7</sup> direct writing methods,<sup>8</sup> and soft lithography.<sup>9</sup>

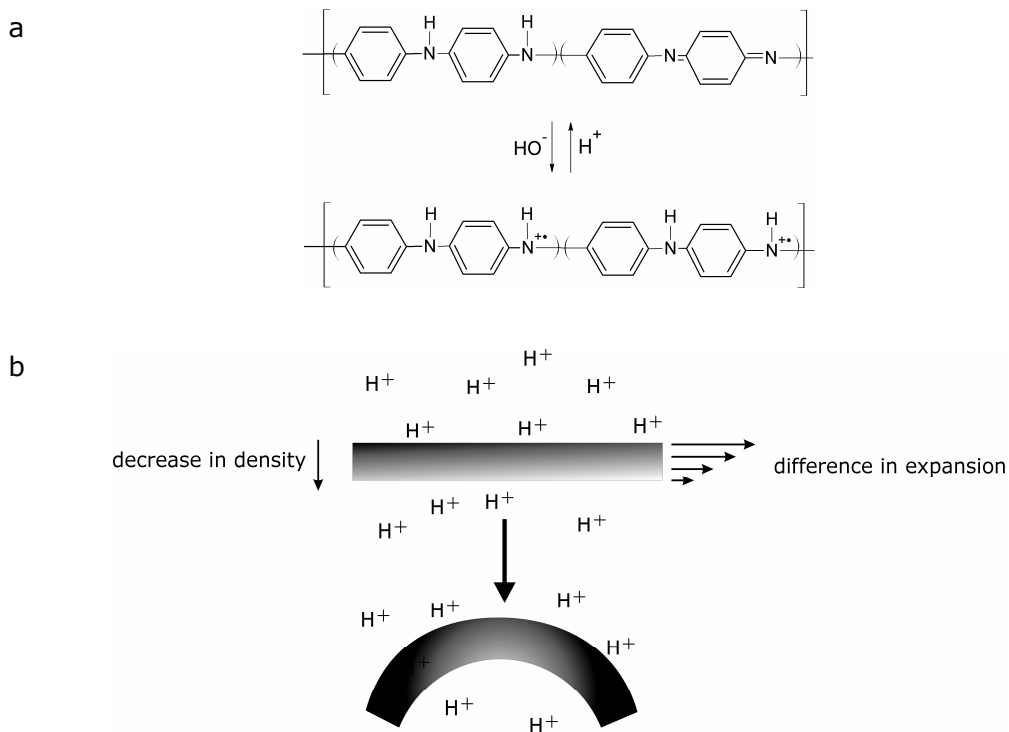
Under certain conditions, using phase separation of polyaniline in its emeraldine base form (PANi EB), thin films are prepared that bend when subjected to a change in pH. The bending response makes these PANi films suitable for use as actuators.<sup>10,11</sup> An electrical potential or the presence of chemical vapors also causes actuation.<sup>12,13</sup> The reason for the bending movement is the asymmetry in the density of the material: the pores are unevenly distributed throughout the film and have a broad size distribution.<sup>14,15</sup> There is a steep decrease in the amount of material from the side of the film that was in contact with the non-solvent, to the side, that was on the substrate during the phase separation. If PANi EB is doped with a proton (see Figure 1a), the result is an increase in volume. The mechanism for the volume change as a result of the doping of PANi EB is an osmotic effect. To compensate the charge of the protons, hydrated counterions are incorporated in the polymer.<sup>10</sup> The presence of ions increases the osmotic pressure and thus forces water to enter the polymer,



which results in expansion of the polymer.<sup>4,16</sup> The density gradient leads to an asymmetric expansion, and the film will bend in response to an external stimulus (see Figure 1b).

There are a few advantages in the use of an asymmetric PANi film as an actuator. First, the fabrication process is simplified, because it is a device from a single material and does not require lamination of the actuating material on other layers. Second, since the actuator consists of a single layer, there is no risk of failure of the device caused by delamination during operation.

Phase Separation Micro Molding (PS $\mu$ M) is a microfabrication method, based on liquid induced phase separation.<sup>17,18</sup> The process therefore gives access to preparation of



**figure1a** Repeat unit of Polyaniline, emeraldine base before (top) and after (bottom) doping with a proton. The protonation is reversed in the presence of hydroxide ions.<sup>10</sup>

**b** Schematic representation of actuation of a PANi film prepared by phase separation, having an asymmetric material distribution. As a result of protonation, the volume of PANi EB increases. Because of the decreasing material density throughout the film the expansion is asymmetric, leading to a bending movement of the film.

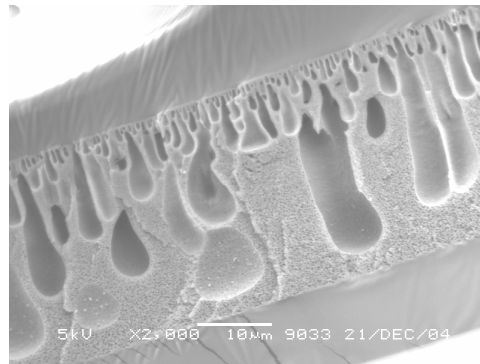


figure 2 Cross-section of an asymmetric thin film of polyaniline, emeraldine base, prepared by phase separation.

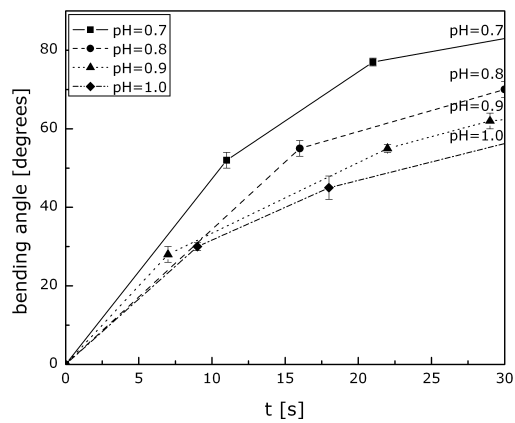


figure 3 Bending of an asymmetric film of polyaniline as a function of time and pH. The thickness of the film was 120  $\mu\text{m}$ .

microstructures, having a density gradient throughout the cross section of the material similar to thin PANi films. This microactuator would also avoid a complex fabrication process and problems related to delamination. In this chapter, first an actuator is prepared on macroscale from a thin, asymmetric PANi EB film. Subsequently the results are used to progress towards preparation of a microactuator by PS $\mu$ M.

## 7.2 results and discussion

Thin, asymmetric films of PANi EB were prepared by liquid induced phase separation. A solution having a high EB concentration was obtained via a gel-inhibitor assisted dissolution route.<sup>10</sup> The solution is spread out in a thin film via casting and immersed in a non-solvent. During the immersion the polymer precipitates and forms a porous film. The polymer film has an asymmetry in the material density, as a consequence of the uneven distribution of pores (Figure 2).

Figure 3 displays the bending of the film as a function of pH and time. Clearly a decrease in pH leads to an increased bending response. Even though the time scale reported in literature for similar actuators is in the same order of magnitude (a few tens of seconds), the response is a bit slower than reported.<sup>10</sup> Apparently, there is room for optimization of the actuator, for instance by adjusting the size of the actuator, the procedure of the solution preparation or the molecular structure of the PANi.

For the preparation of a microactuator by PS $\mu$ M a similar phase separation recipe is used. The polymer solution is then applied on a mold by casting. The top level of the solution after application on the mold is in proximity of the protrusions on the mold. Subsequently the mold and solution are immersed in a non-solvent, causing the solution to phase separate and solidify. The mold perforates the polymer film during the phase separation, creating freestanding PANi microstructures. This phenomenon is described more in detail in Chapter 4.

The possibility to create a completely open microstructure is exploited in the fabrication of the microactuator to create small bars of PANi, having typical dimensions of 25 x 500  $\mu$ m. Figure 4 shows that the PANi microstructure clearly displays an asymmetry in the material distribution, similar to the PANi thin film that was prepared by phase separation (Figure 2). The PANi film, containing the strips, is then integrated with a fluid reservoir, prepared from PDMS.

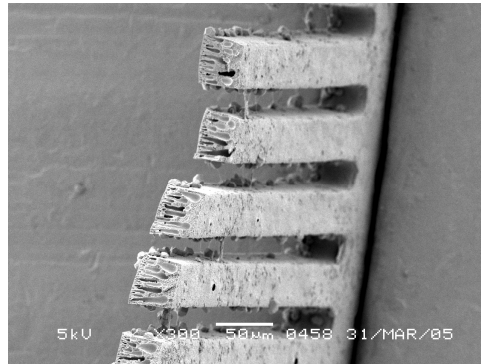


figure 4 *Cross-section of a perforated microstructure of polyaniline. The fractured surface reveals the asymmetry in the material distribution.*

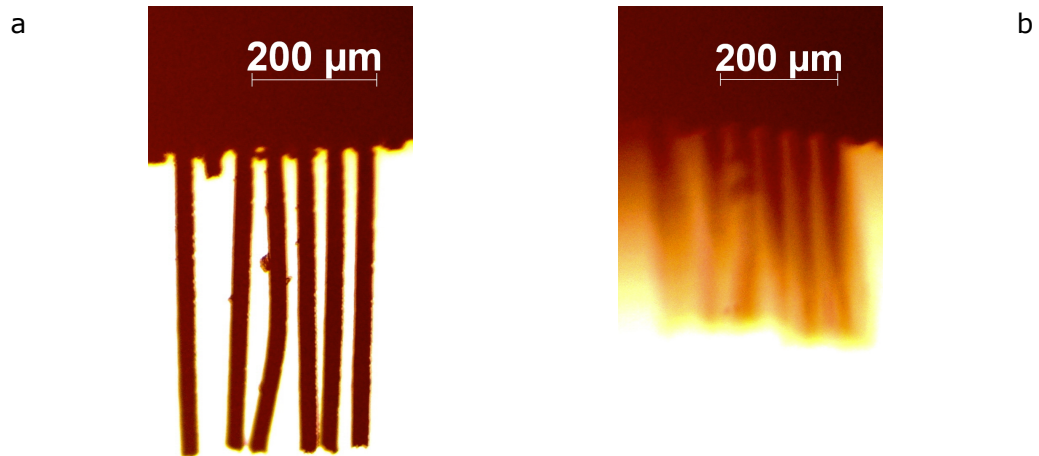


figure 5 *Polyaniline microactuator in water (a) and a HCl solution (concentration 2.1%, pH=1.7). The focus of the microscope was not adjusted between the two images.*

The response of the microactuators to a change in pH was observed using a microscope (Figure 5). Initially the fluid reservoir was filled with water. Then gradually water is replaced by an acidic solution. The microactuators react to the presence of protons by bending out of the focal plane of the microscope (Figure 5b). The reduction in projected length of the microactuators in Figure 5b indicates that the loose ends of the microstructures have bended away. From the projected length the position of the loose end of the actuator is estimated to have moved at most 340 micrometer out of the focal plane. From Figure 5 it is concluded that indeed microstructures have been prepared, which display pH sensitive actuation. The device shares the advantage of hydrogels that no external power supply is necessary for operation. The response times are in the order of a few tens of seconds, which is comparable with hydrogel-based devices<sup>5</sup> and promises a fast device performance.

### 7.3 conclusions

Microactuators have been prepared of polyaniline by PS $\mu$ M. The phase separation process results in an asymmetric cross-section; a gradient in the material density in the microactuator. The uneven distribution of material is responsible for asymmetric expansion and thus bending when the device is subjected to a change in pH. The extent of actuation is determined by the proton concentration. The time necessary to respond to a pH change is comparable to hydrogel-based devices, promising a fast performance of the device. In comparison with other microactuators based on conjugated polymers, advantages are found in the simple and cost effective fabrication process and the use of a single layer of material for actuation. The actuation is purely diffusion driven, and therefore the device does not require an external power source.

### 7.4 experimental

Polyaniline (Aldrich,  $M_w \approx 65.000$ ) was dissolved in a concentration of 19.0 wt% in N-methyl-2-pyrrolidinone (Acros, 99%), which made up 68.6 wt% of the solution. Solutions of PANi EB generally tend to form a gel at high concentrations. Therefore addition of a gel inhibitor to the solution is necessary.<sup>10,11,12,13,19,20,21</sup> Heptamethyleneimine (Fluka, 99%) was added to prevent gelation of the solution, at a concentration of 12.4 wt%.<sup>10,13</sup> First, NMP and HPMI were mixed and heated to 30 °C. Then, PANi was added gradually over approximately three minutes, and dissolved under constant stirring (100

rpm) for one hour. A homogeneous solution is obtained, which reveals no signs of gelation within the time span in which the actuators are prepared.

The thin PANi EB films were prepared on a flat silicon wafer by casting. The height of the casting knife can be adjusted with micrometer accuracy (see experimental section in Chapter 2). Immersion precipitation was performed using tap water. For the film used for the measurement in Figure 3 the solution was cast at a thickness of 200  $\mu\text{m}$ , resulting in a thickness after phase separation of 120  $\mu\text{m}$ . The films were cut in strips of 0.3 x 3 cm, and subsequently

immersed in an aqueous HCl solution at room temperature. The strips were clamped at one end, leaving the other end free. The solution was stirred slowly. The pH was measured using a Metrohm 691 pH meter. An angular scale was placed in front of the actuator to measure the bending angle of the strips. The bending angle is determined as the angular position of the loose end of the strip.

The microactuator was prepared on a mold, having a forked pattern of blocks 500  $\mu\text{m}$  in length and 25  $\mu\text{m}$  in width. The blocks were spaced at a distance of 25  $\mu\text{m}$ . The mold was prepared from silicon by photolithography and etching. The etching was performed on a Plasmatherm SLR 770, using a standard Bosch process ( $\text{C}_4\text{F}_8$ ,  $\text{SF}_6$  and Ar gas). The silicon substrate was maintained at a temperature of 20  $^\circ\text{C}$ . One cycle consisted of 2s of deposition, 2s of removal and 6s of etching. The final mold depth was 53  $\mu\text{m}$ . The solution was applied a few micrometer above the protrusions on the mold. Phase separation resulted in a thickness of the microactuators of 26  $\mu\text{m}$ .

The microactuator was integrated with a fluid reservoir, which consisted of a ring of approximately 0.5 cm thick PDMS (Sylgard 184, Dow Corning.) The volume of the fluid that was contained in the reservoir was 1.2 ml. The PANi film containing the microactuators was placed on a microscopic glass slide. The PDMS was sealed on the glass, clamping the

PANi where the microactuators were connected to the film. Two syringes punched through the PDMS enabled controlled addition and removal of fluid to the reservoir. Optical microscope images were taken on a Zeiss Axiovert 40 MAT Optical microscope. During the microscopic observations, the position of the glass slide, the microscopic table and the syringes were fixed, so that addition and removal of fluid did not affect the microscopic observation. The images taken by the microscope (which detected reflected light) were enhanced by placing a mirror on top of the fluid reservoir. HCl 32 % (analytical quality, Merck) was slowly added to the reservoir while the same volume of water was removed. The fluid reservoir then contained an aqueous HCl solution having a concentration of 2.1 % (pH=1.7). The image was taken after approximately two minutes, when the microactuators had not changed position anymore for at least a minute.

The SEM observations were performed on a JEOL 5600 LV electron microscope. An acceleration voltage of 5 kV was applied. Previous to imaging the polymeric samples were coated with a thin layer of platinum (approximately 25 nm thick) to avoid charging of the samples. To prepare the cross-sections, the polymer was immersed in ethanol, subsequently frozen in liquid nitrogen and broken.

## references

- <sup>1</sup> E. W. H. Jager, E. Smela, O. Inghanas, *Science* **2000**, 290, 1540.
- <sup>2</sup> E. Smela, *Adv. Mater.* **2003**, 15, 481.
- <sup>3</sup> R. H. Baughman, *Synthetic Met.* **1996**, 78, 339.
- <sup>4</sup> M. Roemer, T. Kurzenknabe, E. Oesterschulze, N. Nicoloso, *Anal. Bioanal. Chem.* **2002**, 373, 754.
- <sup>5</sup> D. J. Beebe, J. S. Moore, J. M. Bauer, Q. Yu, R. H. Liu, C. Devadoss, B. H. Jo, *Nature* **2000**, 404, 588.
- <sup>6</sup> S. Holdcroft, *Adv. Mater.* **2001**, 13, 1753.
- <sup>7</sup> C. J. Drury, C. M. J. Mutsaers, C. M. Hart, M. Matters, D. M. de Leeuw, *Appl. Phys. Lett.* **1998**, 73, 108.
- <sup>8</sup> H. Siringhaus, T. Kawase, R. H. Friend, T. Shimoda, M. Inbasekaran, W. Wu, E. P. Woo, *Science* **2000**, 290, 2123.
- <sup>9</sup> Y. Xia, G. M. Whitesides, *Angew. Chem. Int. Ed.* **1998**, 37, 550.
- <sup>10</sup> H. L. Wang, J. Gao, J. M. Sansinena, P. McCarthy, *Chem. Mater.* **2002**, 14, 2546.
- <sup>11</sup> J. M. Sansinena, J. Gao, H. L. Wang, *Adv. Funct. Mater.* **2003**, 13, 703.
- <sup>12</sup> J. Gao, J. M. Sansinena, H. L. Wang, *Synthetic Met.* **2003**, 135-136, 809.
- <sup>13</sup> J. Gao, J. M. Sansinena, H. L. Wang, *Chem. Mater.* **2003**, 15, 2411.
- <sup>14</sup> M. Mulder, *Basic principles of membrane technology*, Kluwer academic publishers, Dordrecht, the Netherlands **1996**.
- <sup>15</sup> R. W. Baker, *Membrane technology and research*, Mc Graw-Hill, New York, U.S. **2000**.
- <sup>16</sup> L. Bay, T. Jacobsen, S. Skaarup, K. West, *J. Phys. Chem. B* **2001**, 105, 8492.
- <sup>17</sup> L. Vogelaar, J. N. Barsema, W. Nijdam, C. J. M. van Rijn, M. Wessling, *Adv. Mater.* **2003**, 15, 1385.
- <sup>18</sup> L. Vogelaar, R. G. H. Lammertink, J. N. Barsema, W. Nijdam, L. A. M. Bolhuis-Versteeg, C. J. M. van Rijn, M. Wessling, *Small* **2005**, 1, 645.
- <sup>19</sup> H. L. Wang, R. J. Romero, B. R. Mattes, Y. Zhu, M. J. Winokur, *J. Polym. Sci. Pol. Phys.* **2000**, 38, 194.
- <sup>20</sup> D. Yang, B. R. Mattes, *J. Polym. Sci. Pol. Phys.* **2002**, 40, 2702.
- <sup>21</sup> B. R. Mattes, H. L. Wang, D. Yang, Y. T. Zhu, W. R. Blumenthal, M. F. Hundley, *Synth. Met.* **1997**, 84, 45.

The research described in this thesis concerns the development of a new microfabrication method, Phase Separation Micro Molding (PS $\mu$ M). While microfabrication is still best known from semiconductor industry, where it is used to integrate electrical components on a chip, the scope has immensely expanded towards technologies including integrated optics, biomedical technology and microfluidics.

PS $\mu$ M is a replication method, based on phase separation of polymer solutions, a technique that is commonly utilized in the preparation of polymeric membranes. In PS $\mu$ M, phase separation is combined with replication of a microstructured mold. The process is described in detail in Chapter 2. Replication methods generally have a few advantages in comparison with photolithography, traditionally the method of choice for microfabrication purposes (see Chapter 1). Replication provides a straightforward and cost-effective alternative, and expands the range of applicable materials, which is necessary for the development of new applications. The latter advantage especially counts for PS $\mu$ M, in which virtually all soluble polymers can be employed. Additional post-processing can also lead to microstructures of carbon and certain ceramics and metals. Therefore PS $\mu$ M further broadens the range of materials applicable for microfabrication.

Another interesting aspect of PS $\mu$ M is the absence of problems like sticking or breaking during the release of the polymer replica from the mold. In most other replication methods, the release is the most critical part of the process. In PS $\mu$ M the polymer shrinks during the phase separation and the replica releases without external force. In this thesis, replication of features having dimensions down to 150 nm and aspect ratio's up to 5, without notable problems is demonstrated. The shrinkage in PS $\mu$ M also leads to very simple fabrication of perforated microstructures. Such microstructures can be applied for instance as polymeric microsieves (very efficient microfiltration membranes) or masks, which can be used for etching or deposition (see Chapter 4).

Using PS $\mu$ M, microstructures that have a freestanding configuration can be fabricated in a single step. The unprecedented simplicity of the fabrication process relies on corner flow of the polymer solution into a polygonal hole in which an air bubble is entrapped. Chapter 3 elaborates on the fabrication of freestanding microstructures by PS $\mu$ M and compares the experimental results to a model describing corner flow.

A unique characteristic of PS $\mu$ M is its ability to prepare microstructures having an intrinsic porosity. The morphology of the porosity can be adjusted by tailoring the composition of the solution and the non-solvent. To support that the above-mentioned characteristics of PS $\mu$ M (porosity, perforation, broad choice of materials and easy process conditions) can indeed be considered as strengths, Chapters 4 until 7 describe examples of applications.

In Chapter 4, the porosity is used to achieve further size reduction by a heat treatment, in which the pores collapse and the microstructure shrinks uniformly. A size reduction over 50% has been realized. Chapter 5 describes how a porous microstructure, prepared from a biodegradable polymer, can be used as a scaffold for tissue engineering. In the scaffold the microstructure enables directional growth of cells, which is crucial for the engineering of several kinds of tissue, while the porosity ensures the necessary transport of nutrients towards the cells.

In Chapter 6 the porosity is exploited to create a hierarchical roughness in a hydrophobic material, leading to superhydrophobicity. The two levels of roughness consist of the microstructure and a superimposed roughness caused by the porosity. This combination mimicks the self cleaning surface of certain plant leaves (the most famous example of which is the lotus). On such surfaces water drops roll like marbles, and drag along dirt particles that come in their way. The surface prepared by PS $\mu$ M shows similar superhydrophobicity: water drops display contact angles well above 160°, and roll off the surface when tilted only 0.5°.

Finally in Chapter 7 a microactuator is developed, making use of the unique possibility of phase separation to realize an asymmetric pore morphology. The device is prepared from Polyaniline, a conducting polymer that expands when subjected to a change in pH. The asymmetry in the material distribution within the microactuator causes an asymmetric expansion and thus bending. In this way the device is able to translate a change in pH into a movement without requiring an external power source.



Het onderzoek beschreven in dit proefschrift heeft betrekking op de ontwikkeling van een nieuwe microfabricage methode, Phase Separation Micro Molding (PS $\mu$ M). Hoewel microfabricage vooral bekend is van de halfgeleiderindustrie, waar het gebruikt wordt om elektrische componenten op een chip te integreren, is de reikwijdte enorm verbreed met technologieën zoals geïntegreerde optica, biomedische technologie en microfluidica.

PS $\mu$ M is een replicatie methode, gebaseerd op fasescheiding van polymeer oplossingen, een techniek die normaliter wordt gebruikt voor de fabricage van polymere membranen. In PS $\mu$ M wordt fasescheiding gecombineerd met replicatie van een microgestructureerde mal. Dit proces wordt in verder detail beschreven in Hoofdstuk 2. Over het algemeen hebben replicatie methoden een aantal voordelen ten opzichte van fotolithografie, van oudsher de meest gekozen methode voor microfabricage doeleinden (zie Hoofdstuk 1). Replicatie voorziet in een eenvoudig en kostenbesparend alternatief, en breidt de reeks toepasbare materialen uit, wat noodzakelijk is voor de ontwikkeling van nieuwe toepassingen. Het laatstgenoemde voordeel geldt in het bijzonder voor PS $\mu$ M, waarvoor praktisch alle oplosbare polymeren kunnen worden gebruikt. Een extra nabewerkingsstap kan ook leiden tot microstructurering van koolstof en bepaalde keramische stoffen en metalen. Daarmee verbreedt PS $\mu$ M het spectrum van toepasbare materialen nog verder.

Een ander interessant aspect van PS $\mu$ M is het ontbreken van problemen als plakken of breken tijdens het losmaken van de polymere replica uit de mal. Bij de meeste andere replicatie methoden is het losmaken de meest riskante processtap. Bij PS $\mu$ M krimpt het polymeer tijdens de fasescheiding en komt de replica vanzelf van de mal los, waarmee eerder genoemde problemen voorkomen worden. In dit proefschrift wordt replicatie aangetoond van structuren met een afmeting tot aan 150 nm en aspect ratio's oplopend tot 5, zonder opmerkelijke problemen. De krimp tijdens PS $\mu$ M leidt ook tot eenvoudige fabricage van geperforeerde microstructuren. Zulke structuren kunnen toepassing vinden bijvoorbeeld als

polymere microzeef (een efficiënt microfiltratie membraan) of als masker, wat weer gebruikt kan worden voor etsen of depositie (zie Hoofdstuk 4).

Met behulp van PS $\mu$ M kunnen microstructuren met een vrijstaande configuratie in een stap gemaakt worden. De niet eerder vertoonde eenvoud van het fabricage proces berust op stroming van de polymeer oplossing door de hoeken van een polygonaal gat waarin een luchtbel opgesloten zit. Hoofdstuk 3 gaat verder in op de fabricage van deze vrijstaande microstructuren met PS $\mu$ M en vergelijkt de experimentele resultaten met een model.

Een unieke eigenschap van PS $\mu$ M is de mogelijkheid om microstructuren te maken die poreus zijn. De porieverdeling kan worden aangepast door afstemming van de receptuur van de oplossing en het niet-oplosmiddel. Om te staven dat eerdergenoemde eigenschappen van PS $\mu$ M (porositeit, perforatie, brede materiaalkeus en eenvoudig proces) gezien kunnen worden als sterke punten, geven Hoofdstuk 4 tot en met 7 voorbeelden van toepassingen.

In hoofdstuk 4 wordt de porositeit gebruikt om een verdere verkleining te bewerkstelligen door middel van een warmtebehandeling, waarin de poriën ineenklappen en de microstructuur uniform krimpt. Een verkleining van meer dan 50% is gerealiseerd. Hoofdstuk 5 beschrijft hoe een poreuze microstructuur uit biodegradeerbaar materiaal gebruikt kan worden als scaffold voor tissue engineering. In de scaffold controleert de microstructuur de groeirichting van de cellen, wat relevant is voor de constructie van diverse typen weefsels, terwijl de porositeit zorgt voor de benodigde toevoer van voedingsstoffen.

In Hoofdstuk 6 wordt de porositeit benut om een hiërarchische ruwheid te creëren in een hydrofoob materiaal, resulterend in superhydrofobiciteit. De twee niveaus van ruwheid bestaan uit de microstructuur en een ruwheid daarbovenop als gevolg van de porositeit. Deze combinatie bootst het zelfreinigend oppervlak van bepaalde planten na (waarvan het bekendste voorbeeld de lotus is). Op een dergelijk oppervlak rollen waterdruppels als knikkers, waarbij ze vuildeeltjes op hun pad meeslepen. Het oppervlak dat gemaakt is met PS $\mu$ M vertoont vergelijkbare superhydrofobiciteit: water druppels laten een contacthoek ver boven 160° zien, en rollen van het oppervlak af wanneer het slechts 0.5° scheef gezet wordt.

Ten slotte wordt in Hoofdstuk 7 een microactuator ontwikkeld, waarbij gebruik wordt gemaakt van de unieke eigenschap van fasescheiding om een asymmetrische porieverdeling te realiseren. De microactuator is gemaakt van Polyaniline, een geleidend polymeer dat uitzet wanneer het aan een verandering in pH blootgesteld wordt. De asymmetrie in de materiaalverdeling in de microactuator leidt tot een ongelijkmatige uitzetting en dus buiging. Op die manier is de actuator in staat om een verandering in pH te vertalen in een beweging, zonder gebruikmaking van een externe energievoorziening.

## curriculum vitae

Laura Vogelaar, geboren 5 september 1975 te Rotterdam.

- 1987-1994    Gymnasium bèta, St. Montfort College, Rotterdam.
  
- 1994-2000    Technische Natuurkunde, Universiteit Twente.  
                  Stage bij British Telecom Labs, Ipswich, UK.  
                  Afstudeeropdracht bij leerstoel Optische Technieken, Universiteit Twente.
  
- 2001-2002    Medewerker Onderzoek, Aquamarijn Micro Filtration.
  
- 2002-2003    ‘Management voor jonge ingenieurs’, professional development programma,  
                  TSM Business School.
  
- 2002-2005    Assistent in Opleiding, Membraan Technologie Groep, Universiteit Twente.
  
- Aug. 2005    Philips Lighting.

